PONTIFÍCIA UNIVERSIDADE CATÓLICA
DO RIO DE JANEIRO

Leo Theodoro d'Azevedo Lemos Bähr

Mechanical Behavior and Numerical Modeling of Textile Reinforced Concrete

DISSERTAÇÃO DE MESTRADO

Dissertation presented to the Programa de Pós-Graduação em Engenharia Civil of the Departamento de Engenharia Civil e Ambiental da PUC-Rio as, partial fulfillment of the requirements for the degree of Mestre em Engenharia Civil.

Advisor: Prof. Flávio de Andrade Silva
Co-Advisor: Prof. Deane de Mesquita Roehl

Rio de Janeiro
December 2016

Pontifícia Universidade Católica
do Rio de Janeiro

Leo Theodoro d'Azevedo Lemos Bähr

Mechanical Behavior and Numerical Modeling of Textile Reinforced Concrete

Dissertation presented to the Programa de Pós-Graduação em Engenharia Civil of the Departamento de Engenharia Civil e Ambiental da PUC-Rio, as partial fulfillment of the requirements for the degree of Mestre. Approved by the undersigned Examination Committee.

Prof. Flávio de Andrade Silva
Advisor
Departamento de Engenharia Civil e Ambiental – PUC-Rio

Profª. Deane de Mesquita Roehl
Co-Advisor
Departamento de Engenharia Civil e Ambiental – PUC-Rio

Prof. Raul Rosas e Silva
Departamento de Engenharia Civil e Ambiental – PUC-Rio

Prof. Givanildo Alves de Azeredo
Universidade Federal da Paraíba

Drª. Lourdes Maria Silva de Souza
Departamento de Engenharia Civil e Ambiental – PUC-Rio

Prof. Márcio da Silveira Carvalho
Vice Dean of Graduate Studies
Centro Técnico Científico - PUC-Rio

Rio de Janeiro, December 21st, 2016.

Leo Theodoro d'Azevedo Lemos Bähr

Leo Bähr graduated in electrical engineering at PUC-Rio, with specialization in optical telecommunications, obtained at TU Braunschweig; having had an extended intercontinental experience. He developed logical thinking abilities in the mathematical and computational areas through his academic and professional experiences, having worked in a German engineering company, financial market and, more recently, in the geomechanics computational group in the TecGraf Institute.

Bibliographic Data

Bähr, Leo Theodoro d'Azevedo Lemos

Mechanical behavior and numerical modeling of textile reinforced concrete / Leo Theodoro d'Azevedo Lemos Bähr ; advisor: Flávio de Andrade Silva ; co-advisor: Deane Mesquita Roehl. – 2016.
98 f. : il. color. ; 30 cm

Dissertação (mestrado)–Pontifícia Universidade Católica do Rio de Janeiro, Departamento de Engenharia Civil, 2016.
Inclui bibliografia

1. Engenharia civil – Teses. 2. Elementos finitos. 3. Concreto têxtil. 4. Análise numérica. I. Silva, Flávio de Andrade. II. Roehl, Deane Mesquita. III. Pontifícia Universidade Católica do Rio de Janeiro. Departamento de Engenharia Civil. IV. Título.

CDD: 624

Acknowledgements

I would like to thank my advisor, Professor Flávio de Andrade Silva and my co-advisor, Professor Deane Roehl for the guidance in this work. Also, I would like to express my gratitude to CAPES for the financial support, the Tecgraf Institute for the work opportunity and financial support and my co-workers in the laboratory and Tecgraf for sharing their knowledge.

Abstract

Bähr, Leo Theodoro d'Azevedo Lemos; Silva, Flávio de Andrade (advisor). **Mechanical Behavior and Numerical Modeling of Textile Reinforced Concrete**. Rio de Janeiro 2016. 98p. MSc. Dissertation - Departamento de Engenharia Civil e Ambiental, Pontifícia Universidade Católica do Rio de Janeiro.

Textile Reinforced Concrete (TRC) offers high-strength and light-weight capabilities combined with ecological potential in construction and architecture spheres. However, important mechanical aspects of TRC are still unresolved, delaying broad utilization of the composite material. An experimental program to measure key parameters of TRC is presented, consisting of uniaxial tension tests in carbon-reinforced TRCs. Different manufacture processes, sizes of test specimen and textile coatings were used. Then, a Finite Elements (FE) model is proposed and validated with experimental data acquired from uniaxial tension and round panel tests. The FE model is made of a sandwich-like structure, containing cementitious matrix, textile and interface elements. A specific constitutive response is assigned to each phase of the composite material. The uniaxial tension tests simulated in the FE model showed excellent agreement with the experimental program, both in the stress-strain curve and stress-transfer mechanisms inside the composite. The results obtained from the simulated round panel tests exhibited differences in the stress-strain curve, but the stress transfer mechanisms were observed.

Keywords

Finite elements; Textile Reinforced Concrete; Numerical Modeling.

Resumo

Bähr, Leo Theodoro d'Azevedo Lemos; Silva, Flávio de Andrade. **Comportamento Mecânico e Modelagem Numérica de Concreto Têxtil**. Rio de Janeiro 2016. 98p. Dissertação de Mestrado - Departamento de Engenharia Civil e Ambiental, Pontifícia Universidade Católica do Rio de Janeiro.

O concreto têxtil é um material compósito com qualidades de alta resistência e peso reduzido, combinadas com potencial ecológico nas áreas de construção e arquitetura. No entanto, importantes aspectos mecânicos seguem irresolutos, postergando a ampla utilização deste material compósito. Um programa experimental é apresentado para apurar os parâmetros-chave do concreto têxtil, composto de ensaios de tração uniaxial em compósitos reforçados com carbono. Diferentes processos de fabricação, tamanhos de corpo de provas e *coatings* de tecido são utilizados. Então, um modelo de Elementos Finitos (FE) é proposto e validado através de dados coletados em ensaios de tração direta e *round panel*. O modelo de EF é composto por uma estrutura sanduíche, contendo matriz cimentícia, tecido e interface. Uma resposta constitutiva específica é atribuída a cada tipo de elemento. Os testes de tração uniaxial simulados apresentaram excelente concordância com os resultados experimentais, tanto nas curvas de tensão-deformação, quanto nos mechanismos de tranferência de esforços entre os componentes do material compósito. Os resultados obtidos dos testes de round panel apresentaram diferença nas curvas de tensão-deformação, mesmo com a presença dos mecanismos de transmissão de esforços no material.

Palavras-chave

Elementos Finitos; Concreto Têxtil; Análise Numérica.

Contents

1. Introduction

Textile Reinforced Concrete (TRC) is a composite material made of open-meshed textile embedded in a fine-grained concrete matrix. When the ultimate strength of the matrix is reached, fracture occurs. The tensile load is then transferred to the textile reinforcement. Depending on the composite's properties, multiple cracking of the matrix may be observed. This load transfer mechanism enables the TRC to support higher tensile loads without critical failure. Having lightweight and slender features. Moreover, when alkaline resistant materials are chosen (polymer-coated yarns, carbon-fiber fabrics and AR glass), textiles exhibit superior durability in alkaline environment of the cement matrix.

From an environmental stand, the ability to create lighter and slimmer concrete structures results in the reduction of Portland cement utilization and lower levels of carbon dioxide emission. This feature places TRC as a sustainable construction material. Further reduction in CO_2 is seen if fuel consumption of logistics is considered. TRC and other new, sustainable building technologies are of great importance when considering the concept of sustainability and environmental concern.

Architecture and design are other stimulating factors for the use of TRC. The possibility of creating larger free spans and slender structures are features of interest. Textile's flexibility allows the creation of numerous TRC shapes: functional and artistic. Applications include furniture design, pre-cast panels, repair of existing structures and structural sandwich elements.

In addition to pre-cast panels advantages in low cost buildings and schedule planning (due to off-site manufacture capabilities), TRC shows energy absorption characteristic after the first crack and can be used to fabricate structural elements. Attributes which make the composite material a topic of interest on fields of seismic, ballistic and impact resistant structures. In recent years attention has been given to carbon TRC and its applications. Advances in the field relate directly to building costs, time optimization and sustainable construction.

The present work investigates the load bearing capabilities in bending and direct tension of TRC and envions to open ground for load bearing production of TRC structural elements. Carbon and basalt open-meshed textiles are used as

reinforcement. Although expensive, carbon was selected for its high tensile strength, corrosion, temperature and fatigue resistance, all of which are important attributes for structures in civil engineering. The purpose of adding basalt-reinforced TRC is the validation of the numerical model, which is based on carbon-reinforced TRC.

Experimental and numerical programs were developed to study the mechanisms present in the behavior of TRC as a whole. The two components of the material (fine-graded concrete matrix and textile reinforcement) and the interface between them were analyzed separately. Experimental data is used to obtain constitutive equations of the matrix and textile for computational simulations. Different textiles, matrices and interfaces were used, aiming to relate changes in parameters of the test specimens to numerical parameters in a finite element solution.

The significance of this research lies on testing commercially available carbon open-meshed textile reinforced concrete, understanding its mechanical behavior as a structural building material and being able to design structural and semi-structural components. To achieve this goal, constitutive equations were obtained from laboratory tests and used as input in a finite elements (FE) software. Furthermore, a numerical model is proposed to reproduce the experimental program.

2. Literature Review

Cement is created by heating limestone and clay to high temperatures (around 1450^{o}C). The thermal reaction produces clinker, cement's core constituent, whose main components are CaO, SiO, Al_2O_3 and Fe_2O_3. These substances become adhesive when mixed with water, being capable of uniting fragments into a single body as a whole. This binding capability is the cement's most notorious characteristic [1].

A binding material was used at an early age (circa 1400-1200 BC) by the Greeks [2] in the Royal Palace of Tiryns. This technique was later brought into the Roman Empire and spread throughout. In Italy, the Romans collected the biding material from the neighborhood of Pozzoli, from which Pozzolana borrows its name. Pozzolana is a substance that, when mixed with lime and water, creates a binder. Due to its extraordinary quality, the name extends its meaning to all minerals of its class.

Mortar quality declined in the Middle Ages. The next remarkable advance in cementitious materials occurred in the 18th century. Then, John Smeaton was assigned to build a lighthouse and studied the cement manufacture process in order to erect a long lasting structure. Continuing with the improvement of cement in Britain, Joseph Aspdin submitted his patent for Portland Cement in 1824 [3], an important fact in mortar's history. Since then, the manufacture process continued to improve, but the name "Portland Cement" remains used until today.

Concrete is the most used building material in the world [4] and is composed by cement and aggregates (coarse and/or fine). Multiple authors have shown [5]-[7] that concrete's ultimate tensile strength is significantly lower than its compressive strength and has a brittle failure mode under tension. To overcome this downside ingenuous solutions have been adopted, one of the first and most common being steel reinforcement of concrete. Downsides of utilizing steel as reinforcement includes high price, transportation, storage, placement in the cementitious structure and corrosion.

An efficient reinforcement material should resist alkalinity of cement (improving durability), bond well to the matrix (not easily slip) and, more importantly, have a high ultimate tensile strength. This combination of properties

enables the structure to support higher stresses without failure.

A more recent reinforcement is made by fibers, in Fiber Reinforced Concrete (FRC). FRC is a discrete reinforced material, where fibers have no specific direction or connection. Its origin dates to ancient times, when horse hair was added to fresh mortar, although in the 1960's the name FRC was broadly adopted [8]. At the time, researches were looking for a high strength, crack resistant and lighter concrete [9]. An improved post cracking behavior is also observed in tensile strain but not in ultimate tensile strength.

Further development, both academic and industrial, in concrete and textile areas resulted in a new combination of materials: textile and concrete, named Textile Reinforced Concrete (TRC). Textile is a continuous material, where filaments and yarns are oriented and connected. A wide diversity of textile types is available, ranging from natural to carbon fibers. The material can take numerous shapes, both artistic and functional. Thinner and lighter elements can be made resulting in lighter structures. Advantages in mechanical properties include the possibility of achieving higher energy absorption after first crack (ductile fracture) under tensile load and considerable improvement in ultimate tensile strength [10]. Fabric Reinforced Cementitious Matrix (FRCM) is a variation of TRC. Donnini [11] describe FRCM as:

> "FRCM is a composite system specifically designed for the repair and rehabilitation of concrete and masonry structures, introducing an alternative to the existing repair methods."

In present days, most common applications of TRC are precast panels, maintenance and repair of structures. Structural and semi-structural elements with lightweight and/or seismic-resistant characteristics, façade systems, barrel shells and more areas are to be explored [12]-[15]. These can be reached in the next years due to today's increasing concern with sustainable materials and global warming. In 2006, the cement industry was responsible for approximately 7% of man generated carbon dioxide, totaling 1.8Gt of greenhouse effect gas released into the atmosphere [16]. Adopting TRC as a standard building material enables slender and lightweight building, reduces cement consumption, and may contribute to lower CO_2 emissions.

An idealized plot of TRC behavior under uniaxial tensile load presents three

states: (I) composite loading, (IIa) crack formation (after matrix failure) and (IIb) stabilized crack pattern, displayed in Figure 2.1. The first (I) consists of loading the composite until failure of the cementitious matrix, in a linear elastic manner. The second (IIa) describes the load transfer from matrix to textile through the interface between them. If bonding is weak, a large interface area is needed to support the matrix's ultimate tensile strength of the matrix and form a new crack and large crack separation is observed whereas stronger bond creates smaller crack spacing. Finally (IIb) load is borne entirely by the textile after multiple cracking. Further bond degradation causes the textile to slip from the matrix and one crack grows wider, causing failure of the material.

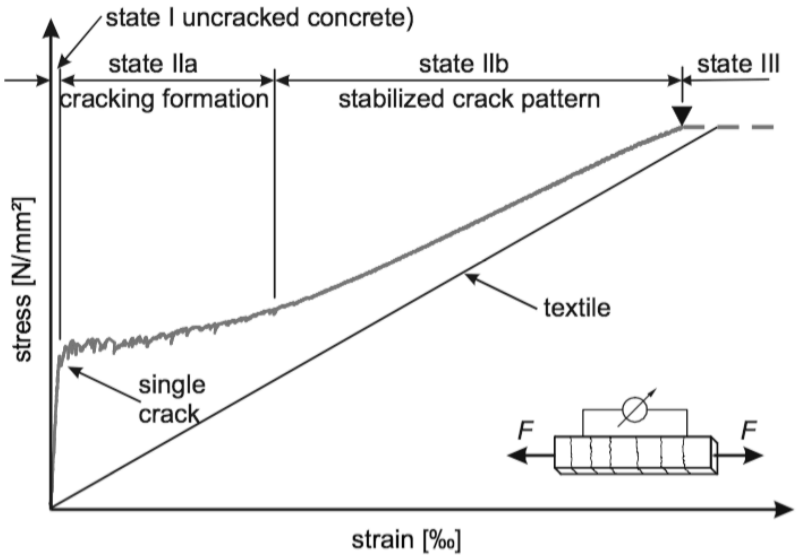

Figure 2.1: Stress-strain diagram of textile reinforced concrete under direct tension [17].

2.1. Textile Grids, Fabrics and Yarns

Fabric (or textile) is a material produced by weaving or knitting of textile fibers. In this work, however, textiles and fabrics assume a more specific definition, being open-meshed, in two or three dimensions, composed by assembling of yarns into patterns. Yarns are defined as bundled individual filaments, in an interweaved or juxtaposed fashion.

Textiles are widely used. Fashion apparel, body armor, tensile structures, reinforced composites and laminated materials are some of its applications. Demand of the material is provided by different manufacture processes of yarns [18] and textiles [19]. The processes affect characteristics and mechanical

properties of the final product. In recent years, growing interest in technical textiles promoted studies on the field, focusing on its mechanical behavior as a stand alone material or integrated with other technologies. Textile materials and approaches used to analyze its structure are presented next.

Fiber materials are classified into two groups: natural and artificial (or man-made). Natural fibers major constituent is cellulose. They are low-cost and biodegradable. However, they present poor matrix bonding, low temperature resistance, variability of properties and hydrophilic nature. These characteristics present major disadvantages when natural fibers are used for load-bearing purposes or in aggressive environments. Therefore, natural fibers are not used in manufacturing high performance TRC [20]. Natural fibers have been successfully employed in producing self-healing concrete [21], due to their water affinity, and non-structural cement based composites.

Man-made fibers present more consistent mechanical properties and wider range of strength (from glass to carbon-fibers). Their properties can be tailored (e.g. matrix bonding or pH resistance) through different processes (e.g. impregnation and/or coating of textile yarns). Hence, they are suitable for manufacture of high performance TRC.

Table 2.1: Comparison of filament yarn properties [19], [20].

Material	Density g/cm3	Strength GPa	Modulus GPa	Elongation %
Aramid	1.44	2.9	60	3.6
Bamboo	.6 ~ 1.1	2.0 ~ 3.5	11 ~ 17	-
Carbon	1.78	3.4	240	1.4
Cotton	1.5 ~ 1.6	.29 ~ .60	5.5 ~ 12.6	3 ~ 7
Glass	2.5	2.0 ~ 3.5	70	2.5
Sisal	1.45 ~ 1.50	.35 ~ .70	9 ~ 22	2 ~ 7
Steel	7.86	1.77	200	1.1

Textile yarns present a non-linear behavior when tested in uniaxial tension. Tensile Young's modulus increases until reaching a linear behavior. Afterwards, a decrease in stiffness may be observed, depending on the failure mode of the fibers (Figure 2.3). The initial, lower modulus is a consequence of the rearrangement of

filaments as the load increases [22]. Parameters which influence the hardening behavior of yarns include material, length and manufacture process (coated, twisted, juxtaposed and others), since they modify the structure of yarns in mesoscopic (i.e. rearrangement of filaments and cross section deformation) and microscopic levels (i.e. friction between filaments and filament failure) [23], [24]. Figures 2.2 and 2.3 show different weaving patterns of textiles and mechanical behavior of yarns of different materials under uniaxial loading.

Figure 2.2: Different weaving patterns. Left, plain weave. Middle, twill weave. Right, satin weave[25].

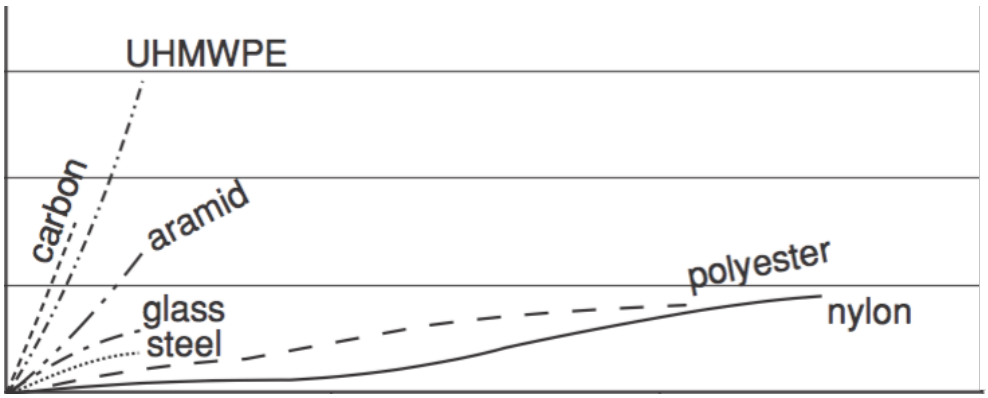

Figure 2.3: Stress-strain relationship for different yarn types [26].

The complex behavior observed in textiles arises from a physical phenomena that occurs inside the material. Understanding these mechanisms is fundamental to address the textile behavior from analytical and numerical perspectives. The main mechanical processes are listed below:

1. Crimp interchange: elongation of the fabric in a direction (yarn waves loses amplitude) and crimping of yarns in another direction, leading to contraction.

2. Locking: increase of fabric deformation resistance due to jamming of interwoven yarns.

3. Contact: shear and normal stresses between yarns and/or filaments. It may stiffen the fabric (or yarn) due to friction and may cause failure.

4. Sliding: relative displacement between warp and weft yarns (in fabrics) or filaments (in yarns).

Peirce [27] proposed a discretization of yarns as smaller, connected elements, linking length of the material (number of elements) to strength probability distribution:

$$F_l(x) = 1 - \left[1 - F_{l_0}(x)\right]^{l/l_0} \tag{1}$$

where $F_{l0}(x)$ and $F_l(x)$ are the strength probability distribution at a gauge length l_0 and at any length l respectively. Assuming a two parameter Weibull distribution [28] to describe $F_{l0}(x)$:

$$F_{l_0}(x) = 1 - \exp\left[-\left(\frac{x}{x_0}\right)^r\right] \tag{2}$$

and replacing (2) in (1):

$$F_l(x) = 1 - \exp\left[-\left(\frac{x}{x_l}\right)^r\right],\ x_l = x_0 \cdot \left(\frac{l}{l_0}\right)^{-1/r} \tag{3}$$

the strength probability is written in term of x_l and r; scale and shape parameters respectively. The shape parameter defines lengths in which failure is expected to occur and the scale parameter defines the maximum length of the yarn.

Realff [29] did a thorough study in both yarn and textile behavior under tensile load. When analyzing yarns, change in failure mode was observed with decreasing gauge lengths, disagreeing with the weakest link theory. In textile structures, the effects of weave texture and structure size were observed, on which larger structures (more yarns) presented more brittle failure. In addition, the study shows that short yarns are more suitable to model the behavior of textiles. However, little information is given for the material composition of the yarns.

Besides geometry and material composition, important parameters such as coating, temperature resistance, moisture absorption and structural design have

been addressed in different researches. Misak et al. [30] compared polyester coated and non-coated carbon nanotubes, observing that coating improved ultimate tensile strength and stiffness. Moreover, failure occurred in one point in coated specimens, versus scattered failure observed in non-coated specimens. Carozzi and Poggi [31] tested single yarns and meshes made of different materials and obtained lower average failure stress for meshes (agreeing with the weakest link equations).

The geometry of textiles and yarns have great influence on the deformation of the material under load. Peirce [32] developed a geometric model for plain weave fabric with round, inextensible yarns from basic parameters: yarn lengths, crimp heights, yarn spacings and sum of yarn diameters. This simplified model (Figure 2.4) allows calculation of the cloth's resistance to mechanical deformation and establishes a relationship between several geometric parameters. Unfortunately, the assumptions are unrealistic and the geometric equations are difficult to solve. Kemp (racetrack model) and Olofsson (elliptical model) made adaptations to Peirce's model, altering the base geometry in an attempt to better predict the mechanical behavior of fabrics [33].

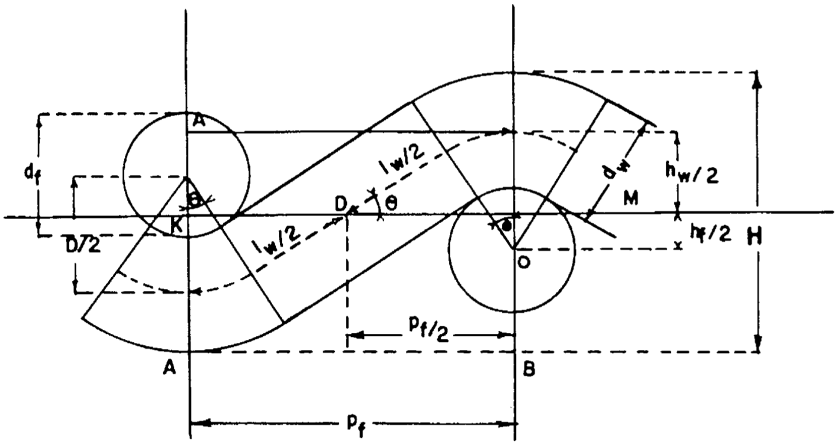

Figure 2.4: Geometry proposed by Peirce, 1937.

Geometrical models are used to better understand mechanical behavior in textiles [34], which are extremely complicated materials and do not conform to any of the ideal geometric assumptions of the previously cited works. Ozgen et al. [35] investigated changes in yarn cross-section along the yarn path, and the effect of yarn and fabric parameters to these changes. Yarn cross section was assumed to be elliptical, with major and minor radii relating to yarn linear density, twist

factor, warp and weft cover.

2.2. Interface

The interface bonds the cementitious matrix and textile together. Bond strength affects stress transfer capacity between the two phases of the composite, balancing forces from high-stressed to less-stressed areas of the material. Multiple cracking behavior of TRC is a consequence of this load-transfer mechanisms, and is observed when the two phases of the composite are well-bonded. A typical bond stress-slip curve is shown in Figure 2.5. The bond strength depends on friction between concrete and textile which, in turn, is affected by coating, material, volume fraction and geometry of textiles, as well as matrix composition. Peled et al. investigated the dependence of interface properties on the fabrication methods of TRC [36] and on textile type [37]. Donnini et al. [11] investigated the mechanical properties of FRCM using carbon fabrics with different coatings. Experimental results showed that stronger bonds generate tougher stress-strain response after matrix cracking.

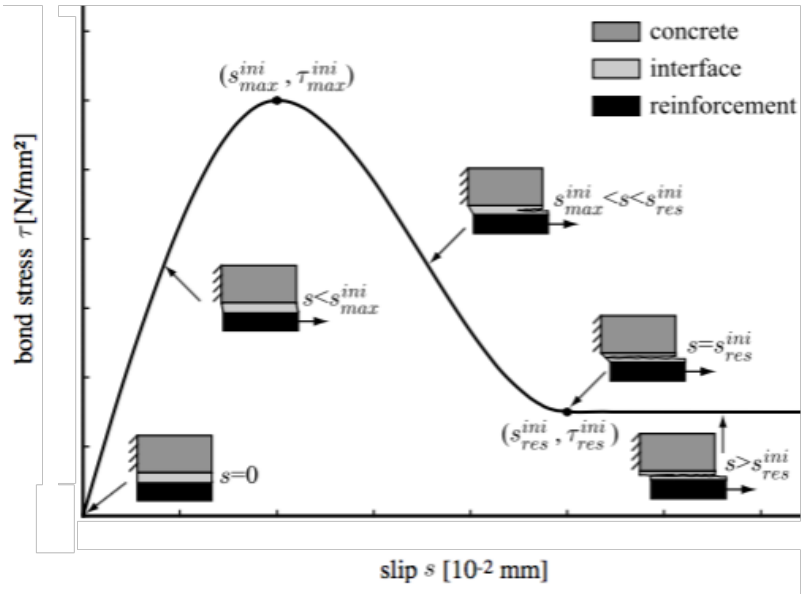

Figure 2.5: Bond stress-slip relationship [38].

Characterization of bond strength is made through pull-out tests. Most common configurations include one-sided and double-sided pull-out tests. More configurations are available, as suggested by Portal et al. [39] with the objective of standardizing test set-ups. Testing consists of applying tensile load to remove

one yarn embedded in the cementitious matrix. During the test, the interface is subjected to the three zones shown in Figure 2.5: bonded zone, debonding zone and sliding zone. Bond properties have been investigated under a series of configurations in [40], [41].

The behavior of the interface under tensile load was investigated by Aveston, Cooper, and Kelly [42], whose work addressed mechanics of matrix toughening after failure when volume fraction of fibers was greater than a critical value. Cox [43] analyzed the stress transfer to fibers embedded in a cementitious matrix and Marshal [44] studied the crack bridging through energy balance and stress intensity in a fiber-reinforced brittle matrix. Wang et al. [45] reviewed the theoretical analyses of fiber pull-out, including the work of Naaman and Shar [46]. Naaman and Shar used elastic and frictional bonding strengths to characterize bond behavior and related the stress in the length of the fiber to the fiber/matrix Young's modulus ratio and fiber cross sectional area. Shortcomings of the model to describe the fiber pull-out experiment include limited fiber geometry, which was assumed to be circular.

The stress-slip curve can be divided into three main segments. Undamaged bond is represented by the initial, linear response. In this state, no relative displacement is observed among the two phases. Non-linearity of the ascending curve is caused by partial debonding of yarns. A mixed behavior of undamaged and debonded yarns is observed until the bond maximum strength is reached. Debonding continues in the post-peak section of the curve, where the bonded length becomes increasingly smaller. Dynamic sliding is observed in the last part of the curve, when the entire length of the yarn is debonded. Derivations of stress distribution for each state of loading can be found in [47]. The experimental stress-slip curve of the interface is used to obtain bond parameters. Reinhardt et al. [48] present useful guidelines to experimental bond testing and several analytical bond models.

More recently, Häussler-Combe and Hartig [49] addressed crack-spacing problem through parameters of textile yarns and concrete matrix. Carozzi et al. [31] made a detailed study in mechanical properties and debonding of FRCM, utilizing a number of textile types and matrix designs. Mobasher et al. [50]

studied hybrid TRCs under tensile and flexural loading and concluded that griping, delamination, interfacial bond and matrix penetrability have a dominant effect in flexure behavior, whereas yarn strength has a larger effect in uniaxial tension.

In [49], crack-spacing is calculated by integrating Equation (4) with x varying from zero, where an initial crack is present, to l_{ct}, the critical length where another crack is expected to occur.

$$A_c \cdot d\sigma_c = n_y \cdot C \cdot \tau(x) dx \tag{4}$$

Where A_c and σ_c are concrete matrix cross-section and stress, n_y the number of yarns, τ the bond stress and x the longitudinal coordinate. After integrating, the critical length is given by Equation (5):

$$l_{ct} = \frac{A_c}{n_y \cdot C} \cdot \frac{f_{ct}}{\tau_{mean}} \tag{5}$$

Mean bond stress, τ_{mean}, and ultimate tensile strength, f_{ct}, are used. Equation (5) demonstrates that decrease in crack-spacing is observed with increasing bond strength.

As discussed, stress is transferred from the cementitious matrix to the textile yarns. Textile yarns are composed by a large number of filaments. These filaments can be directly connected to the interface, named sleeve filaments, or not, named core filaments. Load reaches the sleeve filaments more easily than the core filaments. Thus, in addition to the textile crimp effect discussed in Section 2.1, a gradual mechanical activation of yarns must be considered when analyzing the load-response of TRC.

Peled et al. [36] investigated bond strength for different textile types and manufacture methods embedded in a cementitious matrix. Bond strength results ranged from 1.54~4.07 MPa. Sueki et al. [41] presented a similar study and compared bond strength obtained from simulated (based on the Naaman pull-out model [51]) and experimental tests. Simulated bond strength values were in the range of 1.10~5.58 MPa, where glass-fiber reported the best values. Park et al. [52] addressed bonding mechanism in carbon and glass-fiber reinforced composite, obtaining larger crack-spacing for the carbon reinforced specimens

(indicating inferior bond strength). Lorenz and Ortlepp [53] analyzed pull-out behavior of carbon-fiber textile embedded in a fine-grained matrix and proposed an analytical model to predict the stress-slip behavior. Good agreement of results was reported.

2.3. Mechanical Behavior of TRC

Textile reinforced concrete (TRC) is a composite material composed of a fine grained concrete matrix and fabric with high mechanical properties. The concrete matrix holds the fabric, maintaining orientation of the yarns and contributing to a high initial rigidity. Yarns are composed by a large number of filaments. Coating of yarns can be used to better distribute stress to core filaments. Mechanical behavior of TRC can be described as a combination of this two components: cementitious matrix and textile, with the interface transferring stresses. Unfortunately, none of their behaviors is simple. As seen, textile has a number of parameters which influence its mechanical behavior, as does the interface. The strong adherence between textile and matrix enables TRCs to exhibit multiple cracking behavior, greater ductility and energy absorption, all of which are desirable properties. Since textiles and fabrics allow only small particles to permeate them, matrices used in TRCs do not contain coarse aggregates. Finer matrices better penetrate the gaps in the textiles and create stronger bonds.

Concrete can be analyzed in micro (10^{-8}~10^{-4} m), meso (10^{-4}~10^{-1} m) and macro (10^{-1}~10^{3} m) scales. At the micro level, atomic structure, unhydrated cement grains and calcium silicate hydrates are distinguished. Moving to the meso scale, pore structure, aggregates, micro cracks and interfacial transition zone (ITZ) are observed. Arriving at the macro scale the material is considered homogenous, with no internal structure. This is the scale in which laboratory tests are performed. Larger levels of observations are used to analyze entire buildings and structures [54].

The concrete stress-strain behavior under uniaxial compressive loading exhibits an ascending branch followed by a peak, named ultimate compressive strength. Afterwards, a descending line and an abrupt decline in compressive strength is observed, representing complete failure. A typical curve is shown in

Figure 2.6a.

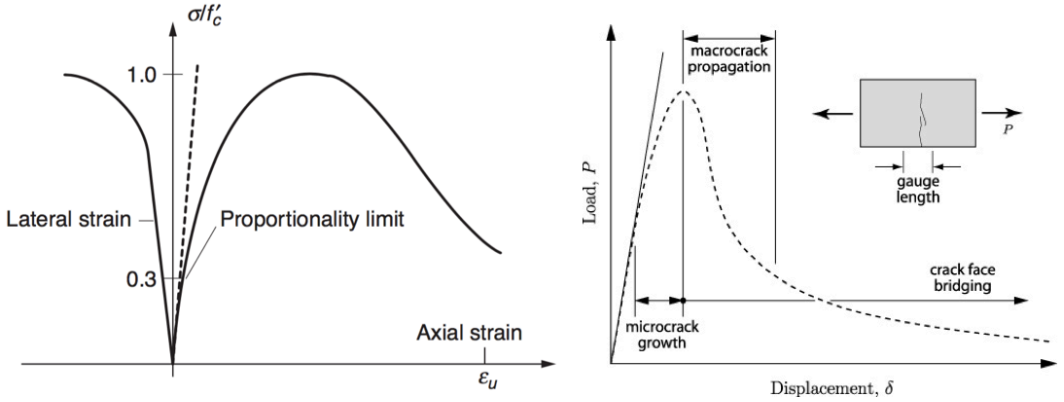

Figure 2.6: On the left, (a) typical stress-strain curve of concrete under uniaxial compressive load [55] and on the right, (b) typical stress-strain curve of concrete under uniaxial tensile load [56].

The initial part of the curve, until σ/f_c'~0.3, presents a linear response. Its slope is the Young's modulus. Micro cracking of concrete is responsible for the slight slope decrease after the ~0.3 mark. Micro cracking continues until ultimate compressive strength is reached. At this point, crack propagation begins and continues until complete failure of the material. Crack propagation behavior is shown in the softening branch of the curve. Under tensile load, concrete behaves similarly. Initially a linear behavior is observed, followed by a slope decline until the ultimate tensile strength is reached. Softening in the stress-strain curve is observed afterwards. Significant difference is seen in slope decline in the ascending branch, more noticeable in compression, and ultimate tensile strength, generally ten times smaller (in modulus) than ultimate compressive strength.

Non-linearity observed in concrete is closely related to cracking. Understanding failure phenomena of concrete is key to correctly predict the behavior of TRC, which undergoes multiple cracking. A series of classical fracture and failure hypothesis can be found in [57], describing failure point of materials.

After the failure point of the material is reached, its mechanical response changes and a new approach must be taken to describe its behavior. Hillerborg [58] proposed a fictitious crack approach, stating the undamaged stress-strain relationship is valid until a limiting strain, ε_L. The corresponding stress value is the tensile strength, f_t. Once ε_L is exceeded, additional displacement is concentrated at the fracture zone and behavior of the material is described by a

stress-displacement (σ-w) curve. The fracture zone has an original width (w) of zero. A width of w is observed after the fracture zone starts to develop. At this stage, the fracture zone is able to transfer tensile stresses (σ) and may be regarded as a fictitious crack. The fictitious crack tip ($w=0$) is the limit between displacement and strain dependent stresses and the crack end ($w=w_L$) is the dividing width between transferring of stresses and zero stress transfer, shown in Figure 2.7.

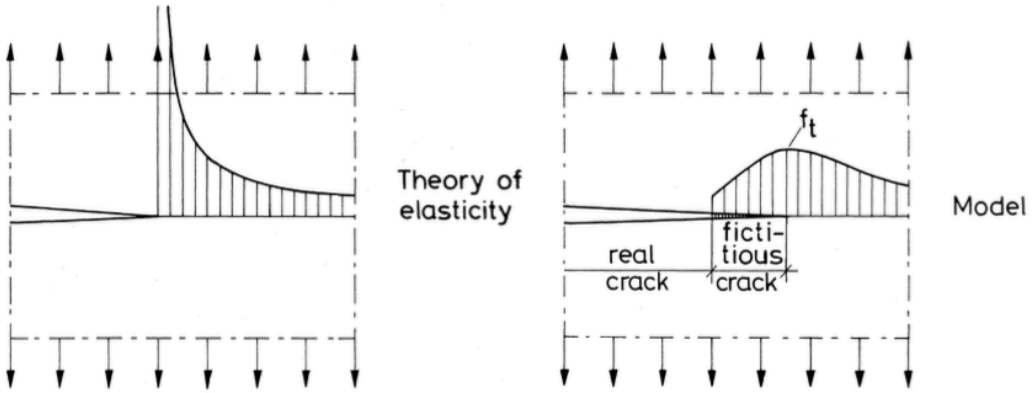

Figure 2.7: (a) Crack stress according to the theory of elasticity and (b) fictitious crack model suggested by Hillerborg, taken from [58].

Crack growth is written in terms of energy absorption and crack propagation occurs when energy absorbed exceeds the energy of the fictitious crack (G_c). This relationship is described by Equation (6).

$$\int_0^{w_L} \sigma \, dw = G_c \tag{6}$$

Equation (6) links the fictitious crack theory to classical fracture mechanics. Graphically, G_c is the area under the stress-displacement curve (Figure 2.6b) after the peak load is reached.

Textile and fiber reinforced concrete differ from unreinforced concrete in post-failure behavior (Figure 2.8). TRC and FRC are capable of transferring stresses through large crack widths, as yarns or fibers bridge cracking zones [59]. Post-failure behavior of TRCs depends on volume fraction of textile, textile properties and bonding between textile and concrete (or interface) [37], [38]. Volume fraction of the TRC material is calculated through Equation (7).

(7) $$V_f = \frac{v_f}{v_m}$$

Where v_f is volume of fibers or textile yarns and v_m is volume of the cementitious matrix. Young's modulus of the composite material can be described in terms of volume fraction by:

(8) $$E_c = E_m \cdot v_m + E_f \cdot v_f$$

Equation (7) can be used in conjunction with the constitutive models of the materials to describe the stress-transfer mechanism of TRC in multiple phases of loading. Constitutive response of textile yarns and concrete depends on several parameters, as discussed previously. The interface is considered infinitesimally thin and does not support load. It only bonds matrix and textile, preventing relative displacement between them until bond strength is exceeded.

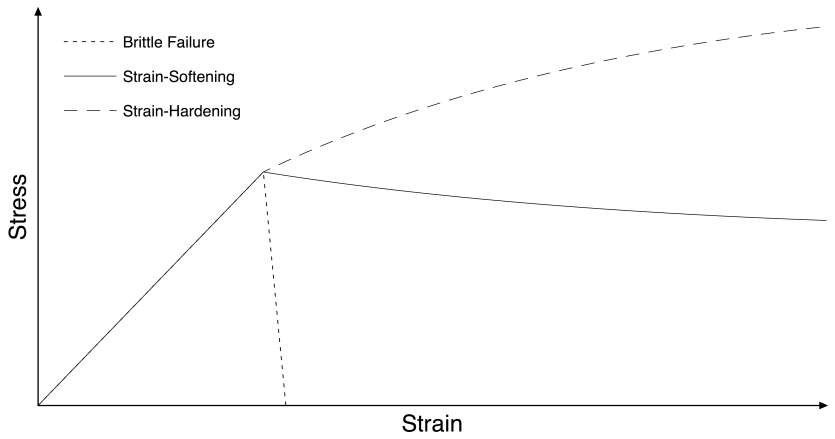

Figure 2.8: Brittle failure (i.e. unreinforced concrete), strain-softening and strain-hardening behavior under uniaxial tension.

Utilizing the constitutive models presented and Equation (8), a physical-mathematical approach can be taken to describe the behavior of TRC under uniaxial tension, shown in Figure 2.1. Adopting the nomenclature displayed on Figure 2.1, state I describes loading of the composite up to rupture. Since the textile has almost no load bearing capacity in this state, Young's modulus of the composite material is, generally, slightly smaller than that of the matrix alone. When failure of the matrix occurs, the curve moves to state IIa, where localized displacements (cracking) are observed. The displacements are large enough for the Young's modulus of the textile to increase and the yarns start to bear load. If

the interface is capable of resisting shear stresses, the textile does not slide and load is transferred entirely to the matrix at a distance *d* from the first crack, where the textile remains relaxed. A new crack appears. Repeatedly, cracking of the matrix occurs following this process. Young's modulus of the composite observed in this state is low. State IIb begins when no new crack zones appear. The interface surface between cracks is unable to support stresses higher than the ultimate tensile strength of the matrix. The curve moves to state III when sliding begins. Stress transfer between textile and matrix declines as bonding degrades, displayed in the last part of the curve in Figure 2.5. A summary of TRC mechanical behavior is presented in Table 2.2.

Table 2.2: Load bearing materials and Young's modulus of TRC during the states of loading. Bond strength is shown in Figure 2.5 and min(a, b) indicates the minimum value between a and b. Since high performance textile is used, generally $E_t > G_{inter}$.

State	Load Bearing Material	Bond Strength	E_c
State I	mostly matrix	$slip < slip_{max}$	$\sim E_m$
State IIa	matrix and textile	$slip < slip_{max}$	~0 (plastic stage)
State IIb	textile and interface	$slip \sim slip_{max}$	$\min(E_t, G_{inter})$
State III	textile and interface	$slip > slip_{max}$	$\min(E_t, G_{inter})$

TRC behavior in the macro scale has been studied by several authors. Papanicolaou et al. [60] investigated the structural behavior of TRC beams cast against thin-walled formwork, reporting higher load-carrying and deformation capabilities in beams reinforced with polymer-coated textiles and higher textile volume fraction. Arboleda [61] evaluated FRCM utilization in structural rehabilitation through research of mechanical behavior of FRCM after exposure to severe environmental conditions. However, no significant degradation was observed for the environments studied. Matzenmiller et al. [62] developed a constitutive model for anisotropic damage to describe elastic-brittle behavior of fiber-reinforced composites. The model allows elaborate dependencies between components of the constitutive tensor and the governing internal variables, making it suitable for implementation in finite elements software. Silva et al. [63] analyzed interface behavior of carbon textile reinforced concrete under elevated

temperatures and found that polymer-coated yarns presented higher pull-out load after being preheated to 150ºC. Changes in performance were attributed to a matrix-polymer interlocking mechanism. Butler et al. [64] investigated aging effect on interface properties of glass fiber TRC. It was found that the performance losses with increased age depended primary on the alkalinity of the pore solution in the matrix. These research fields are essential for TRC to replace (at least partially) conventional steel-reinforced concrete in the future.

This work aims at the macro scale of TRC, specifically at dimensioning of semi-structural components. To achieve this, a numerical model is proposed and its validation is made through comparison with experimental results.

2.4. Numerical Modeling

A numerical solution is needed when experimental testing is impossible, undesirable and/or cost/time consuming. Numerical models are mathematical models that use numerical time-stepping procedure to obtain the behavior of a system over time. Validation of the model is needed and is accomplished through comparison between the physical and mathematical systems, demonstrating similarities between them [65]. Common choices for numerical solutions are the finite elements method (FEM), finite difference method and finite volume method. The FEM is the most widely used and was chosen for this work. Simulation of results was performed by Abaqus, developed by Dassault Systemes.

Carlos Felippa [66] described discretization in the FEM in his book:

> "The basic concept in the physical FEM is the subdivision of the mathematical model into disjoint (non-overlapping) components of simple geometry called finite elements or elements for short. The response of each element is expressed in terms of a finite number of degrees of freedom characterized as the value of an unknown function, or functions, at a set of nodal points. The response of the mathematical model is then considered to be approximated by that of the discrete model obtained by connecting or assembling the collection of all elements."

TRC mechanical behavior is described by a combination of textile, interface and concrete. Other aspects as geometry and size also influence the behavior of the material. An experimental program to test every parameter available would be extremely time-consuming. Hence, numerical modeling of TRCs is an important tool for researchers.

At an early stage of computational engineering a finite element (FE) model,

capable of simulating concrete damage was presented in [67]. Realistic results were reported regarding failure, crack formation and crack propagation. As computational systems advanced, powerful FE softwares were developed and a wide range of models became available. These models objectives are to simulate the behavior of important phenomena such as concrete and steel mechanical response to loading. Making use of this technology, authors have [62], [68] addressed the identification of parameters used in the concrete damaged plasticity model in Abaqus. This specific model simulates loss of strength and rigidity in concrete [68]. Also using Abaqus, Chaudhari and Chakrabarti [69] presented guidelines for modeling a concrete cube utilizing the smeared crack model and concrete damaged plasticity model.

Numerical approach to behavior of woven fabrics is of interest in numerous applications. Currently no commercial-implemented model captures all important aspects of fabric behavior and is capable of predicting macroscopic and mesoscopic response of the material. The main reason is the variability of requirements for fabric models in different applications [70], [71]. Hence, ingenious solutions must be found in order to simulate the fabrics in a virtual environment. The FE model should replicate the macroscopic behavior of fabrics, which is usually nonlinear and depends strongly on the heterogeneities on the microlevel, i.e. on the structural assembly of the fibers and contact interaction between them [72].

Eischen et al. [73] addressed textile modeling to help in manufacture automation. Other authors [74]-[76] also approached textile modeling through micro-geometry of the material, reporting similarity between experimental tests and numerical results. However, micro-modeling should be treated carefully in larger models, since it is not a computational efficient approach. Boisse et al. [22] implemented macro scale parameters in their textile model, i.e. yarn hardening in uniaxial tension and biaxial behavior, to test feasibility of drawing of a given fabric into a given 3D shape.

One of the simplest approaches used to model fabrics is to homogenize the behavior of the mesostructure and approximate the fabric as an anisotropic continuum. Continuum models provide greater computational efficiency and are

easily integrated into multi-component systems [71]. A continuum approximation is shown in Figure 2.9. In another work, Boisse et al. [77] proposed a simplified numerical model of fabrics, based on results of single cell approach. Finally, [72] et al. introduced a multi-scale homogenization method for textile models, which combines a macroscopic shell with a microscopic representative volume element, connecting macro and micro scales. Homogenization of textiles may have undesirable consequences when modeling concrete composites, since interconnection of matrix layers is not possible.

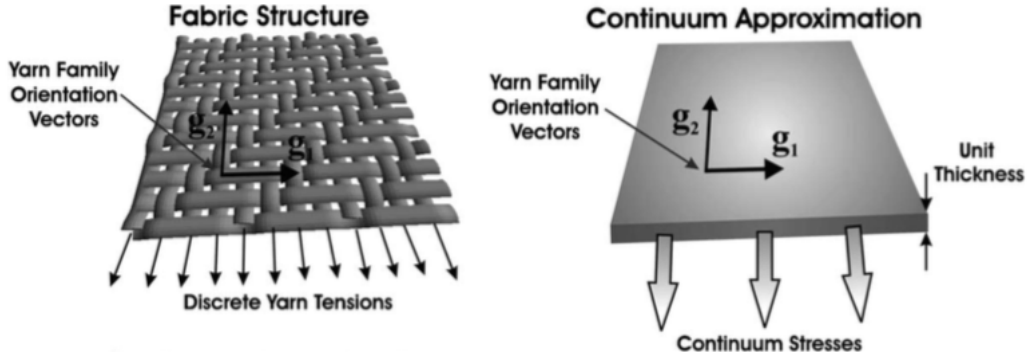

Figure 2.9: Fabric structure and continuum approximation [71].

In this work, numerical representation of the interface was accomplished with use of cohesive elements. Cohesive elements have a great number of applications and have been successfully utilized to model tensile cracks in thin film coatings [78] and crack propagation [79], [80]. Zachariah et al. [81] used spring connector elements to simulate the interface in a laminated material, a time-consuming task, since no automated method for placing these elements is available. In TRC models, researchers have used cohesive elements in interfacial modeling as well [78], [82], although other options are available [38].

Numerical models of textile reinforced concrete must capture all attributes of the material. A common approach is to unite concrete, textile and interface into one system [83], [84]. Homogenization of the phases differ according to the objectives of each study. A detailed model was proposed by Sejoha et al. [83], being capable of modeling imperfections and porosity of the matrix and geometry of the textile, whereas Azzam et al. [84] described the behavior of TRC through a simpler geometry.

Lapczyk et al. [82] modeled a fiber reinforced material in Abaqus. The

interface was described by triangular-shaped cohesive response and mesh-dependency of the system was addressed. Portal et al. [85] proposed a TRC 2D-numerical model based on experimental four-point bending test results. Although the problem was approached at macro level (contact area between textile and matrix was not measured), agreeing results were obtained. Larrinaga et al. [86] compared experimental and numerical results of basalt textile reinforced mortar, obtaining consistency of results, however, interface parameters were found to have a small impact in the behavior of the material. Salviato et al. [87] compared size effects in textile composites through intra-laminar fracture energy. The results show a remarkable size effect dependency, in agreement with the work of Bazant [88]. The works cited show a trend in numerical analysis of concrete composite materials. This research aims to understand mechanisms behind TRC behavior and reproduce them in a virtual environment. This approach allows a parametric study of the material, catalyzing its investigation.

3. Experimental Program

This chapter describes the process in which the concrete matrix was mixed, molded and cured to produce the TRC. Information regarding testing equipments, loadings and set-ups is also reported.

3.1. Material Description

Two composites were investigated in this work. Carbon-reinforced composites were analyzed in the experimental and numerical programs, whereas the basalt-reinforced composite was studied exclusively in the numerical program. Hence, a detailed description of the manufacturing method and materials of the carbon-TRC is given and the basalt-TRC components are described briefly.

The 2D carbon mesh used was the SITgrid017KB made by V. Fraas. Information listed in their data sheet states: 79 rovings per meter in both directions, 90 degree angle between warp and weft directions, cross section of 142.82 mm^2/m in both directions, 580 g/m^2, density of 1.77 g/cm^3, elastic modulus of 250 GPa and tensile strength of 4000 MPa.

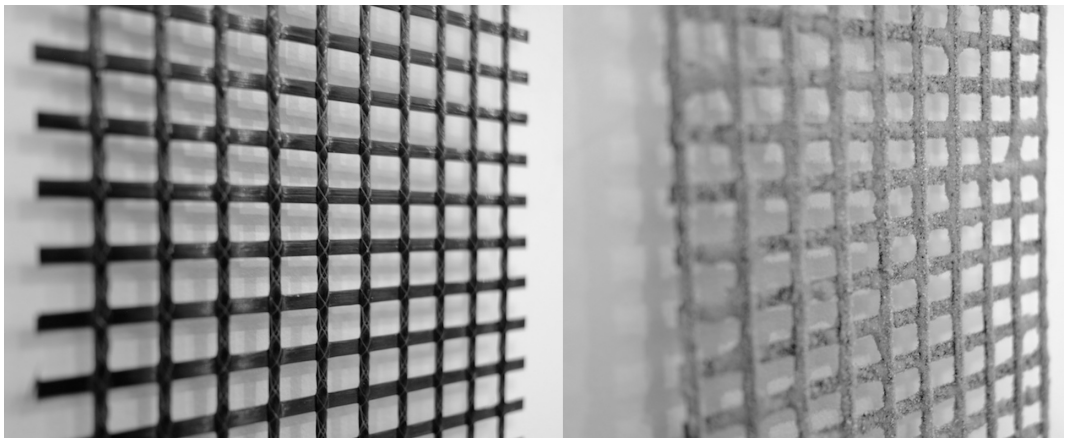

Figure 3.1: Left: plain carbon-fiber textile. Yarns' filaments were juxtaposed and weaving was not interlaced. Right: sand-coated carbon textile.

TRCs reinforced with plain and sand-coated (Figure 3.1) carbon textile were tested. Sand coating was added by hand-spreading a layer of epoxy adhesive (Sikadur®) to each side of the textile and pressing it against a sand-covered, flat surface. The material was visually inspected and sand was added to less-coated parts. No additional concern was given to the amount of sand or epoxy adhesive used. Coating lengths of 200 and 1000 mm were used: 200 mm as strengthening

factor in shear stress concentration areas (caused by gripping surfaces) and 1000 mm to study interface effects on the behavior of TRC.

Manufacture of carbon-reinforced TRC utilized a fine grained cement matrix composed of sand, cement, fly ash, microsilica, super-plasticizer and water as described in the work of Silva et al. [89]. Quantities and properties of each material are listed in Table 3.1. To facilitate mixing all materials, except the super-plasticizer, were weighted beforehand. Super plasticizer was weighted and added at the time of mixing.

Table 3.1: Weights to produce one liter of concrete.

Material	Weight g
Sand (1.18 mm)	947.0
CP2 cement	632.0
Water	284.5
Fly ash	265.0
Microsilica	50.5
Glenium (super plasticizer)	3.75 (95 drops)

The concrete was mixed at room temperature (22~30^{o}C), using a planetary mixer (Amadio, model 20LA). Firstly, all dry materials were added in order of finest to coarser, to avoid loss of the finer material. The powder was mixed for two minutes at low speed (125 RPM). In a second stage, the bowl was removed and the material manually mixed, pulling trapped grains from the bottom. With the bowl back in the mixer, the components were mixed for one minute more in low speed. Super-plasticizer was added to the water, the mixture stirred and poured into the bowl containing the dry materials. The concrete was mixed for one minute at low speed, and one minute more at medium speed (220 RPM). In the final stage, the bowl was removed and the concrete manually mixed. With the bowl back in the mixer, the concrete was stirred for one minute at high speed (450 RPM).

Still in the bowl, the concrete was set on a vibrating table for one and a half minutes to eliminate entrapped air from the mix. Due to the complexity of the molding procedure, vibrating was easier at this stage.

Flow table test, according to [90], was done to characterize the concrete. A cone with top and bottom diameters of 80 and 125 mm and 65 mm high was used and a slump of 250 mm in diameter was measured with fresh concrete, as shown in Figure 3.2.

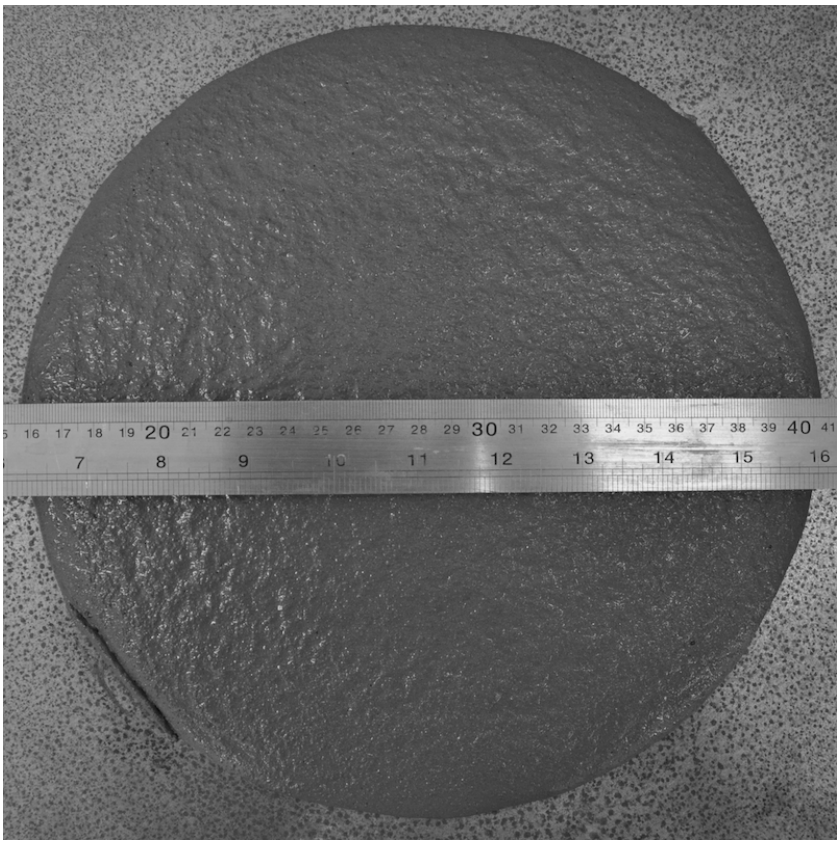

Figure 3.2: Table flow test. Diameter of 250 mm was measured.

Basalt textile reinforced concrete was produced with a calcium aluminate cement matrix. Its components, fabrication and molding processes are described in the work of Rambo et al. [91]. Calcium aluminate concrete matrix is suitable for high temperature performance, as an increase in strength is seen at 1200+^{o}C [92]. Characteristics of the basalt fibers used in this composite include corrosion in alkaline environment of the cement matrix (as do glass fibers) and lower Young's modulus than carbon fibers.

3.2. Molding, Curing and Cutting Processes

A cylindric, stainless steel formwork was used to produce test specimens for concrete compression tests. Concrete was poured into the 100 mm high by 50 mm in diameter formwork in three stages. Each stage consisted of filling one third of

the formwork's volume. Between stages, the formwork was vibrated for 30 seconds and tapped on the sides with a wooden rod, removing entrapped air from the concrete.

Rectangular TRC test specimens for uniaxial tension tests were produced in two different formworks: one made of acrylic and the other of steel. The acrylic, cuboid formwork measured 500x212 mm. Plastic spacers, measuring 5 mm in height, were used on the outside border to separate and straighten the carbon fabric sheets. Top and bottom were sealed with 8 millimeter thick acrylic plates as displayed in Figure 3.3. This formwork was used to produce the smaller (500x60 mm) test specimens.

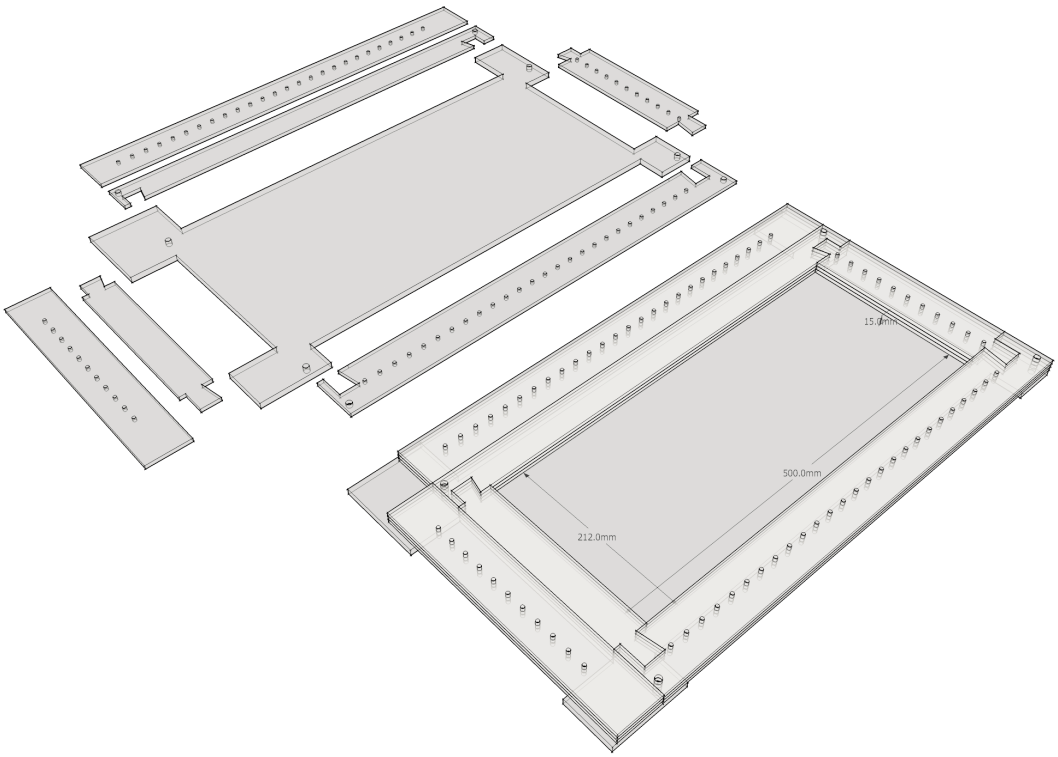

Figure 3.3: Scheme of the acrylic formwork design with three spacers positioned, used to produce 500x60x11.5 and 500x60x18 mm test specimens with one and two layers of reinforcement. Internal measures: 212 (left), 500 (middle) and 15 (right) mm.

The steel formwork (Figure 3.4) was used to manufacture larger (1000x120 mm) and smaller (500x60 mm) test specimens. A simpler design did not allow fixture of the textile on the sides of the formwork. Fabric was held at the upper and lower ends of the formwork. Spacers measuring 3 mm in height were used to separate textile layers.

The carbon fabric was cut with steel scissors. Rectangles of 600x400 and

1020x120 mm were cut to fit in both formworks. After cutting, weight was added on top of the textile sheets to reduce its curvature. The carbon fabric was then placed and aligned in the formwork.

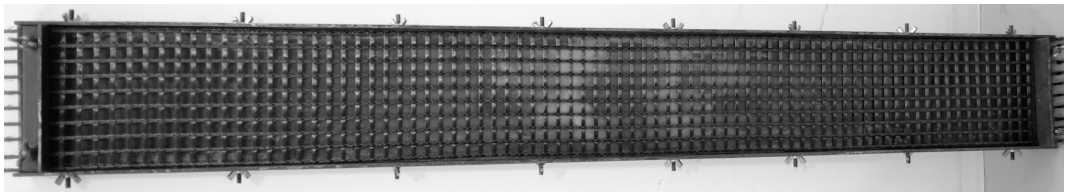

Figure 3.4: Steel formwork with textile. Used to produce 1000mm long test specimens.

Molding in the acrylic formwork consisted of producing a sandwich-like structure, composed of (in this order) acrylic base, spacer, textile, spacer, textile and spacer was built. Once in the correct place, the parts were fixed on the lower and left sides. Before fixing the right side, the carbon fabric was tensioned by hand in this direction, straightening the mesh surface. Three bolts were used on each side to hold the carbon fabric in place. The upper side was not used.

The formwork was tilted before being filled with mortar. This helped concrete flow and filling of corners. Concrete was poured onto the raised edge and lightly pressed against the carbon fabric, filling beneath and between layers of carbon textile. Transparency of the formwork permitted checking for large pores in the concrete. The top lid was not closed until the formwork was completely filled, minimizing entrapped air. After completely filled, an extra hundred milliliters of concrete was added and the top lid fixed with four bolts. At this point, exceeding mortar escaped through the upper side.

The formwork was placed vertically (longer side down) and tapped vigorously with a wooden rod. This procedure enabled better settling of the paste in the formwork without segregating water from the mixture. The vibrating table was not used because high vibrating frequencies would segregate water from the mixture, causing unwanted effects, i.e. change in water/cement ratio.

The composite rested inside the formwork for 24 hours at room temperature, in vertical position. Then, the top lid was removed and the test specimen lifted from the formwork. The end result was a flat, smooth piece of composite, measuring 500x212 mm. Height of the test specimen varied throughout its length.

Height differences of 0.5 to 2.0 mm were observed. After removed, the test specimens were cured inside a closed plastic container filled with 20 liters of water and calcium oxide mixture, at room temperature, for 27 days.

A table saw with water lubricated diamond blade was used to cut three test specimens from the larger piece. After cut, each test specimen measured 500x60 mm. Height varied according to the number of carbon sheets: ~11.5 mm for test specimens with one textile layer and ~18 mm with two layers.

A second set of test specimens was manufactured with the steel formwork. Due to differences in the formworks, molding procedures varied. In the steel formwork, concrete was weighted and poured in ~3 mm layers, as this was the dimension of the spacers. This was achieved by placing the spacers on both ends of the formwork followed by the addition of ~900g of concrete and one layer of textile. Then, two more spacers were put in place, another ~900g of concrete and a second layer of textile added. Lastly, two spacers were placed and ~900g of concrete added. In each phase, concrete was hand-pressed against the textile. A plastic film was used to seal the system for the next 24 hours. Afterwards, TRC test specimens were removed from the mold and sealed with plastic film, where they would cure, at room temperature, for 27 days. In addition to 1000x120 mm test specimens, four 500x60 mm were created by cutting the larger composite.

According to Equation (7), textile volume fraction of TS1~6, TS7~12, TS13~22 were: 4.68%, 6.16% and 9.68%.

Table 3.2: TRC test specimens specifications. Cross section is represented by X-Sc and was calculated multiplying width of test specimens by their average height.

Control	Carbon Sheets	Length mm	Free Span mm	Width mm	X-Sc. mm^2	Properties	Bolts	Torque Nm
TS1	1	500	260	60	710	plain	4	22
TS2	1	500	260	60	740	plain	4	20
TS3	1	500	260	60	700	plain	4	18
TS4	1	500	260	60	730	plain	4	16
TS5	1	500	260	60	740	plain	4	14
TS6	1	500	260	60	730	plain	4	12
TS7	2	500	260	60	1110	plain	8	12

Control	Carbon Sheets	Length mm	Free Span mm	Width mm	X-Sc. mm^2	Properties	Bolts	Torque Nm
TS8	2	500	260	60	1110	plain	8	12
TS9	2	500	260	60	1110	plain	8	12
TS10	2	500	260	60	1120	plain	8	12
TS11	2	500	260	60	1090	plain	8	12
TS12	2	500	260	60	1120	plain	8	12
TS13	2	1000	700	120	1440	plain	8	15
TS14	2	1000	700	120	1420	plain	8	15
TS15	2	1000	700	120	1460	plain	8	15
TS16	-	-	-	-	-	-	-	-
TS17	2	1000	700	120	1240	sand on edges	8	15
TS18A	2	500	260	60	750	plain	8	12
TS18B	2	500	260	60	740	plain	8	12
TS19	2	1000	700	120	1340	sand on edges	8	15
TS20	-	-	-	-	-	-	-	-
TS21	2	1000	600	120	1360	plain	8	15
TS22	2	1000	600	120	1520	sand full length	8	25

3.3. Matrix Compression Test

Ultimate compression strength and compressive Young's modulus were measured using a MTS testing system composed of a hydraulic actuator attached to a steel custom frame and data acquisition channels,. Young's modulus was measured with test specimens measuring 100 mm in height and 5 mm in diameter.

To determine Young's modulus of the cementitious matrix, four cylindric test specimens were used. They had two strain gages glued to their sides, 180^o apart and the results were calculated by averaging both measured strains. One misaligned test specimen suffered premature failure and its result was discarded. Test specimens were linearly loaded and unloaded four times, with a maximum force of 23 kN (compression) and minimum of 0 kN. Each cycle had the duration of 60 seconds. Afterwards, they were loaded from 23 kN to their ultimate compressive strength at a rate of 3.5 kN/s [93].

Ultimate compressive strength was measured with the previously described MTS equipment. A displacement rate of 0.2 mm/min was applied to the test specimens until complete rupture.

3.4. Carbon Yarn Uniaxial Tension Test

Data was obtained from the carbon-fiber textile through uniaxial tension tests. Different lengths, number of yarns, textile directions and clamping techniques were used. Tests were performed using MTS Frame Model 311.31. Fabric manufacturer data stated warp and weft yarns had cross section of 1.81 mm^2. Three weft direction samples were analyzed under an electron microscope and measured cross sections are listed in Table 3.3. Length, cross-section and clamping parameters were changed, and their effect over the mechanical behavior of the yanrs observed in the obtained results.

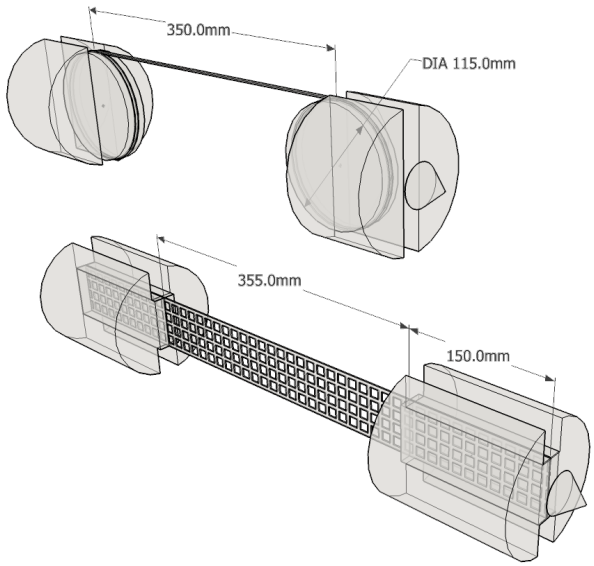

Figure 3.5: On top, the uniaxial tension test of a single yarn, utilizing the cylindric adapters. On the bottom, the uniaxial tension of the textile structure, utilizing aluminum clamps.

The initial set-up (Figure 3.5) consisted of placing each end of the test specimens in between aluminum plates measuring 150x60 mm. The plates were fitted in the holding mechanism of the MTS Hydraulic Actuator and pressed with 8.3 MPa. Test specimens containing one and four yarns (in textile structure form) were submitted to uniaxial displacement of 0.1 mm/min. The aluminum clamp would deform under pressure, creating a tailored anchorage area. Yarn failure did not occur near the clamps, indicating no shear stress concentrations on those

areas. The aluminum clamps worked well with the first tests. However, it would become unusable due to severe deformation after a few tests.

A second setup (Figure 3.5) consisted of rolling the test specimens around a cylindrical stainless steel adapter. The yarn contoured the cylinder two times and was fixed at the ends by an anchor like mechanism. The stainless steel cylinder measured 115 mm in diameter and 20 mm in height. A displacement rate of 0.1 mm/min was applied. Yarn failure did not occur on the cylinder or its proximities, implying no shear stress concentration on those areas. Due to dimensions of the cylinder, no more than one yarn could be tested at a time. Table 3.3 summarizes test specimens parameters utilized.

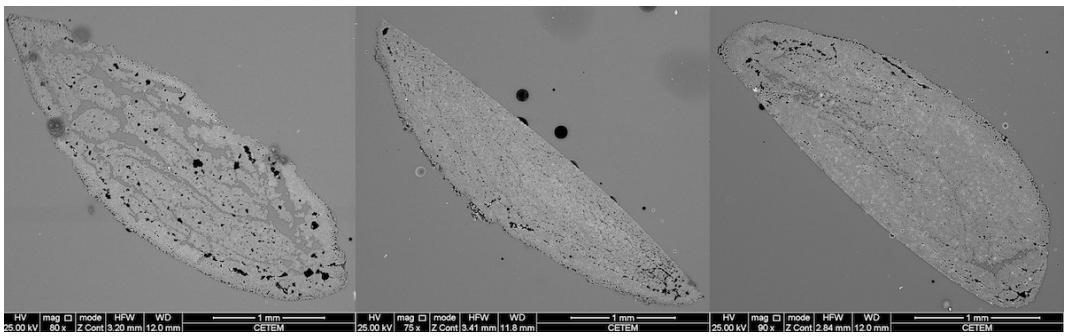

Figure 3.6: Area of carbon yarns measured by image analysis.

Cross-sectional area of carbon yarns was measured by image analysis (Figure 3.6). The test specimens were cold embedded in epoxy resin to form cylindrical blocks of 30 mm diameter and about 30 mm high. These blocks were ground and polished with diamond suspensions down to 1 μm in an automatic polishing machine following the traditional metallographic sample preparation. Cross-sections were covered with evaporated carbon to make them conductive and suitable for conventional scanning electron microscope (SEM) analysis. A SEM FEI Quanta 400 was used to acquire back-scattered electron images. This kind of image presents atomic number contrast and consequently allows the discrimination among fibers, coatings, and the epoxy resin. Image analysis was performed through an automatic routine implemented as a script in the Zeiss Axiovision software. The routine starts by segmenting fibers. It was carried out through intensity thresholding using the Otsu [94] automatic method. The average result for the weft yarns was 3.20 mm² obtained from three independent

measurements, as shown in Table 3.3.

Table 3.3: Carbon yarn test specimens.

Control	Length mm	Free Span mm	Yarns	X-Sc. mm^2	Boundary Condition	Property
CY01	2125	680	1	3.79	cylinder	weft
CY02	1795	350	1	2.84	cylinder	weft
CY03	1795	350	1	2.98	cylinder	weft
4Y01	655	355	4	12.00*	clamp	weft

* cross-section was based on other test specimens

3.5. TRC Uniaxial Tension Test

Test specimens were placed in a steel adapter, which was attached to MTS Frame Model 311.31. The adapter prevented test specimens from being crushed by the holding mechanism of the actuator. Furthermore, it enabled precise control over the pressure applied onto the test specimen and allowed freedom of movement (Figure 3.7). Two set of adapters were used: one for the 500x60 mm test specimens and a second for the 1000x120 mm. The larger adapters measured 300x160x10 mm and the smaller adapter measured 200x100x10 mm. The smaller and larger adapters held test specimens with a maximum of 8 bolts.

Test specimens measuring 500 mm long, reinforced with one carbon layer were tightened with torque between 12 and 22 Nm, according to Table 3.2. Higher values were adopted first and gradually decreased until sliding occurred. Torque selected was the last non-sliding value, aiming to minimize shear stress concentration. Test specimens containing two layers of reinforcement had eight bolts with a torque of 12 Nm holding them. Torque was measured with a torque wrench. Test specimens were positioned 120 mm inside the adapters, providing a contact area of 7500 mm^2 on each face, with a total of four faces.

Test specimens measuring 1000 mm long had two layers of reinforcement and eight bolts fixing them. Torque values (on each bolt) ranged from 15 to 25 Nm, according to Table 3.2. When sliding occurred, torque was increased in the next experiment. Anchorage length varied from 150 to 200 mm, since test specimens presented high ultimate tensile strength. These lengths provided a contact area of 18000 or 24000 mm^2 on each face.

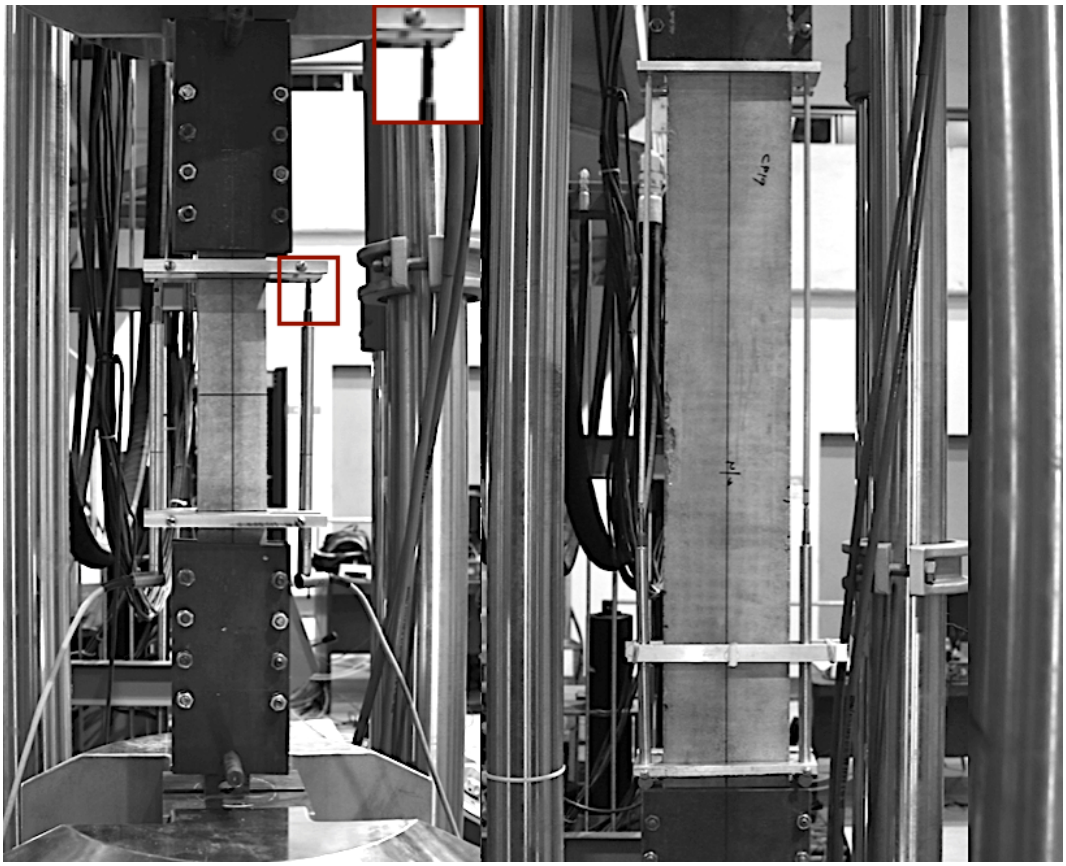

Figure 3.7: TRC uniaxial tension test set-up. Length of test specimen: 500 mm (left) and 1000 mm (right). One of the LVDT's supports is marked in red.

The top end of the adapter was positioned inside the top holding mechanism of the actuator, which was then closed with a pressure of 8.3 MPa. Afterwards, the experimental setup was aligned with a laser level. Tilting the bottom of the specimen from left to right and/or frontwards and backwards assured correct alignment with the load mechanisms. Front and side facets were checked. The bottom grip was closed with a pressure of 8.3 MPa after correctly placing test specimens into the frame. This procedure ensured minimization of shear stresses concentration (due to misalignment).

When positioned in the MTS actuator, two LVDTs (Linear Variable Displacement Transformer) were connected to the specimen, one on each side. Test specimens measuring 500 mm long had the LVDTs positioned 15 cm from the top and bottom edges with two aluminum adapters, having an initial span of 200 mm. Both adapters were tightened together, clamping the sample. One adapter held the LVDT fixed at the bottom while the other provided the upper limit for the LVDT's measuring tip, as seen in Figure 3.7.

Larger test specimens, measuring 1000x120 mm had LVDTs placed bordering the steel adapters, having identical value to the free span, according to Table 3.2. Aluminum extensions, 400 mm long, had to be built and attached to LVDTs' end to measure the longer length.

Testing consisted of controlled displacement at a rate of 0.5 mm/min. Axial force, time, displacement and both LVDT's displacement data were captured by the testing equipment for analysis. Testing was stopped when residual sliding forces were observed, usually after forty minutes. All of the described test setups followed recommendations of RILEM [95].

Uniaxial tests of basalt-reinforced TRC consisted of prescribed displacement rate of 0.1 mm/min applied to one end of the test specimens, which contained five layers of textile. Test specimens measured 1000x120x20 mm and were tested between 8 and 10 days of age. Free-span was 650 mm. Other aspects of the experimental set-up were identical to those described in the carbon-reinforced uniaxial tension tests. Dimensions of the uniaxial tension tests are shown in Figure 3.8.

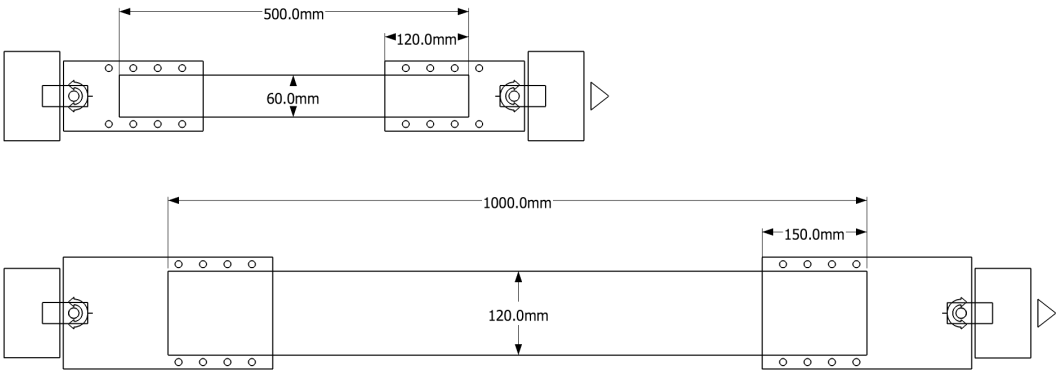

Figure 3.8: Dimensions of the composites and direction of load (indicated by the arrow).

3.6. TRC Round Panel Test

Experimental round panel tests (Figure 3.9) made on basalt-reinforced TRCs followed the recommendations of the ASTM C1550-12a [96]. Three symmetrically arranged pivots, measuring 50 mm in diameter, were placed tangent to the external radius of the test specimen while load was applied to their center. Load was applied by a MTS servo-controlled hydraulic actuator through a stainless steel ball point with a radius of 86.1 mm.

Test specimens were tested until failure under a load rate of 0.1 mm/min. The deflection response was measured using a LVDT positioned at the central part of the bottom surface of the test specimens. Crack opening in the bottom surface was measured using a triangle shaped system of three LVDTs with three equal sides of 120 mm. Test specimens measured 800 mm in diameter and 20 mm in height (Figure 3.10). Reinforcement was composed of five layers of basalt textile. Orientation of the reinforcement layers had three distinct directions, i.e. warp yarns: 0^o, 60^o, 120^o; weft yarns: 90^o, 150^o, 210^o.

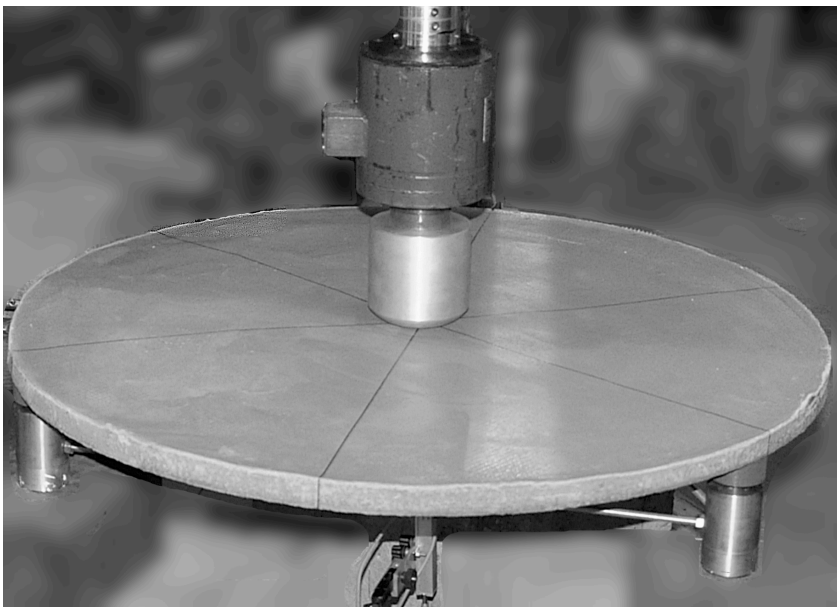

Figure 3.9: Round panel test experimental set-up. Deflection response was measured with the LVDT in the center of the bottom surface.

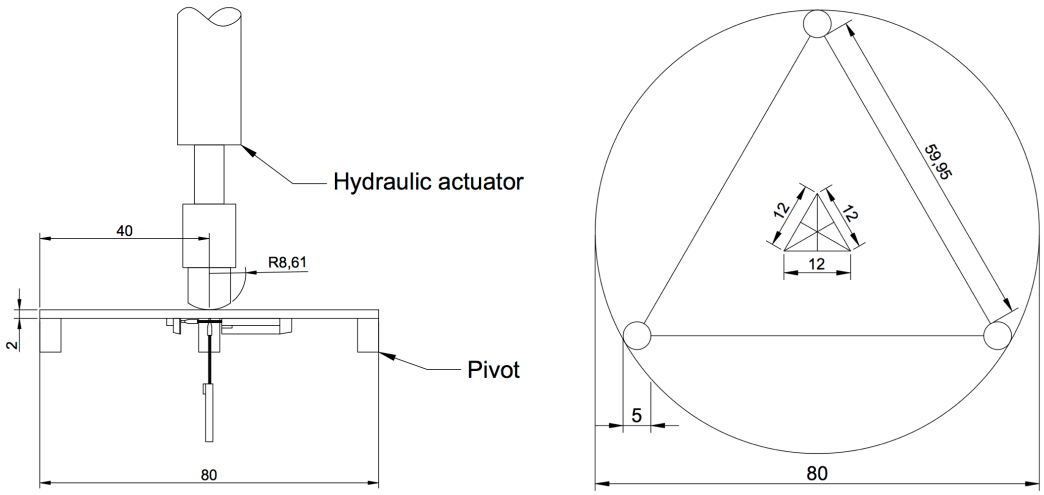

Figure 3.10: Schematics of the round panel test. The triangle in the center of the disc indicates the presence of three LVDTs. Distances are shown in centimeters.

4. Experimental Results and Analysis

Tensile stresses were calculated dividing the reaction force by the cross section of test specimens, hence a uniform stress field was assumed throughout the entire length of the test specimens. An uniform stress field is a realistic approach when observing points far from the load, as the Saint-Venant's principle states. However, once points observed move closer to boundary conditions, this hypothesis is no longer valid. Displacement was measured through the displacement acquisition channel of the actuator.

4.1. Matrix of Carbon Reinforced TRC

The matrix average ultimate compressive strength was 75 MPa. Hysteresis of concrete stress-strain curve shows $\Delta(\sigma)$ equals to 10.2MPa and $\Delta(\varepsilon)$ equals to 285μm/m, resulting in a Young's modulus of 35.79 GPa for the concrete matrix under uniaxial compression.

Ultimate tensile strength and Young's modulus of the matrix were obtained through analysis of the TRC uniaxial tension experiments. Test specimens TS08~12 were chosen due to smaller textile volume fraction, larger cross section and overall quality. Stress-strain curves of the initial loading of these specimens is shown in Figure 4.1a. An average Young's modulus of 5.88 GPa was observed for the concrete matrix under uniaxial tension. The measured average ultimate tensile strength was 3.15 MPa.

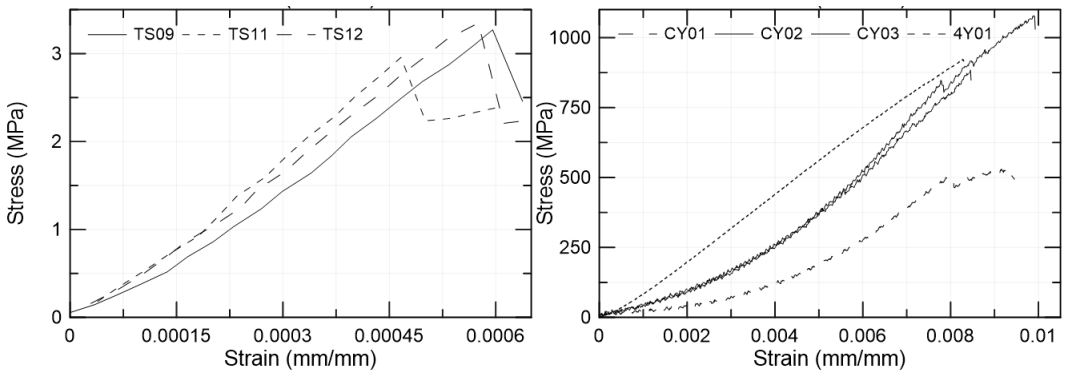

Figure 4.1: On the left, (a) zoom in the matrix behavior. An average Young's modulus of 5.88 GPa and ultimate tensile strength of 3.125 MPa was measured. On the right, (b) stress-strain curves obtained from the carbon textile uniaxial tension tests. Yarn length affects the hardening behavior.

4.2. Carbon Textile

Carbon textile was tested under uniaxial tension in two configurations:

single yarn and in textile structure. Two different approaches in boundary conditions were taken. The textile structure was held with aluminum plates and single yarns with cylindric, stainless steel adapters. Strain was measured utilizing the free-span in the textile structure setup, whereas total length was used to measure strain in the single yarn tests.

The results show a hardening stress-strain curve, agreeing with the literature [47], [97], [98]. Length dependency can be assumed, phenomenon displayed in Figure 4.1b. Longer test specimens presented a slower hardening behavior whereas shorter test specimens showed faster hardening. Results in the literature show faster hardening in larger gauge lengths [47]. Difference in results was associated to data acquisition method. Here, displacement data was gathered directly by the hydraulic actuator LVDT while other works utilize strain gages attached to the yarns to capture strain data.

Ultimate tensile strength results do not correspond with the weakest link theory and the work of Moreton [99]: the shortest test specimen did not present the strongest failure-stress. This could be attributed to an ill-formed textile test specimen, damage caused to a test specimen during manipulation or different cross section of yarns. However, the most probable cause was the difference in the holding mechanisms that was used in the present work.

4.3. Carbon Reinforced TRC Tensile Behavior

The experimental program of carbon-reinforced TRC presented here is focused at studying the behavior of the material under uniaxial tension. Fabrication method, size, bond strength and volume fraction of fibers are analyzed.

TS1-6 (acrylic formwork, 1 layer of reinforcement, 500x60 mm): The three states of loading can be seen in Figure 4.2a. Matrix was loaded until failure, under tensile stress varying from 2.5 to 3.5 MPa. Then, cracking began. Few failure zones are observed throughout the curve, represented by the abrupt decreases of stress. The observed behavior was consequence of poor bond strength, caused by small volume fraction of textile and manufacture method. Most test specimens presented two to three cracks. Usually near the ends of the composite. Stabilized crack pattern was observed from 0.02 strain until maximum tensile strength was

reached, raging from 3.5 to 5.5 MPa. Slow strain-hardening behavior confirmed poor bond strength. Next, the textile reinforcement slid from the matrix and caused complete failure of the material near one of the holding mechanisms. The fractured composite is shown in Figure 4.2b.

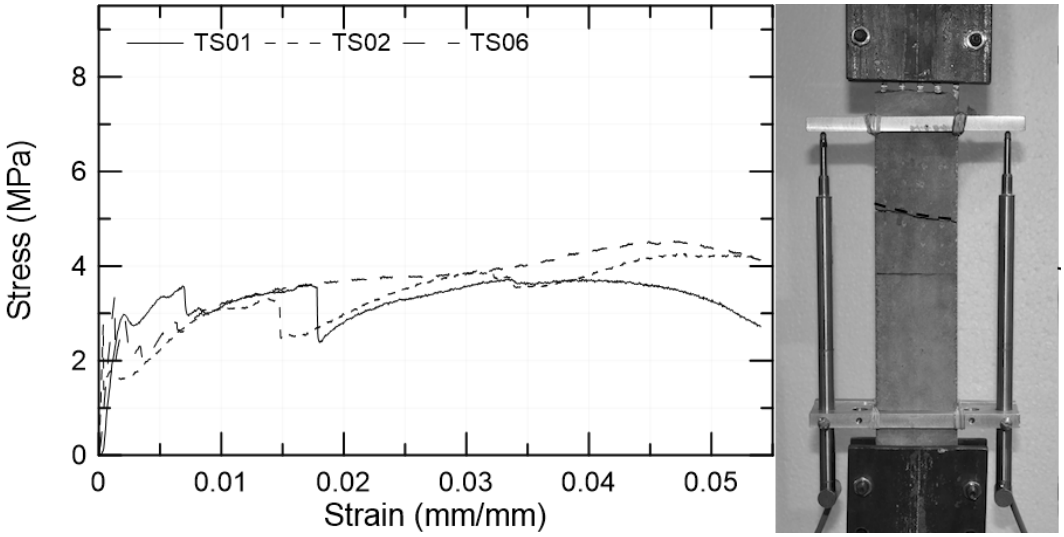

Figure 4.2: (a) Stress-strain curve for TRCs reinforced with one layer of carbon fabric, molded in the acrylic formwork. Specimen dimensions were 500x60x12 mm. (b) Photo of TS1 after the uniaxial tension test. Failure occurred near the top holding mechanisms and one crack was formed slightly above the center (the faded line in the center was drawn with a pen).

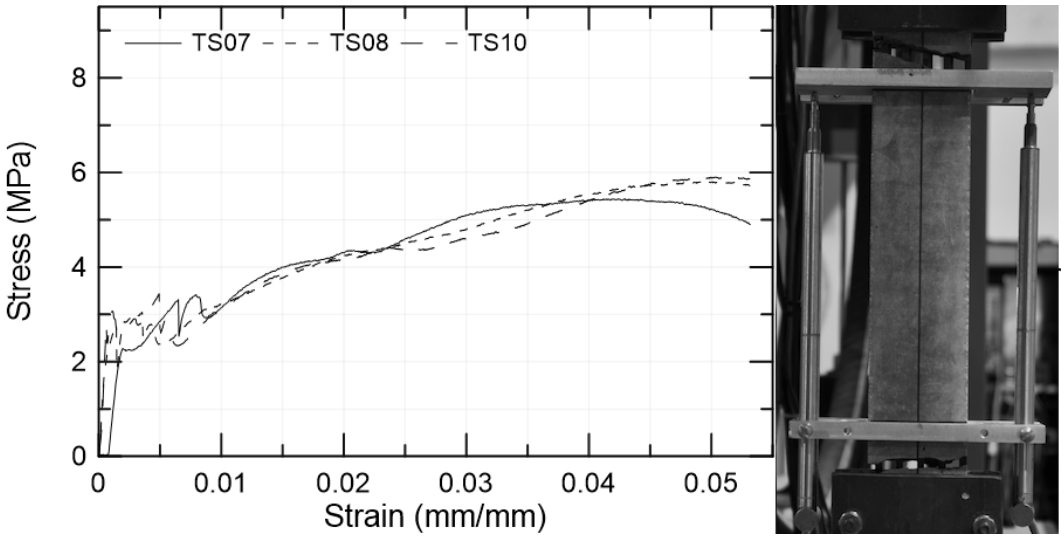

Figure 4.3: (a) Stress-strain curve for TRCs reinforced with two layers of carbon fabric, molded in the acrylic formwork. Specimen dimensions were 500x60x18.5 mm. (b) Photo of TS10 after the uniaxial tension test. Failure occurred exclusively near the holding mechanisms.

TS7-12 (acrylic formwork, 2 layers of reinforcement, 500x60 mm): In the first state, matrix was loaded until tensile failure, which occurred between 2.5 and 3.0 MPa. The cracking state followed. Sudden decreases of stress represent the

few cracks formed in the composites. The small number of failure zones was consequence of poor bond strength, caused by small volume fraction of textile and manufacture method. Most test specimens presented two cracks, always near the ends of the composite. Stabilized crack pattern was observed from 0.01 strain until maximum tensile strength was reached, raging from 5.5 to 6.0 MPa. Slow strain-hardening behavior confirmed poor bond strength. Sliding of the textile began at 0.045~0.050 strain and caused complete failure of the material near one of the holding mechanisms. The described stress-strain curve is shown in Figure 4.3a and the fractured composite is displayed in Figure 4.3b.

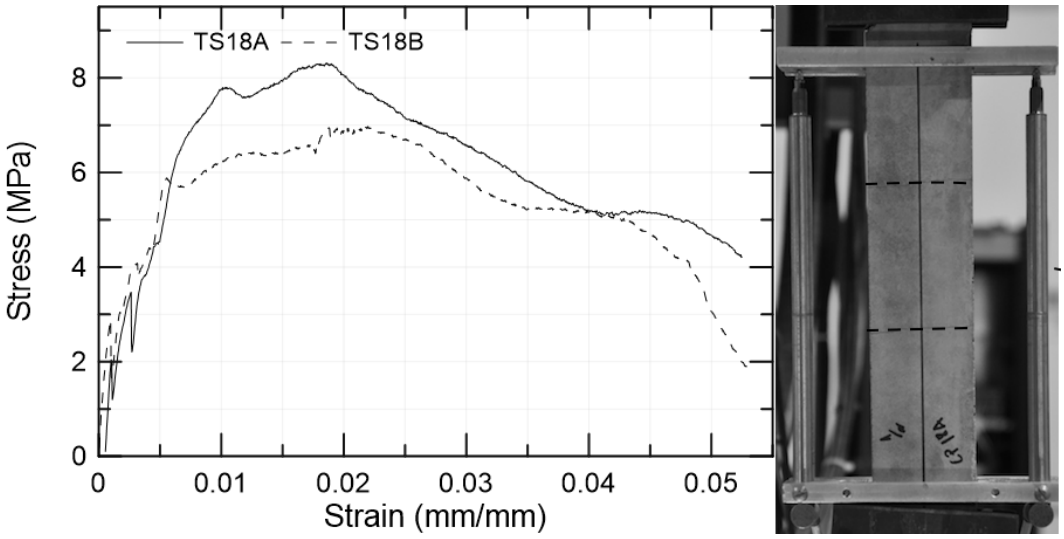

Figure 4.4: (a) Stress-strain curve for TRCs reinforced with two layers of carbon fabric, molded in the steel formwork. Specimen dimensions were 500x60x12.4 mm. (b) Photo of TS18A after the uniaxial tension test.

TS18A,B (steel formwork, 2 layers of reinforcement, 500x60 mm): First crack of the matrix occurred in the range of 2 to 3 MPa, followed by the quick formation of three additional cracks. In both test specimens two cracks were formed in the vicinity of the holding mechanisms and the other two in the center of the composite, indicating good bond strength. Stabilized crack pattern was observed from 0.005 to 0.02 strain, during a fast strain-hardening behavior until the maximum tensile strength was reached (7~8.3 MPa). Next, sliding of the textile reinforcement began, represented by the softening branch of the stress-strain curve (Figure 4.4a). Lastly, complete failure of the material was observed near one of the fixing adapters. A total of 2 cracks were observed in the free-span of the composite, resulting in an average crack-spacing of 130 mm

(Figure 4.4b).

TS14-15 (steel formwork, 2 layers of reinforcement, 1000x120 mm): In the first state, the matrix was loaded until its ultimate tensile strength, ranging from 1.8 to 2.2 MPa. Next, multiple cracking occurred, ranging from 0.0005 to 0.0035 strain and represented by the saw-shaped branch of the stress-strain curve (Figure 4.5a). Multiple cracking behavior indicated an efficient stress transfer mechanism through well bonded materials, consequence of increased volume fraction of reinforcement and manufacture method. Stabilized crack pattern was observed from 0.0035 until 0.015 strain. Once the ultimate tensile strength of the composite was reached, sliding of the textile reinforcement was observed, which resulted in complete failure of the material. A total of 10 cracks were observed, resulting in an average crack-spacing of 70 mm (Figure 4.5b).

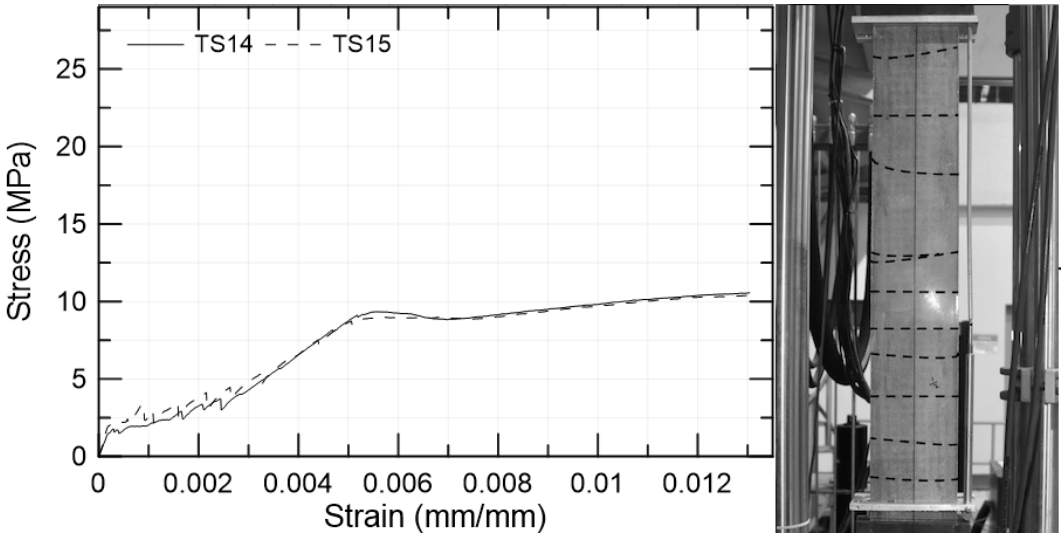

Figure 4.5: (a) Stress-strain curve for TRCs reinforced with two layers of carbon fabric, molded in the steel formwork. Specimen dimensions were 1000x120x12 mm. (b) Photo of TS14 after the uniaxial tension test.

TS22 (steel formwork, 2 layers of sand-coated reinforcement, 1000x120 mm): The three states of loading can be clearly seen in Figure 4.6a. Matrix was loaded until failure, under tensile stress of 2.5 MPa. Then, multiple cracking began. A great number of failure zones is observed throughout the curve, represented by the saw-shaped branch of the stress-strain curve. The observed behavior was consequence of an excellent bond strength, caused by coating of the textile, increased volume fraction of reinforcement and manufacture method. Stabilized crack pattern was observed from 0.002 strain until maximum tensile

strength of 25 MPa was reached. Fast and homogeneous strain-hardening behavior confirmed great bond strength. Next, the composite slid from the holding mechanism, ending the test. A total of 22 cracks were observed in the 600 mm span of the composite, resulting in an average crack-spacing of 27.3 mm. The fractured composite is shown in Figure 4.6b.

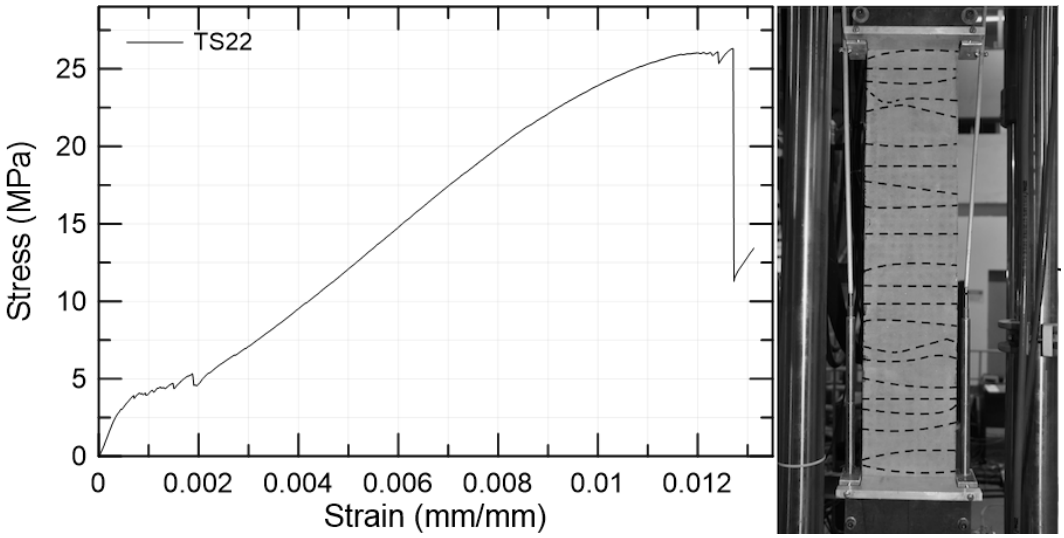

Figure 4.6: (a) Stress-strain curve for TRCs reinforced with two layers of sand-coated carbon fabric, molded in the steel formwork. Specimen dimensions were 1000x120x10.7 mm. Curves show stress-strain behavior until slippage of the test specimens occurred due to insufficient torque on the clamping mechanism. (b) Photo of TS22 after the uniaxial tension test.

Three sets of 500 mm long test specimens were manufactured. Two were produced in the acrylic formwork with 1 and 2 layers of reinforcement, and the third in the steel formwork with 2 layers of reinforcement. Differences between results were seen in post cracking behavior and maximum tensile strength. Both were related to stress-transfer mechanisms in the composite. Stronger bond strength was observed in the test specimens molded in the steel formwork, which had hand-pressed concrete and higher textile volume fraction. Test specimens produced with the acrylic formwork had the concrete simply vibrated during the manufacture process. Hand-pressing the textile produced a less-straightened surface inside the matrix, creating a larger bond surface and faster load-coupling of the textile. Peled et al. [37] reported faster load-coupling in stronger-bonded textiles (2 mm loop vs. 4 mm loop) and dependency of bond strengths on fabrication method of TRCs [36]. Curing conditions may have some effects as well, but those are not discussed here.

Size effect in the composite affected the number of cracks, crack-spacing and change in ultimate tensile stress (Figure 4.7). Larger crack-spacing was observed in the 500 mm long test specimens. A more heterogeneous stress field was observed in smaller test specimens, which caused localized failure. Areas of stress concentration failed first, and, although load was transferred through the phases of the composite, higher, localized stresses caused crack growth rather than multiple cracking. Larger crack-spacing observed in the 500 mm long test specimens confirmed this hypothesis.

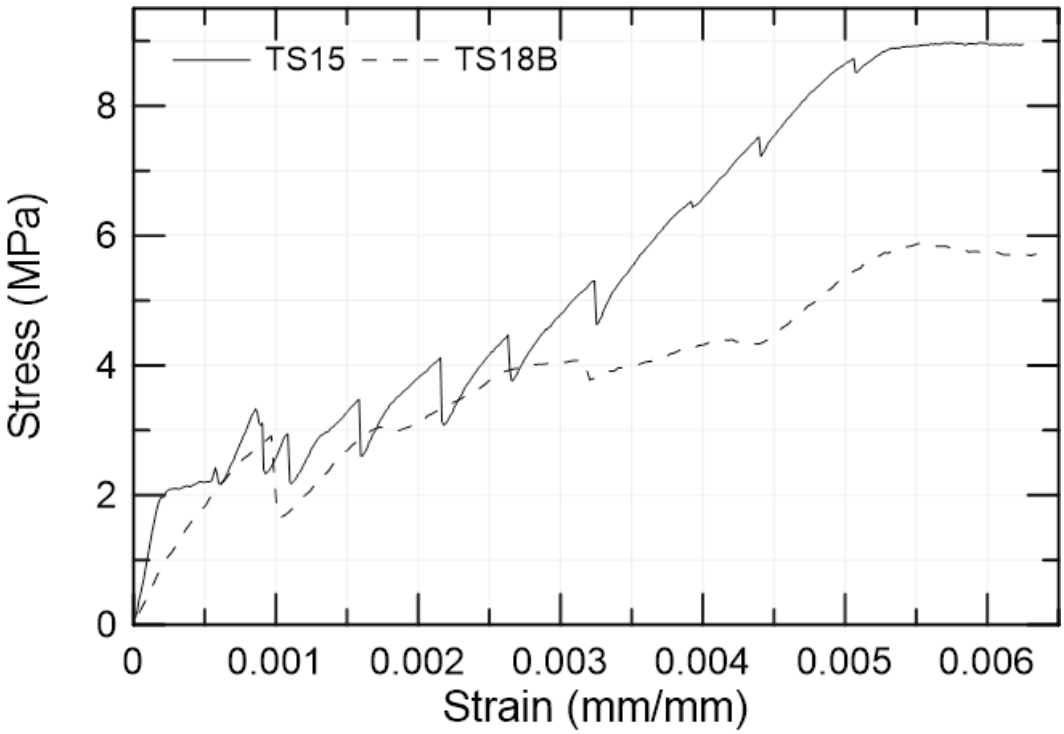

Figure 4.7: Size comparison of test specimens: TS15 (1000x120 mm) versus TS18B (500x60 mm).

Comparison of TRCs reinforced with plain and sand-coated carbon textile refers to mechanisms of bonding. Interface rigidity was not affected, as Young's modulus in the post-cracking branch of the stress-strain curves are extremely similar for both TS14 and TS22 (shown in Figure 4.8a). However, interface shear strength of the sand-coated reinforced TRC was higher, since smaller crack-spacing and higher ultimate tensile strength were observed. Crack-spacing was directly affected by shear strength of the interface, as represented by Equation (5) and discussed in Section 2.3. The results observed in the experimental program agree with results from the literature [11], [37]. The plain-coated test

specimen presented an average crack-spacing of 70.0 mm and the sand-coated specimen presented an average crack-spacing of 27.3 mm. Results are shown in Figures 4.8a-c.

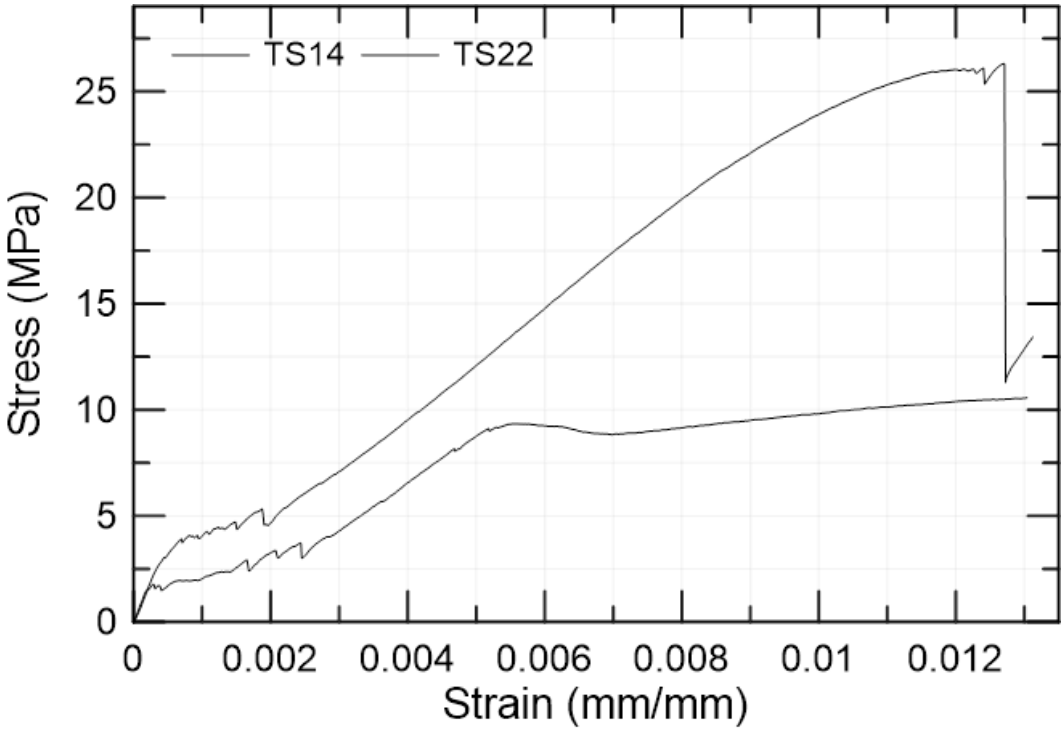

Figure 4.8a: Interface comparison between plain and sand coated carbon-reinforced TRC. Plain textile is displayed in the lower curve (TS14) with ultimate tensile strength of ~10 Mpa. Sand-coated reinforcement was used in TS22, reaching an ultimate tensile strength of ~25 MPa. Significant decrease in stress observed in TS22 in due to slippage of the composite from the holding mechanism, not failure of the material.

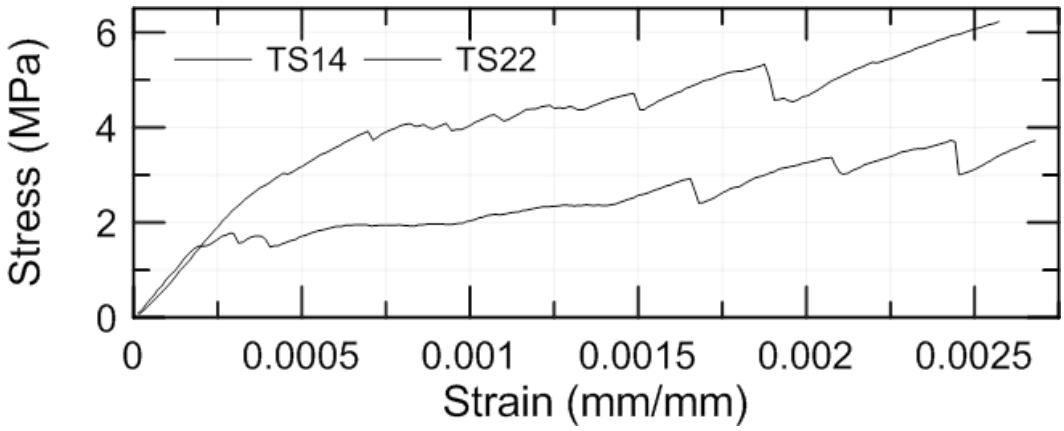

Figure 4.8b: Stress-strain curve of TS14 (lower curve) and TS22 (upper curve) during multiple cracking.

Figure 4.8c: On the left, crack-spacing after uniaxial tension test of TS14 (plain-coated carbon textile) and, on the right, crack-spacing after uniaxial tension test of TS22 (sand-coated carbon textile).

5. Numerical Modeling of TRC in Abaqus

Numerical modeling is a powerful tool for the simulation of materials in all levels of observation. However, caution is necessary to correctly model the problem. This work approaches TRC modeling as single materials: matrix, textile and interface, which are coupled. Matrix calibration was done individually at an initial stage. Textile and interface were added afterwards. During the modeling process, the Abaqus manual version 6.14 [100] was consulted and proved to be a substantial source of information. All parameters listed in this section are explicitly described in the Appendix I: Lua Code and Appendix II: Fortran Routine through commented sections in the code.

Several authors have studied concrete-composite materials with assist of numerical simulation tools [82], [85]-[87], [101]-[103]. However, detailed models or modeling guidelines are scarcely found. In this section, modeling steps utilized in Abaqus are explained in detail.

5.1. Matrix

Concrete model used in Abaqus was *Concrete Damaged Plasticity* and its constitutive behavior is presented in Figure 5.1. This model is designed for applications in which concrete is subjected to monotonic, cyclic, and/or dynamic loading under low confining pressures and can be used to describe the mechanical behavior of plain concrete. The model has two failure mechanisms, i.e. tensile cracking and compressive crushing. Strains in compression and tension are divided into elastic and plastic.

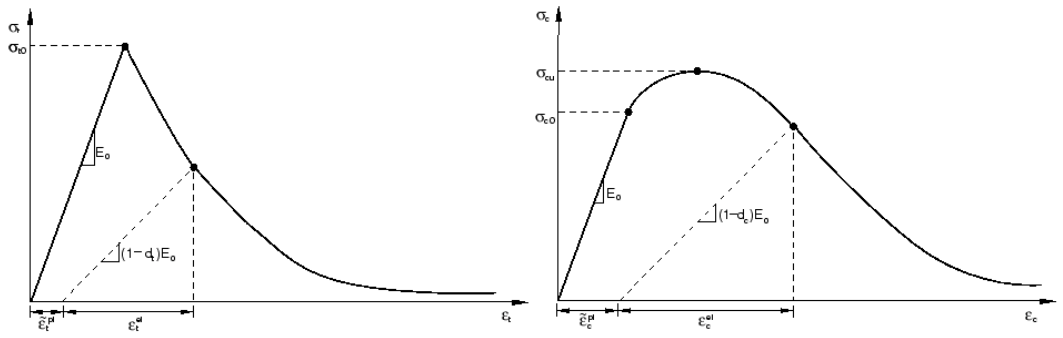

Figure 5.1: Concrete damage plasticity model. On the left, the mechanical behavior of concrete under tensile load is shown. On the right, the behavior of concrete under compression. Taken from Abaqus manual [100].

Plastic strain is utilized to describe damage evolution through softening of concrete, under the *Concrete Compression Damage* or *Concrete Tension Damage* options. Decrease of Young's modulus as function of plastic strain is displayed in Figures 5.1 and 5.2. These options aim to reproduce the mechanical behavior of concrete in cyclical loadings, or where the material is subjected to stresses after plasticity has occurred. Unfortunately, these parameters were not measured in the experimental program and damage parameters for concrete were left blank, meaning that loss in rigidity was not represented. However ultimate tensile strength was lowered after failure.

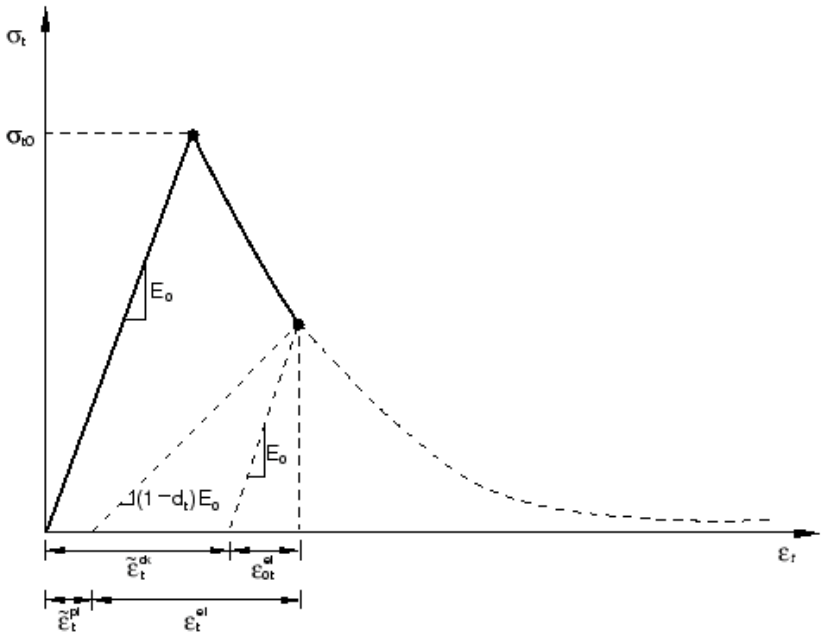

Figure 5.2: Concrete tension stiffening and damage. Taken from Abaqus manual [100].

Tension stiffening was associated with displacement due to reasons discussed in Section 2.3. Post-failure behavior is described as function of the cracking displacement, defined as the total displacement minus the elastic displacement. In the simulations of this work, elastic displacement is present until the maximum tensile strength is reached. Then, tabular data is entered to describe maximum tensile strength as a function of cracking displacements. A detailed description of the concrete model used is found in the Abaqus user manual [100], in Section 22.6.3: Concrete damaged plasticity.

The behavior of the concrete elements under compression was represented as linear elastic, i.e. no damage or change in stiffness were added. This decision

was based on the nature of concrete failure. Here, it is assumed that even in uniaxial compression, concrete failure is a consequence of concentrated tensile stresses in the heterogeneous structure of the material, as discussed in [54]. This decision is also justified by the nature of the tests performed (uniaxial tensile tests and round panel tests), on which failure is caused by tensile stresses.

5.2. Textile

Textile was added as an isotropic, plain linear elastic material in the first models. This was an intuitive, simple approach. However, it neglected complex behavior of textile as textile crimp and load-activation of filaments. A second approach was made associating Young's modulus of the textile to simulation time. The objective was to reproduce the hardening behavior of the material as the prescribed displacement increased, seen in Figure 4.1b. This model was capable of generating multiple cracking behavior in the first loading steps. Yet, load transfer from high-stressed to lower-stressed areas was not correct since Young's modulus of textile was constant throughout the entire length of the composite.

The two first textile models adopted made clear that a third, more realistic textile model should be used. Correct stress distribution among the phases of the composite would only be achieved if the behavior of the textile was strain-dependent, assuring higher Young's modulus in the vicinity of failure zones, and lower Young's modulus in undamaged parts of the matrix. The strain-dependency was added to the model through a Fortran Routine, shown in Appendix II: Fortran Routine. The Fortran Routine sets the Young's modulus of the textile according to the strain observed in each gauss point of the model.

Abaqus reads the Fortran Routine when solving the numerical model, as it is not part of the model itself. Young's modulus of textile is set at run time by a user defined table in the code. Abaqus expects the **USER MATERIAL* keyword in the model description to correctly assign the values present in the Fortran Routine to the material. Value updating is done through a step function.

5.3. Interface

Cohesive elements were chosen to reproduce the interface. The Abaqus manual [100] states cohesive elements are suitable to model adhesives between

two components and to model interfacial debonding. Constitutive response of cohesive elements using traction separation and linear failure is shown in Figure 5.3. Resemblance with the bond constitutive model, displayed in Figure 2.5, can be observed. Cohesive elements allow the combination of several damage mechanisms, each consisting of three parameters: damage initiation criterion, damage evolution law, and a choice of element removal upon reaching a completely damaged state.

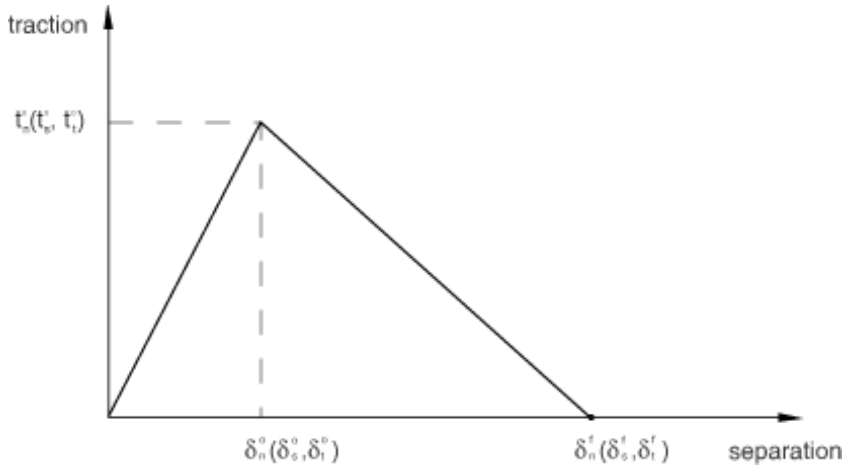

Figure 5.3: Typical traction separation response of cohesive elements. Taken from Abaqus manual [100].

Cohesive elements present a linear response until the damage initiation criterion is reached. After this point, damage occurs and behavior is defined through a damage evolution law. Damage is assumed to initiate when the maximum nominal stress ratio reaches the value of one, according to Equation (9). Alternatively, a strain-based damage criterion can be established, following the same rule.

$$\max\left\{\frac{\langle t_n \rangle}{t_n^0}, \frac{\langle t_s \rangle}{t_s^0}, \frac{\langle t_t \rangle}{t_t^0}\right\} = 1 \tag{9}$$

t_n, t_s and t_t are defined through the nominal stresses, accessed in the *Maxs Damage* option in *Edit Material* window.

Damage evolution was set to linear softening, based on displacement. This failure criterion receives one parameter: effective displacement at complete failure. Strength of the material linearly decreases from its maximum strength to

zero in this length interval. Additionally exponential softening or tabular data can be used to model bond behavior after failure initiation.

5.4. TRC Uniaxial Tension Model

The composite material model merges information of the cementitious matrix, textile and interface. When correctly calibrated, it should be capable of describing the results observed in the experimental tests. The TRC model is composed by a sandwich-like structure, generated through the Lua code. The user defines basic characteristics: number of reinforcement layers, height of each material, width and depth of the composite, material properties and number of nodes in the *x* and *y* directions. From these parameters, the code creates the nodes and elements of the model and assigns the corresponding material properties. The nodes are equally spaced in the *x* and *y* directions and depend on the height of each layer in the *z* direction. This arrangement creates a model more similar to a laminar composite than a TRC structure, since matrix layers are not interconnected. The code positions the layers in a specific order, as displayed in Figure 5.4. The matrix-matrix-interface-textile-interface arrangement is repeated from one to the number of textile layers. At the end, two layers of matrix are added to complete the TRC finite elements model. The mechanical attributes of the layers are then assigned as described in Sections 5.1, 5.2 and 5.3.

The Lua code includes parameters to set the number of steps and load incrementation for each step. In the code in Appendix I, those are configured to replicate the experimental program, at a rate of 0.5 mm/min during an estimated time of 20~40 minutes. Boundary conditions are set according to the length inputed by the user. The code calculates the number of nodes present in the defined length on the left and right ends of the model. The nodes on the left end are fixed in all directions and those on the right end have the prescribed displacement applied in the *x* direction. The mechanical response of the model is then visualized as a set of changing parameters over time. These parameters are defined by the user through the **OUTPUT* keyword. Node, element and contact parameters are available for saving. The complete FE model is shown in Figure 5.5.

The solver options include a series of parameters and are set by the user.

These values have a profound impact in convergence of the result and run-time of the model. The mechanical response of TRC includes a series of non-linear phenomena, i.e. multiple cracking. Therefore, low values should be assigned for initial, minimum and maximum increments and the maximum number of iterations should have a high value.

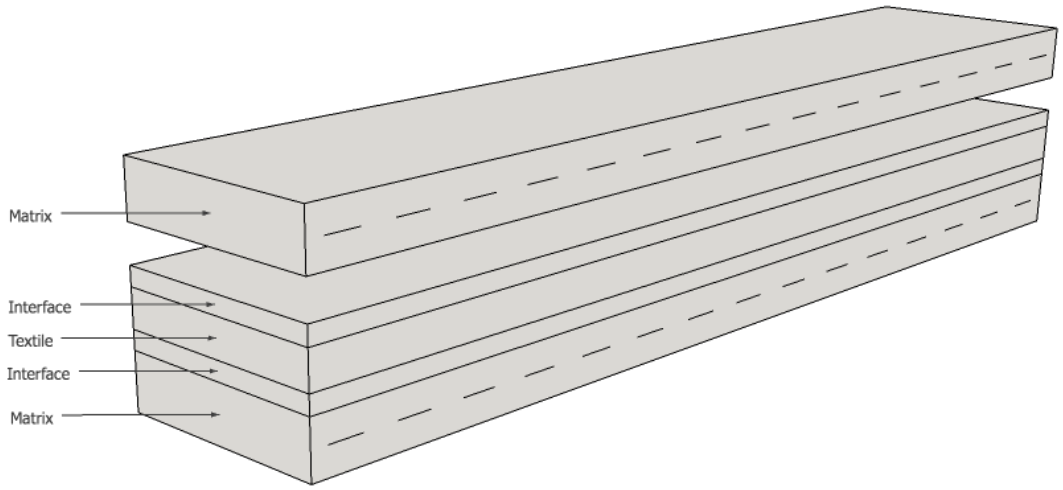

Figure 5.4: Repetition pattern of layer arrangement. Dashed lines represent the borders between the two layers of matrix elements.

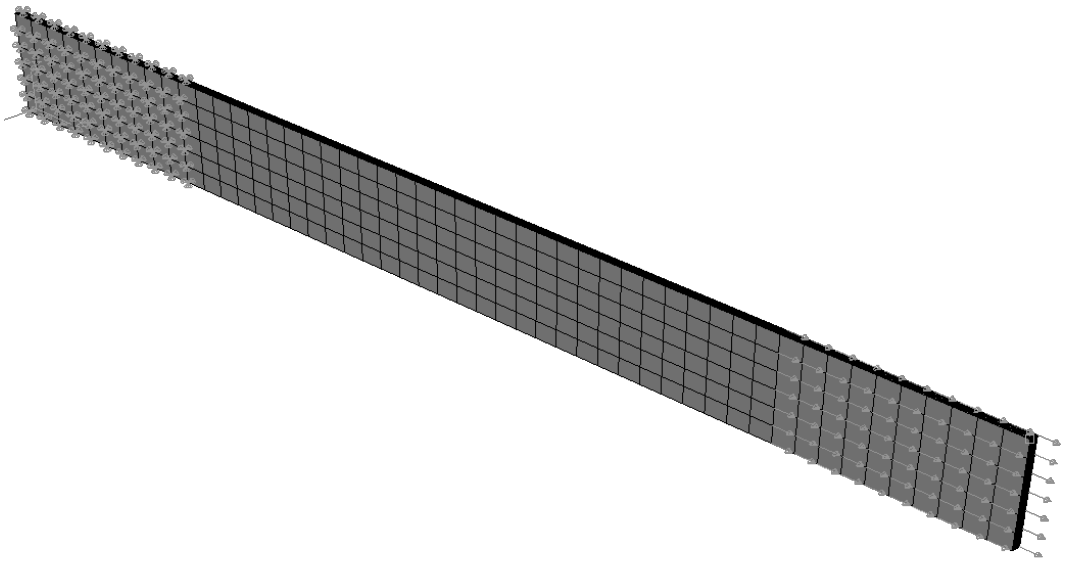

Figure 5.5: Abaqus model of uniaxial tension test. Surface nodes on the left end are fixed while a prescribed displacement is applied to surfaces nodes on the right end. Length of boundary condition is defined through the *bc* variable in the Lua code.

5.5. TRC Round Panel Model

The mesh of the round panel was manually created in a spreadsheet. A cylindric structure, measuring 400 mm in radius and 20 mm in height was divided: its radius into 20 mm segments, separated by 10^{o} angles and its height

into 27 layers, i.e. 12 layers of matrix, 10 of interface and 5 of textile. Thus, each layer contained 720 elements and the whole model contained 19440 elements. The layer arrangement followed the pattern described in Figure 5.4. All elements were represented by linear hexahedral elements (8 nodes) and the geometry of all materials (i.e. matrix, textile and interface) was the same.

Prescribed displacement was applied in the *-z* direction to the top surface of a cylindric structure with 100 mm diameter and a ball-point (r=86.1 mm) at one end. Three support elements (r=380~400 mm), separated by 120º angles, were added to the bottom surface of the system (*z=0*) and their lower surface was fixed (*x*, *y* and *z* directions). Therefore, the supporting elements did not represent correctly the behavior of the pivots present on the experimental round panel test. The described system is shown in Figure 5.6.

In uniaxial tension models, textile hardening behavior depended on strain in the *x* direction and the textile was considered isotropic. This approach was acceptable, since stress and strain components in the *x* direction greatly exceeded components in other directions. However, when modeling the round panel, stress and strain components are present in all directions. Therefore, the textile was altered to simulate an anisotropic material (through its stiffness matrix, **D**, shown below) and its hardening behavior was set to increase with strain magnitude of the *xx* and *yy* directions (i.e. $\sqrt{\varepsilon_{xx}^2+\varepsilon_{yy}^2}$).

$$\mathbf{D}=\frac{1}{k}\cdot\begin{pmatrix} E\cdot(1-\nu_{23}^2) & E\cdot(\nu_{13}\nu_{23}+\nu_{12}) & E\cdot(\nu_{12}\nu_{23}+\nu_{13}) & 0 & 0 & 0 \\ E\cdot(\nu_{13}\nu_{23}+\nu_{12}) & E\cdot(1-\nu_{13}^2) & E\cdot(\nu_{12}\nu_{13}+\nu_{23}) & 0 & 0 & 0 \\ E\cdot(\nu_{12}\nu_{23}+\nu_{13}) & E\cdot(\nu_{12}\nu_{13}+\nu_{23}) & E\cdot(1-\nu_{12}^2) & 0 & 0 & 0 \\ 0 & 0 & 0 & k\cdot G_{23} & 0 & 0 \\ 0 & 0 & 0 & 0 & k\cdot G_{13} & 0 \\ 0 & 0 & 0 & 0 & 0 & k\cdot G_{12} \end{pmatrix}$$

Where $k=1-(\nu_{12})^2-(\nu_{13})^2-(\nu_{23})^2-2\cdot(\nu_{12}\nu_{13}\nu_{23})$, $E=E_1=E_2=E_3$ and $G=E/(2\cdot(1+\nu))$. Utilizing the shear modulus of the textile caused convergence problems. The value was altered to a linear interpolation between the shear modulus of the textile and matrix, according to Equation (10), which improved convergence and can be understood as a physical degradation of the matrix and the textile becomes slowly

tensioned.

$$G = \left(E_{tex} \Big/ E_{tex}^{\max} \right) \cdot G_{tex} + \left(1 - E_{tex} \Big/ E_{tex}^{\max} \right) \cdot G_{matrix} \tag{10}$$

In Equation (10) E_{tex} is the current Young's Modulus of the textile, E_{tex}^{max} the maximum Young's modulus of the textile, G_{matrix} and G_{tex} are the shear modulus of the matrix and textile. All parameters listed are user defined in the Fortran Routine or Lua Code. This approach failed to capture warp and weft yarn interaction and presumed the biaxial behavior of the textile to be identical to the uniaxial behavior of its yarns.

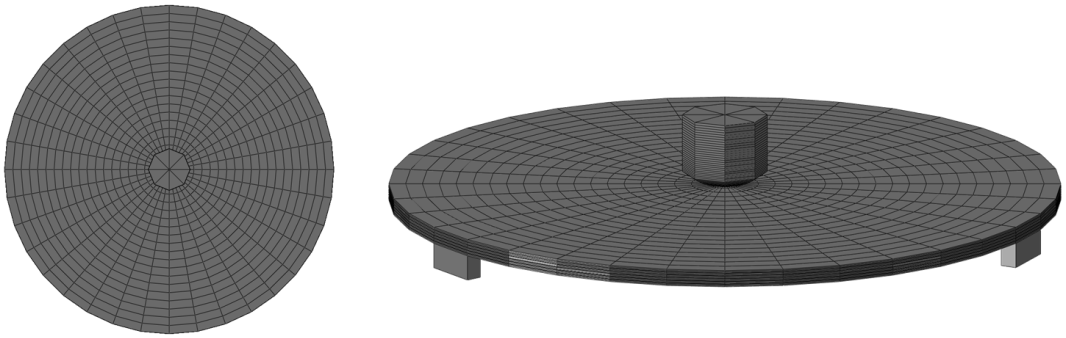

Figure 5.6: Abaqus model of round panel test. The lower surface of the three supports were fixed (*x*, *y* and *z*) and all nodes of the punch were fixed (*x* and *y* directions) while displacement was applied (-*z* direction) to nodes on its top surface.

6. Numerical Results

Numerical simulation of TRC was made in phases. Concrete matrix and textile were modeled independently. Later, the interface was added and calibrated in conjunction to the previously modeled materials. Methodology of the calibration and comparison with experimental results are addressed in this section.

6.1. Carbon-Reinforced TRC

Experimental results obtained from test specimens reinforced with carbon textile and molded in the steel formwork were compared with simulated results obtained from Abaqus. Composites used in this section are TS15 (1000x120 mm, 2 layers of plain carbon textile), TS18 (500x60 mm, 2 layers of plain carbon textile) and TS22 (1000x120 mm, 2 layers of sand coated carbon textile). The finite elements model was composed of 1000x120x7.54 mm or 500x60x7.54 mm composites containing 50x6x12 elements. Matrix, textile and interface total heights were 6.54 mm, 0.6 mm and 0.4 mm respectively. Hence, a virtual textile volume fraction of 9.17% was obtained (excluding interface volume). In addition to the mesh described here, more refined meshes were used o test convergence of the models.

Numerical uniaxial tension test of the concrete matrix is shown in Figure 6.1a. It exhibits similar stress-strain relationships in the pre-failure area for different lengths. After failure, longer specimens exhibit faster decline in stress. This behavior was in agreement with the failure criterion suggested by Hillerborg [58], discussed in Section 2.3. Simulated results were compared with the TS12 experimental uniaxial tension test. TS12 presented an above average ultimate tensile strength and, therefore, lower ultimate tensile strength was observed in the curve of the virtual models. The curves obtained from the numerical simulations show no instability or highly non-linear behaviors, proving the suitability of the matrix model for analysis of TRC.

The curves obtained from the finite elements (FE) model of the textile (Figure 6.1b) were similar to those obtained from experimental testing, being capable of simulating the strain-hardening behavior of the material. The yarn length versus hardening relationship was set through a third degree polynomial function (described in the Fortran Routine). The function sets the strain

magnitudes at which the change of rigidity occurs. Larger lengths present increase of rigidity at shorter strain magnitudes, whereas shorter lengths present a slower hardening behavior. This approach enables the simulation of different textile lengths and different load-activation rates of filaments. In the Fortran Routine, the *L1* parameter adjusts the load-activation of the core yarns (smaller values cause faster hardening) and *dT0* sets the initial strain at which change in Young's modulus of the textile occurs.

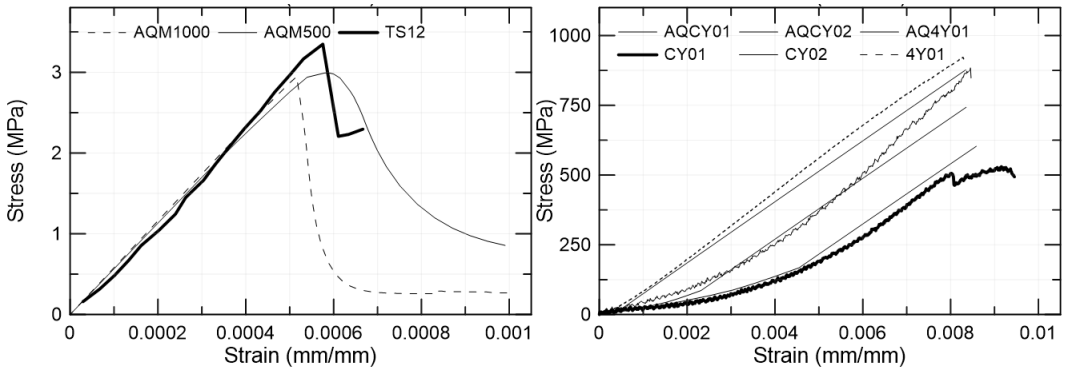

Figure 6.1: On the left, (a) concrete matrix numerical and experimental comparison, AQM1000 represents 1000x120 mm tests specimens and AQM500 represents 500x60 mm test specimens. On the right, (b) textile numerical and experimental comparison between three different lengths, 2125 mm (CY01), 1795 mm (CY02) and 355 mm (4Y01).

Since no interface experimental data was collected, a parametric study was conducted to understand the effects of parameters in the mechanical response of the numerical model. Interface parameters studied were: *MAXS* (maximum shear strength before damage), d_f (displacement from damage initiation until complete failure) and *T* (rigidity of the interface). Textile and matrix parameters were constant in this stage of testing. The chosen interface control values were: d_f=1.5 mm, *MAXS*=1.00 MPa and *T*=5880 MPa, based on the work of Lorenz and Ortlepp [53] and Azzam and Richter [84]. Stress-strain curve of the model with the control set of parameters is shown in Figure 6.1. A linear damage evolution model was adopted at this stage due to its simplicity (Figure 5.3).

Values of d_f adopted were 0.125, 0.25, 0.50 and 1.50 mm. In these scenarios d_f=1.50 mm did not undergo complete failure, whereas other values of d_f showed complete failure prior to the total displacement imposed. In addition, smaller values of d_f presented failure at lower stresses. No change in rigidity of the interface was observed.

Evaluation of the interface strength included testing *MAXS* with values of 0.25, 0.50, 1.00 and 2.00 MPa. Correlation between interface bond strength and load-coupling of the textile can be observed: higher values of *MAXS* show faster-increasing stresses. The curve on which *MAXS*=0.25 MPa shows complete failure, indicating larger relative displacements between matrix and textile. No convergence was observed for the values of 0.50 and 2.00 MPa. The error was attributed to the interface failure model (linear), which has no strength after the designated displacement value was reached, in addition to a rigid interface model, which loads and unloads rapidly. In this scenario, Abaqus may have trouble performing calculations. Moreover, interface failure, represented by dents in the hardening part of the curve, was more present for lower values of *MAXS*. This resembles the behavior observed in Figure 4.10.

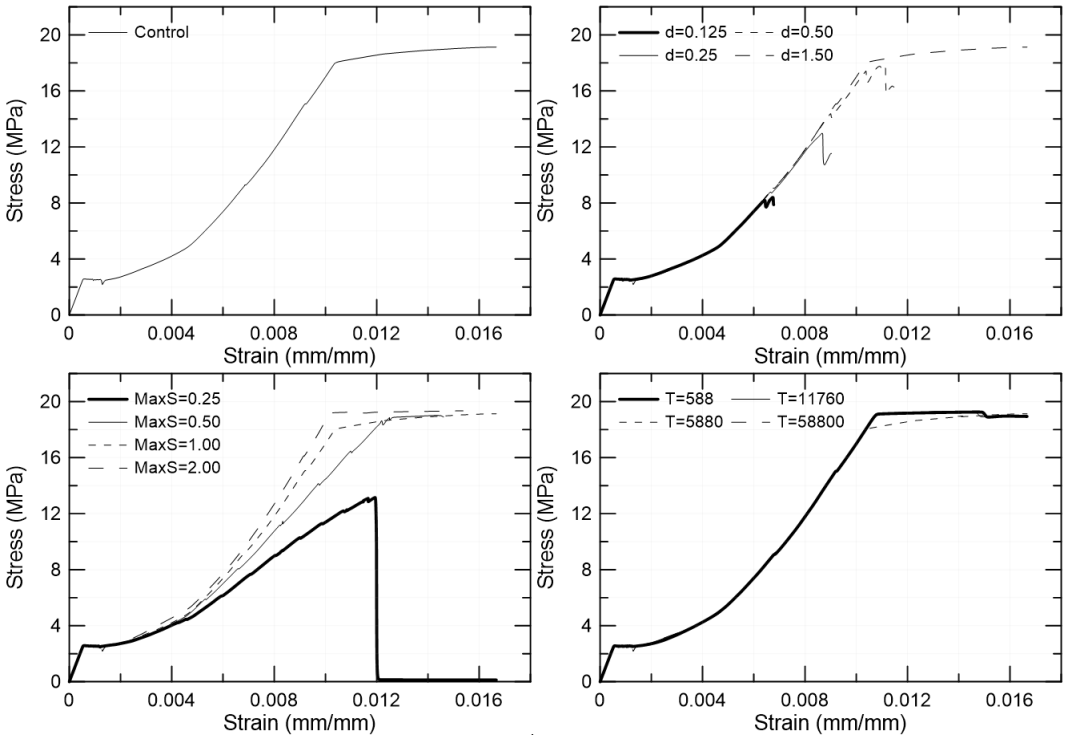

Figure 6.2: Simulated results of the interface parameters. Change in d_f, *MAXS* and *T* are observed in comparison to a control set of parameters (d_f=1.50 mm, *MAXS* = 1.00 MPa and *T*=5880 Mpa).

Interface rigidity (*T*) did not show an evident influence on the overall behavior of the models with values between 600~60000 MPa. These values were tested with *MAXS* set to 0.25, 1.00 and 2.00 MPa. A similar set of results was obtained in all simulations. The main alteration was in the multiple cracking behavior, calculation time and convergence. Smaller values of *T* presented a faster

calculation time and more homogenous cracking behavior, with smoother variances of stress. Additionally, smaller values of *T* showed better convergence, since loading and unloading of the interface material became smoother. These conclusions were especially useful when replicating the experimental program of TRC in virtual environment. All interface simulation results are shown in Figure 6.2.

The results presented show the capacity of the numerical model in simulating all of the TRC characteristics, including multiple cracking behavior. The main disadvantage observed was failure criterion of the cohesive elements, which could better represent interface behavior. Changing failure criterion from linear to exponential or tabular addresses this problem. Unfortunately, the tabular model was abandoned due to lack of information in the Abaqus user manual [100] and disparity of results obtained when comparing the build-in, linear and exponential failure models with the tabular model, calibrated to simulate these failure equations.

Numerical TRC model had the failure criterion of the interface altered from linear to exponential. Moreover, parameters were changed: *MAXS* was set to 1.50 MPa, d_f to 0.65 mm and *T* to 2500 MPa. The numerical results of the TRC were compared with the experimental data and a retro-analysis was made to calibrate bond strength. Calibration of the model consisted of altering the values of *MAXS*, d_f, α and *T*, according to the observations made in the parametric study to obtain results similar to those measured in the laboratory.

Exponential behavior better represents the physical phenomenon of bond failure and assists in convergence of the model. In addition to displacement from damage initiation until complete failure (d_f), a damage ratio parameter (α) is needed. The exponential failure behavior is described by Equation (11) .

$$D = 1 - \left\{ \frac{d_0}{d_{\max}} \right\} \cdot \left\{ 1 - \left[\frac{1 - \exp\left(-\alpha \cdot \left(\frac{d_{\max} - d_0}{d_f - d_0} \right) \right)}{1 - \exp(-\alpha)} \right] \right\} \tag{11}$$

Where D is the damage parameter, d_0 is displacement at damage initiation, d_f is displacement at complete failure and d_{max} the maximum displacement measured. These parameters define the behavior of the interface after damage initiation. Activation of core yarns and load-coupling of the textile were influenced by *MAXS* (as shown in the parametric study) and parameters of the textile in the Fortran Routine.

Lengths of boundary condition (on each end) were 120 mm, for the 500 mm long TRC, and 200 mm, for the 1000 mm long TRC. The moving end being on the right and the fixed end on the left.

Calibration of the model was done with the 1000x120 mm test specimen reinforced with plain carbon textile. This configuration was chosen due to similarities with the smaller test specimens (i.e. reinforcement-type) and the sand-coated carbon reinforced composites (i.e. size). *MAXS* was altered first, configuring the ultimate tensile strength of the material. *MAXS* was considered calibrated when ultimate tensile strength of the FE model reproduced the value measured in the laboratory. In this case, 0.16 MPa was adopted. Displacement until complete failure (d_f) and alpha (α) were calibrated next. These configure behavior of the TRC after ultimate tensile strength was reached. A soft decay in stress is wanted, in order to model slow failure of the interface and smooth slippage of the textile. In this case, d_f and α were set to 30 mm and 0.1. Lastly, rigidity of the interface was chosen. The value should correctly model the heterogeneous stress field in the composite, but still allow convergence of the model. *T* was set to 2500 MPa. Load activation parameters of the textile were set to 1795 mm (*L1*) and 0.0012 (*dT0*). Experimental and numerical results are displayed in Figures 6.3a-d.

Alterations to simulate the 500x60 mm test specimens were limited to size of the test specimen. Comparison of results are shown in Figures 6.4a-d.

Test specimens reinforced with sand-coated carbon textile had textile and interface parameters changed. Measured load-activation of the core yarns was slightly faster hence *L1* was set to 1650 mm and *dT0* to 0.0011. The maximum Young's modulus of the textile was lowered from 120 to 90 GPa. Interface parameter *MAXS* was set to 0.50 and 0.55 MPa, representing a stronger bond

between matrix and textile. Matrix ultimate tensile strength was changed to 4.25 MPa. Results obtained from this simulation are shown in Figures 6.5a-d.

Stress of the FE model was calculated by summing reaction forces of all moving nodes and dividing it by the cross-section of the TRC. Strain was obtained by dividing the prescribed displacement of the moving nodes by the initial free-span of the composite.

The simulations of the three test specimens (Figures 6.3-6.5) show the stress transfer mechanism from concrete matrix to textile. Utilizing the nomenclature of Figure 2.1, at the end of state I (Figures 6.3b, 6.4b and 6.5b), the concrete in the FE model is responsible for supporting most of the applied load. As the displacement increases and the curve reaches the end of the state IIa (Figures 6.3c, 6.4c and 6.5c), a mixed load bearing behavior is observed: matrix and textile are loaded, creating a non-uniform stress field. Moreover, less stressed regions of the concrete matrix correspond to higher stressed areas of the textile. Lastly, at the end of state IIb (Figures 6.3d, 6.4d and 6.5d), the external load applied to the system is mostly bore by the textile reinforcement. The stress transferred to the textile depended on the interface strength: stronger bond strengths lead to higher load transfer to the textile. The states observed in the simulations agree with the experimental results previously shown and the analytical analysis available in the literature.

The FE model was unable to simulate complete failure of the matrix (cracks) and concrete plastic strain was used to simulate loss of rigidity, i.e. failure zones of the material. A comparison between crack patterns of the experimental tests and plastic zones of the numerical model is shown in Figure 6.6. The FE model simulated correctly the stress-transfer behavior of the composite, as bond strength showed direct effect in crack spacing. Moreover, smaller test specimens presented inferior stress-transfer, as discussed in Section 4.3.

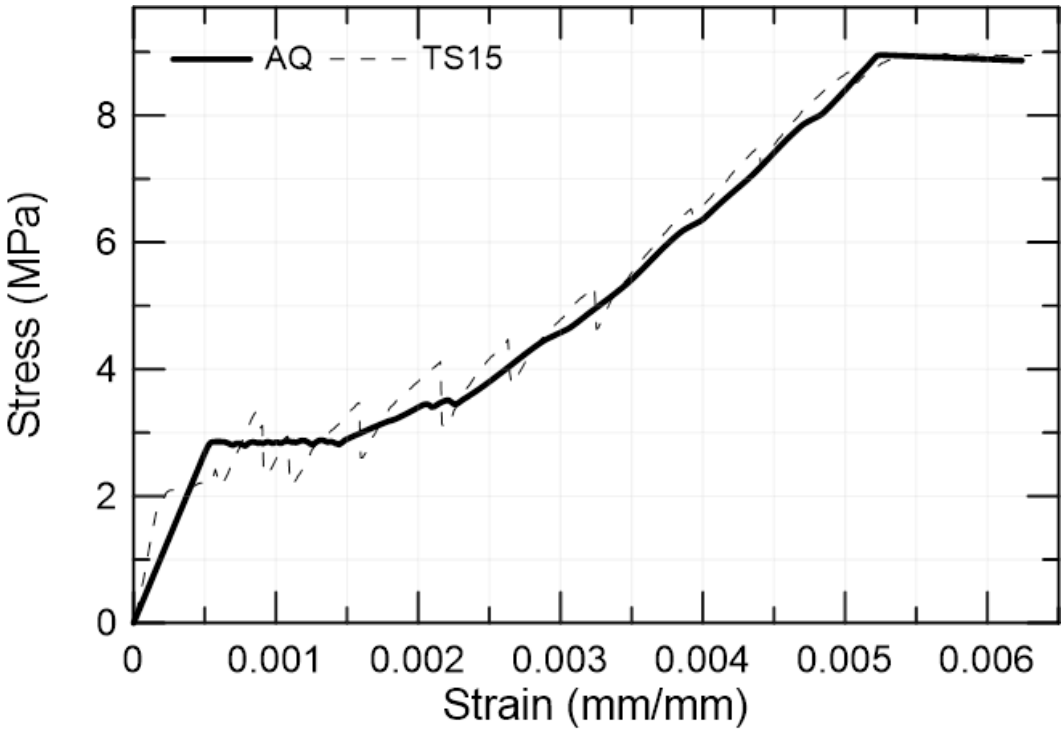

Figure 6.3a:Abaqus simulation (AQ) of TS15: 10000x120 mm and 2 layers of plain carbon textile. Interface parameters: d_0=30 mm, α=0.1, T=2500 MPa and MAXS=0.16 MPa. Textile parameters: L1=1795 mm, L2=2125 mm, dT0=0.0012 mm/mm.

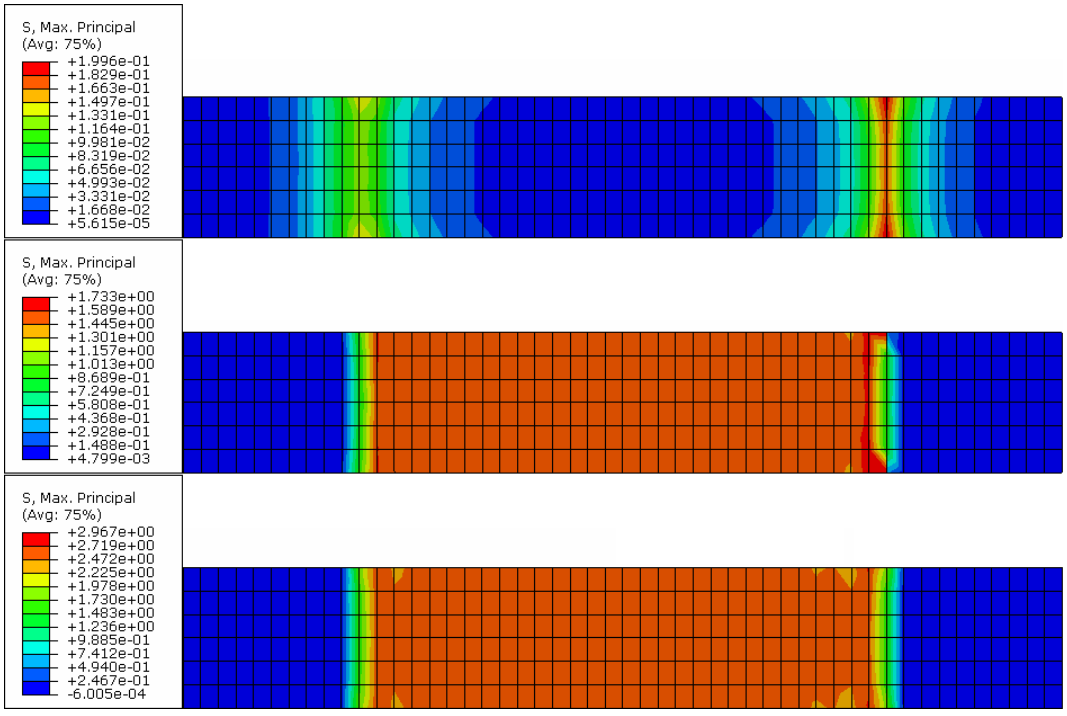

Figure 6.3b: Maximum principal stress. From top to bottom: Interface, Textile, Matrix (outer). Strain=0.00043 mm/mm.

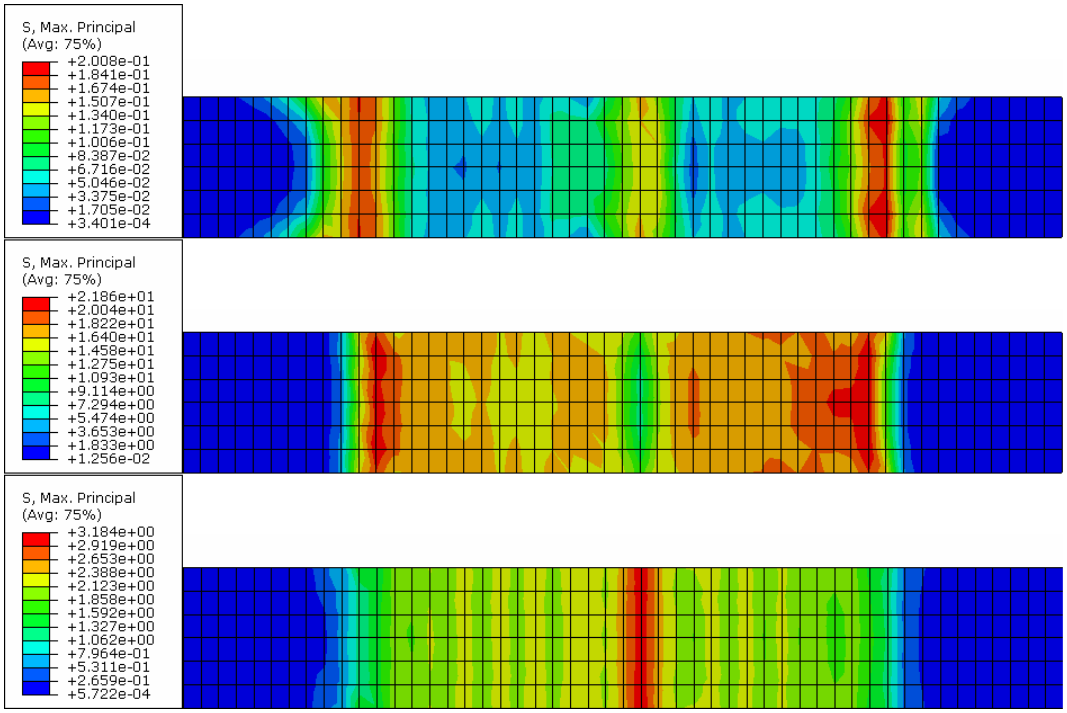

Figure 6.3c: Maximum principal stress. From top to bottom: Interface, Textile, Matrix. Strain=0.0019 mm/mm.

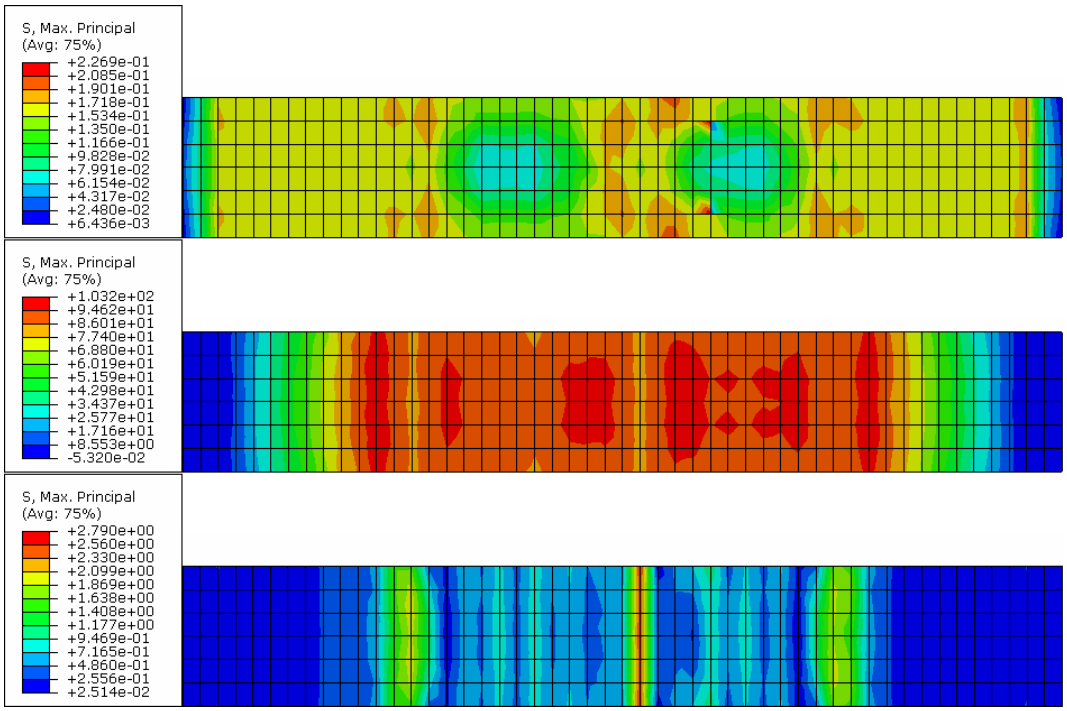

Figure 6.3d: Maximum principal stress. From top to bottom: Interface, Textile, Matrix. Strain=0.0048 mm/mm.

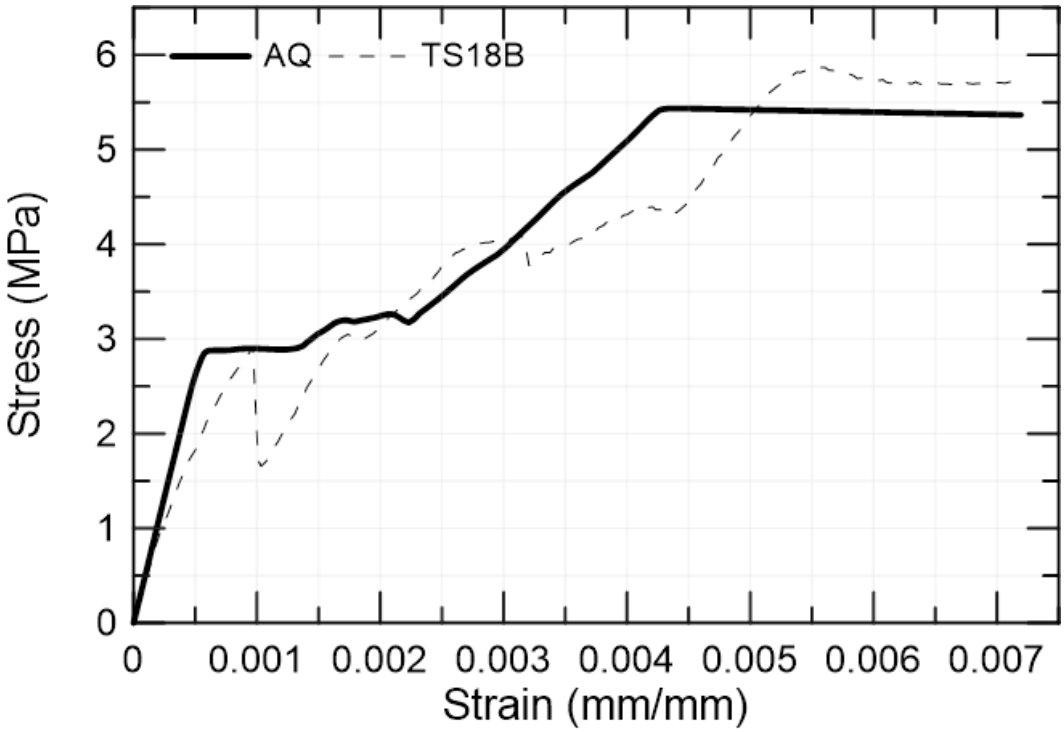

Figure 6.4a: Abaqus simulation (AQ) of TS18B: 500x60 mm and 2 layers of plain carbon textile. Interface parameters: d_0=30 mm, α=0.1, T=2500 MPa and MAXS=0.16 MPa. Textile parameters: L1=1795 mm, L2=2125 mm, dT0=0.0012 mm/mm.

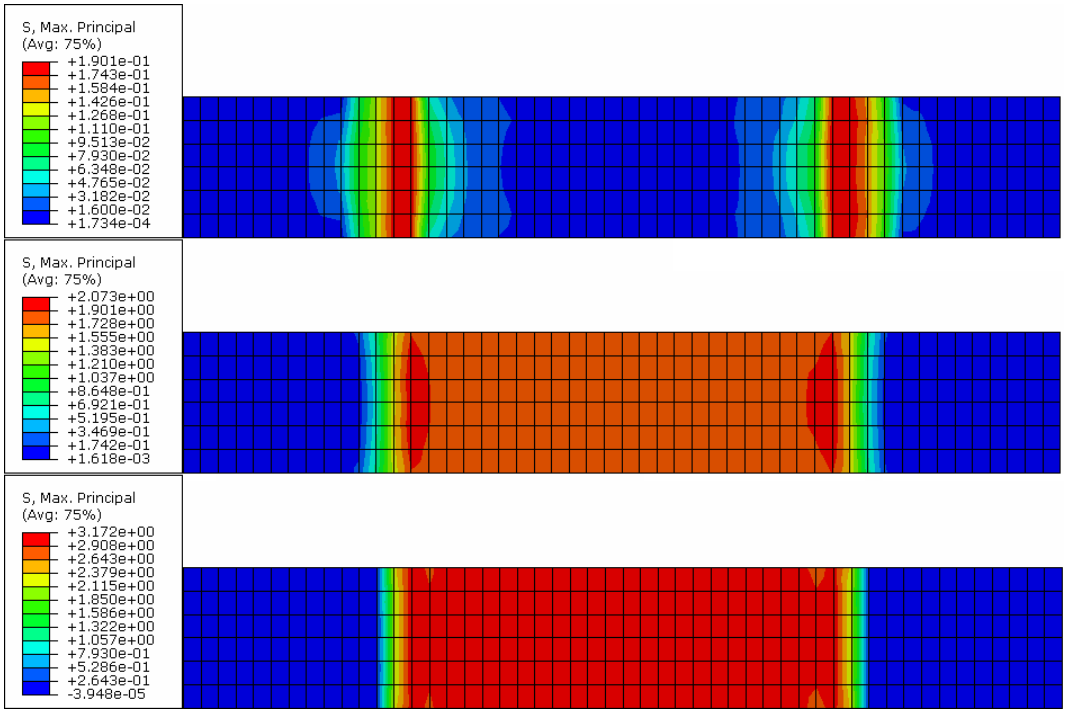

Figure 6.4b: Maximum principal stress. From top to bottom: Interface, Textile, Matrix (outer). Strain=0.00055 mm/mm.

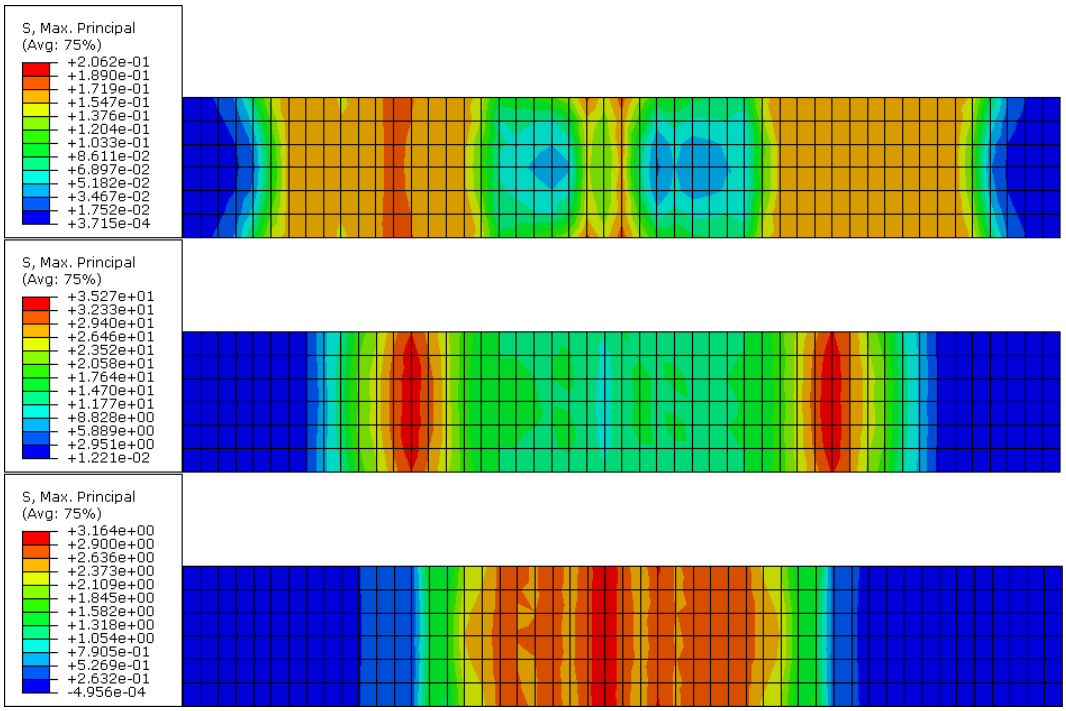

Figure 6.4c: Maximum principal stress. From top to bottom: Interface, Textile, Matrix (outer). Strain=0.0025 mm/mm.

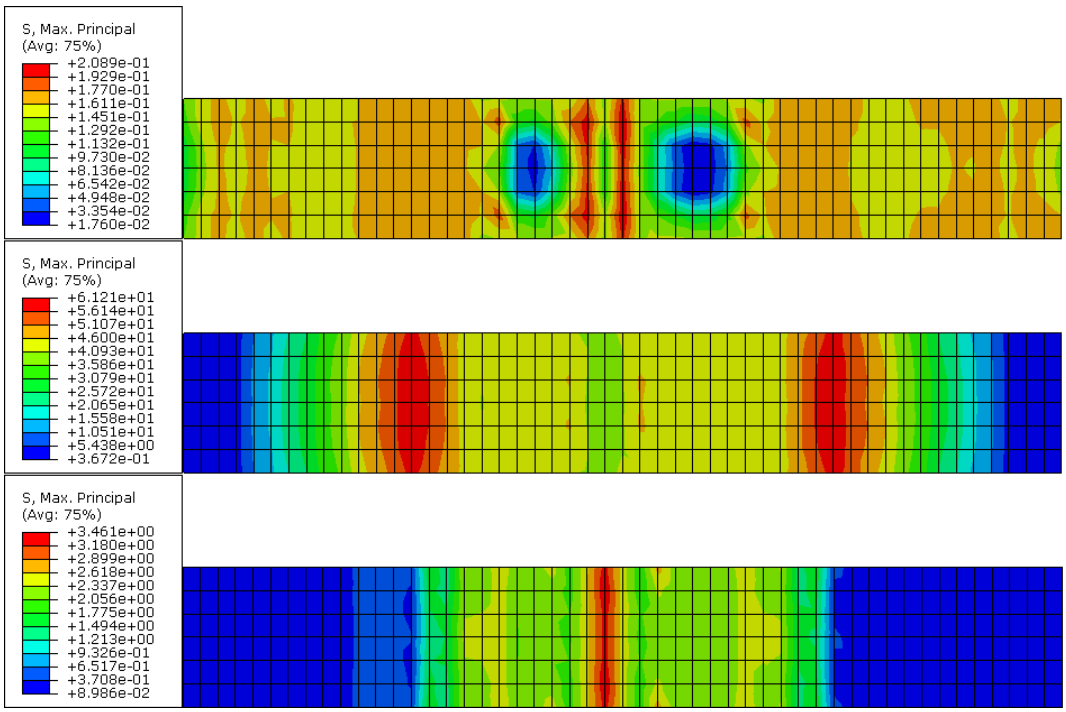

Figure 6.4d: Maximum principal stress. From top to bottom: Interface, Textile, Matrix (outer). Strain=0.0042 mm/mm.

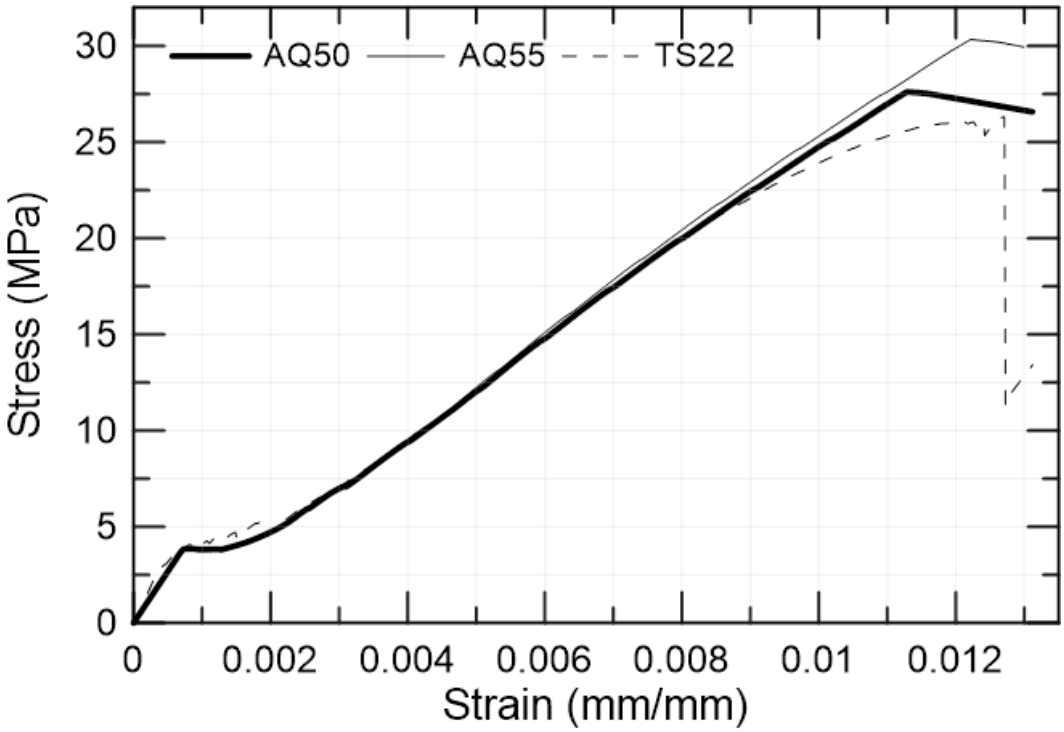

Figure 6.5a: Abaqus simulation (AQ50 and AQ55) of TS22: 1000x120 mm and 2 layers of sand-coated carbon textile. Interface parameters: d_0=30 mm, α=0.1, T=2300 MPa. MAXS=0.50 MPa for AQ50 and MAXS=0.55 MPa for AQ55. Textile parameters: L1=1650 mm, L2=2125 mm, dT0=0.0011 mm/mm, Young's modulus limited to 90 GPa.

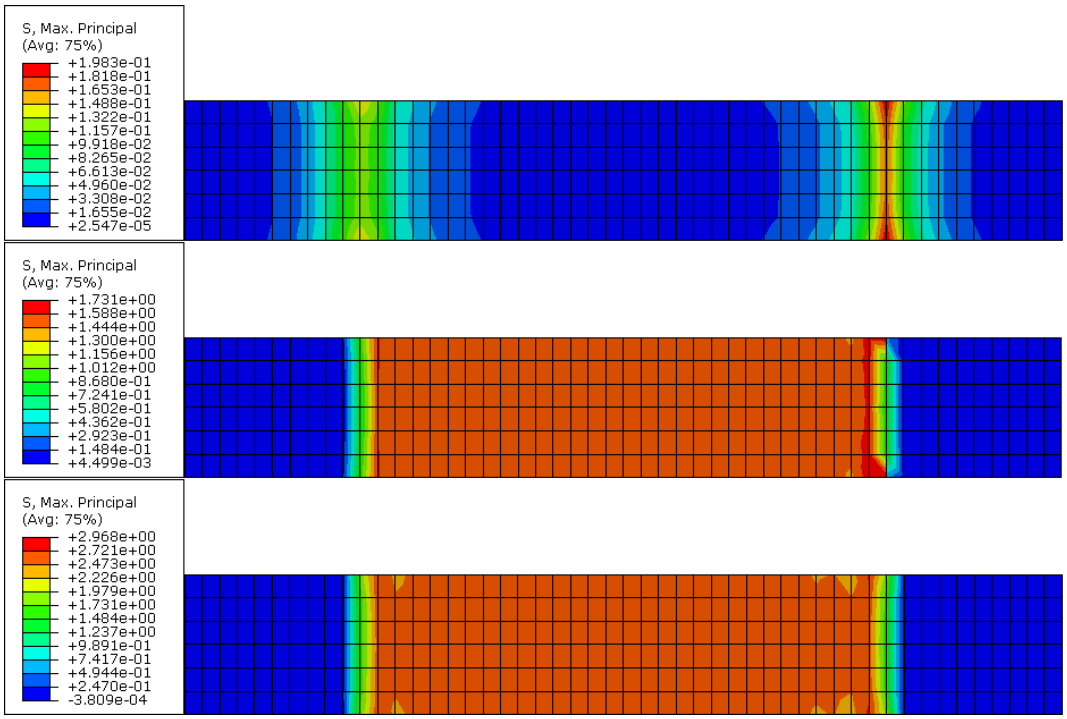

Figure 6.5b: Maximum principal stress (AQ50). From top to bottom: Interface, Textile, Matrix (outer). Strain=0.00043 mm/mm.

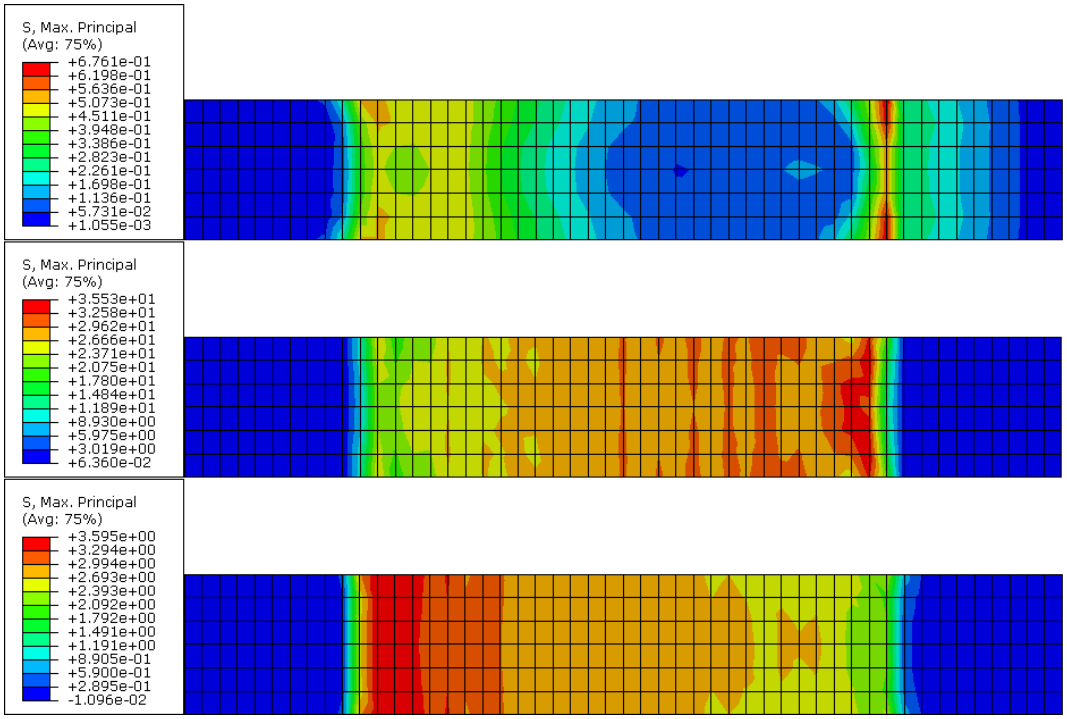

Figure 6.5c: Maximum principal stress (AQ50). From top to bottom: Interface, Textile, Matrix (outer). Strain=0.0020 mm/mm.

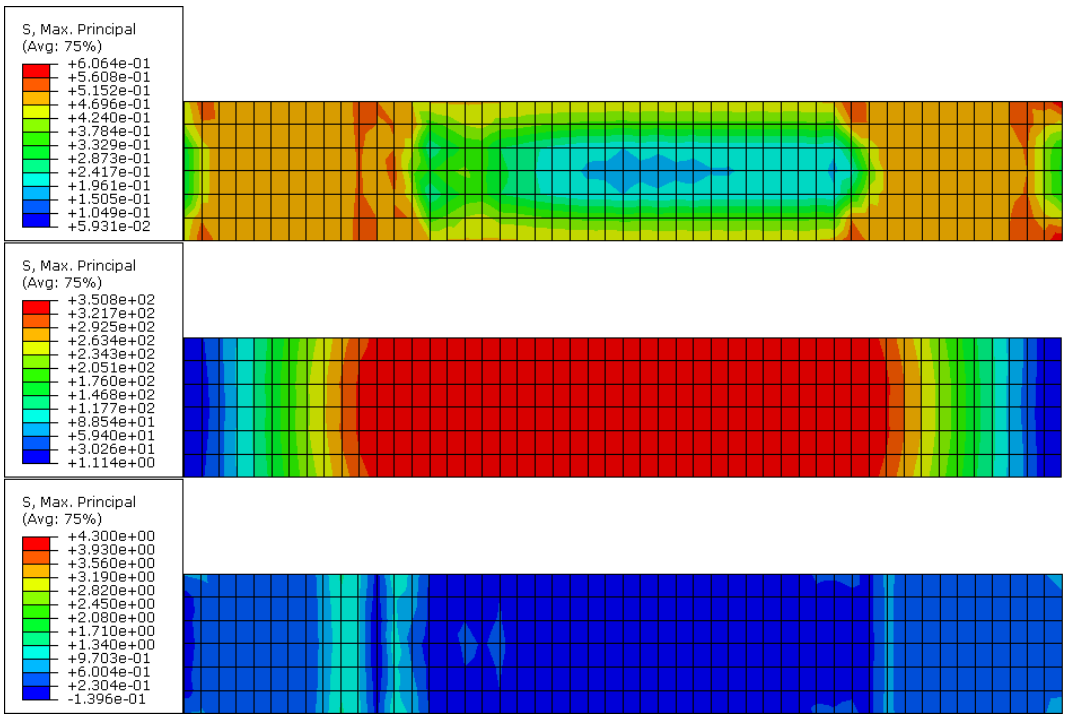

Figure 6.5d: Maximum principal stress (AQ50). From top to bottom: Interface, Textile, Matrix (outer). Strain=0.0110 mm/mm.

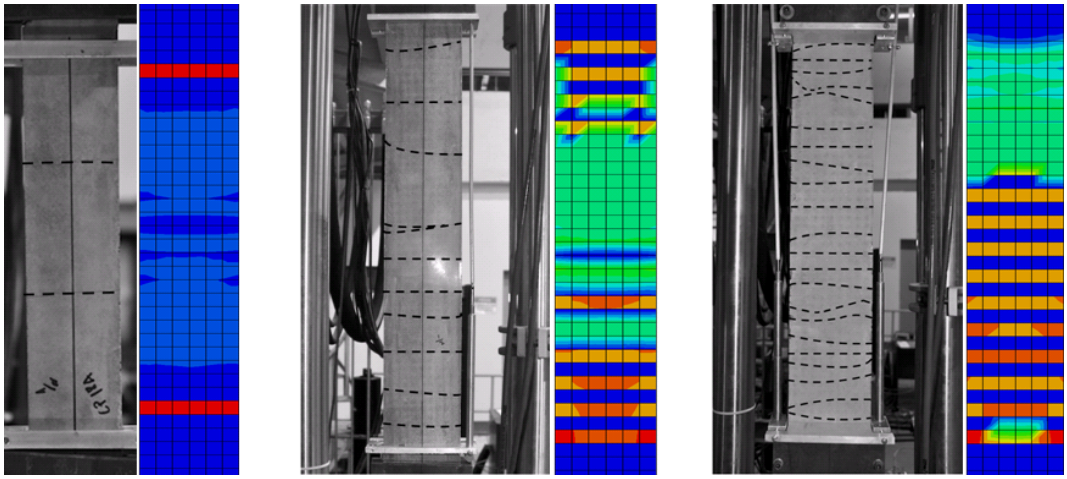

Figure 6.6: Principal plastic strain of the concrete matrix at the end of the multiple cracking state. From left to right: 500x60, 1000x120 with plain-coated textile, and 1000x120 with sand-coated textile.

6.2. Basalt-Reinforced TRC

The model described in Section 5 was altered to correctly predict the behavior of basalt-reinforced TRC. Parameters were calibrated through retro-analysis of basalt-reinforced TRC uniaxial tension tests. Variables of the FE model were changed until good agreement between numerical and experimental results was obtained. Then, a FE model simulating the round panel was created and compared with experimental results.

Simulation of the basalt-reinforced TRC under uniaxial tension required alterations to matrix, textile and interface parameters. Matrix was configured to present higher ultimate tensile strength and more brittle failure. Textile maximum Young's modulus was lowered to 48 GPa and its hardening curve modified. Lastly, interface parameter *MAXS* was calibrated to correctly represent ultimate tensile strength of the basalt-reinforced TRC. These changes were made based on the experimental uniaxial tension stress-strain curve of the composite material, since individual material data was not available. Comparison between experimental and numerical results are shown in Figures 6.6a-d.

The same stress transfer mechanism described in the carbon-reinforced simulations can be observed in the basalt-reinforced results. The stress migrates from the concrete matrix in an early stage to the textile reinforcement as the imposed displacement increases and the strength of the matrix deteriorates.

The round panel test was first modeled with the same parameters used in the uniaxial tension test. Constitutive changes were made to the stiffness matrix of textile (DDSDDE in the Fortran Routine) and its hardening curve was set to increase with strain modulus of the *xx* and *yy* directions, as discussed in Section 5.5. After the initial test results, alterations were made to the ultimate tensile strength of the matrix and the hardening curve of the textile.

The results obtained from the round-panel simulations are presented in Figures 6.7a-c. The stress-transfer mechanism between matrix and textile is clearly seen: once failure starts, lower stressed areas in the matrix correspond to higher stressed areas in the textile. Additionally, the overall shape of the force-displacement curve is similar to the one obtained experimentally, with sustained load after matrix failure. This indicates a well-balanced model, capable

of simulating important aspects and mechanisms of TRCs. However, lack of material parameters and the absence of pivoting supports in the boundary conditions of the model resulted in a great offset between the experimental and numerical values. An initial stiffness had to be introduced to the textile material in three dimensions (i.e. shear modulus interpolation), which was done to improve convergence of the model, but created a stiffer curve.

Other difficulties in obtaining agreeing results were associated to the manufacture method of the test specimens, which affects their mechanical behavior, as discussed in Section 4.3. In this case, the manufacture method of the round panel was assumed to be identical to the manufacture method of the uniaxial tension test specimens.

Overall, simulation results of the round panel test were unsatisfactory, although the force-displacement curve showed some similarities to experimental data and the load-transferring mechanism could be observed, there are still improvements to be made before the model can correctly simulate a multiaxial state of stress. From the simulation results, it is estimated that the constitutive response of the textile should be altered. Mobasher et al. [50] studied hybrid TRCs under tensile and flexural loading and concluded that griping, delamination, interfacial bond and matrix penetrability have a dominant effect in flexure behavior, whereas yarn strength has a larger effect in uniaxial tension. The parameters analyzed by Mobasher and al. were not addressed in the present study and could have a profound effect on the simulation results.

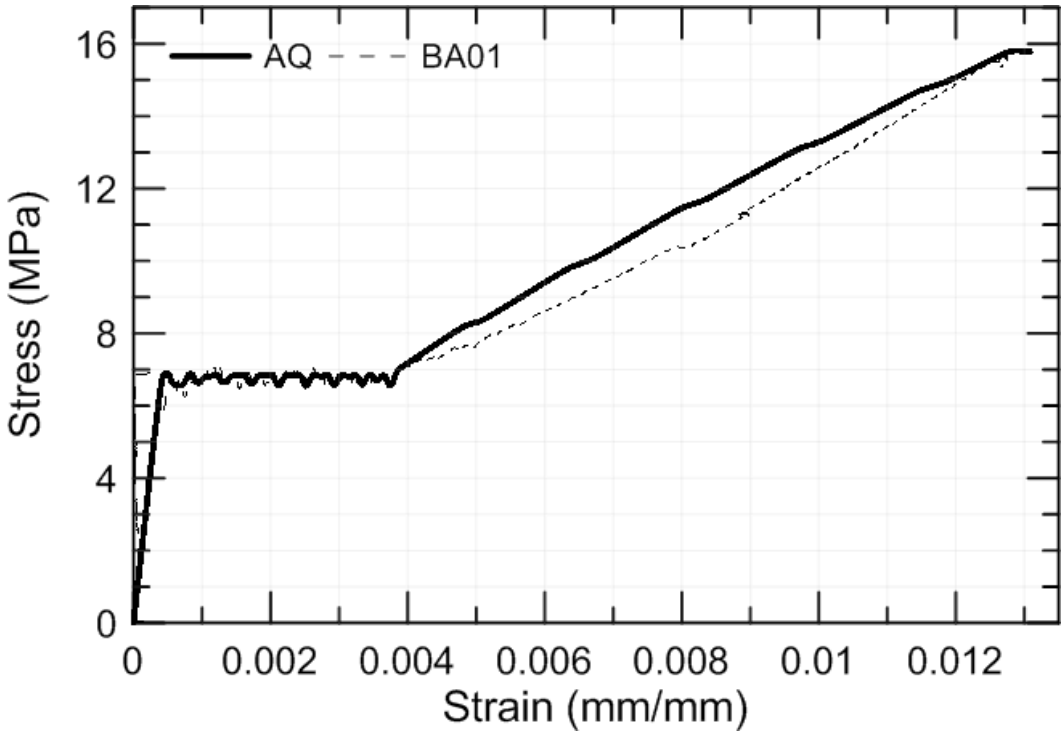

Figure 6.6a: Abaqus simulation of basalt-reinforced TRC: 1000x120 mm and 5 layers of textile. Interface parameters: d_0=30 mm, α=0.1, T=1000 MPa. MAXS=0.82 MPa. Textile parameters: L1=1700 mm, L2=2125 mm, dT0=0.0012 mm/mm, Young's modulus limited to 48 GPa.

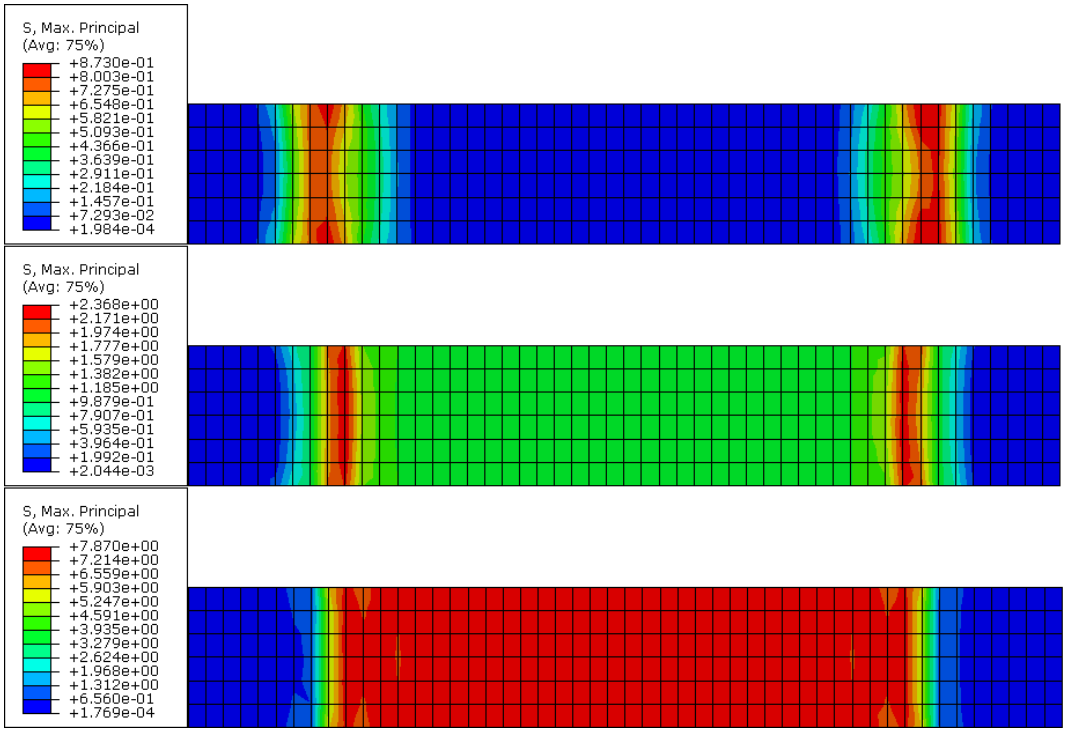

Figure 6.6b: Maximum principal stress. From top to bottom: Interface, Textile, Matrix (outer). Strain=0.00045 mm/mm.

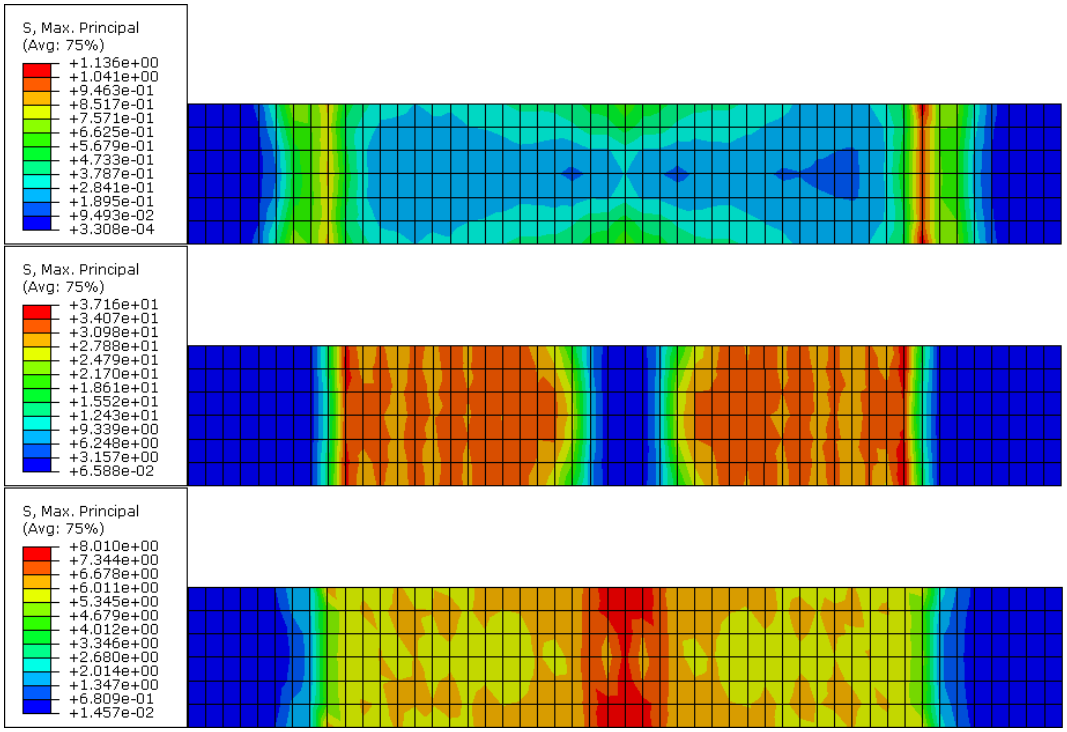

Figure 6.6c: Maximum principal stress. From top to bottom: Interface, Textile, Matrix (outer). Strain=0.0034 mm/mm.

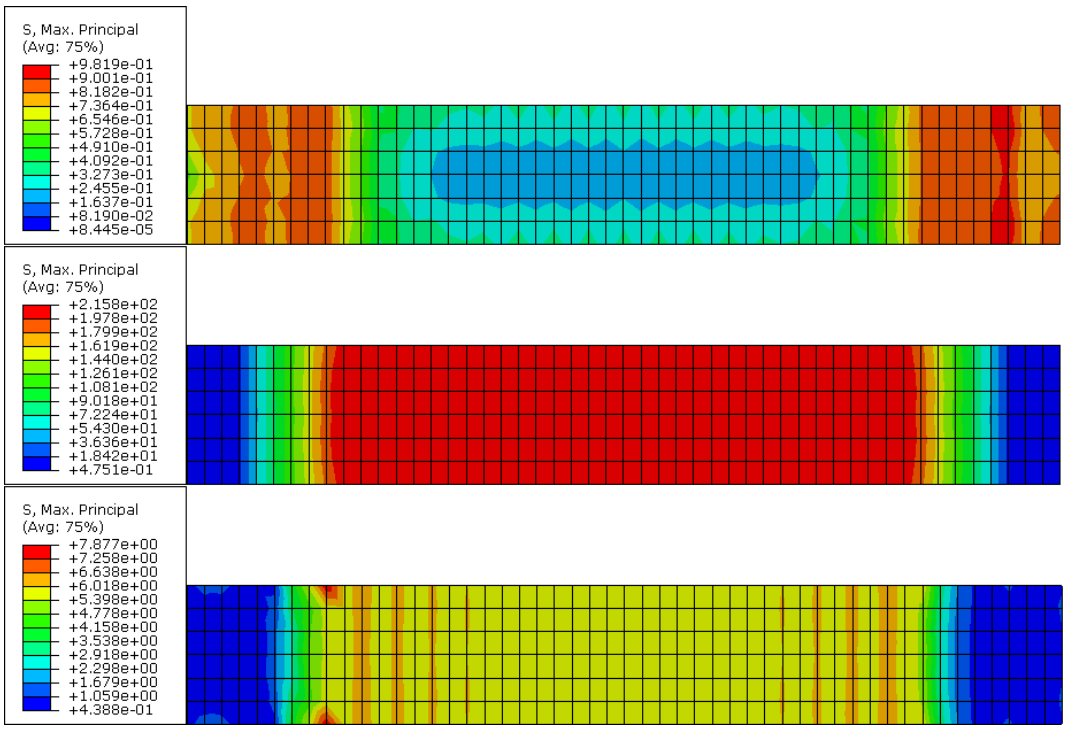

Figure 6.6d: Maximum principal stress. From top to bottom: Interface, Textile, Matrix (outer). Strain=0.0125 mm/mm.

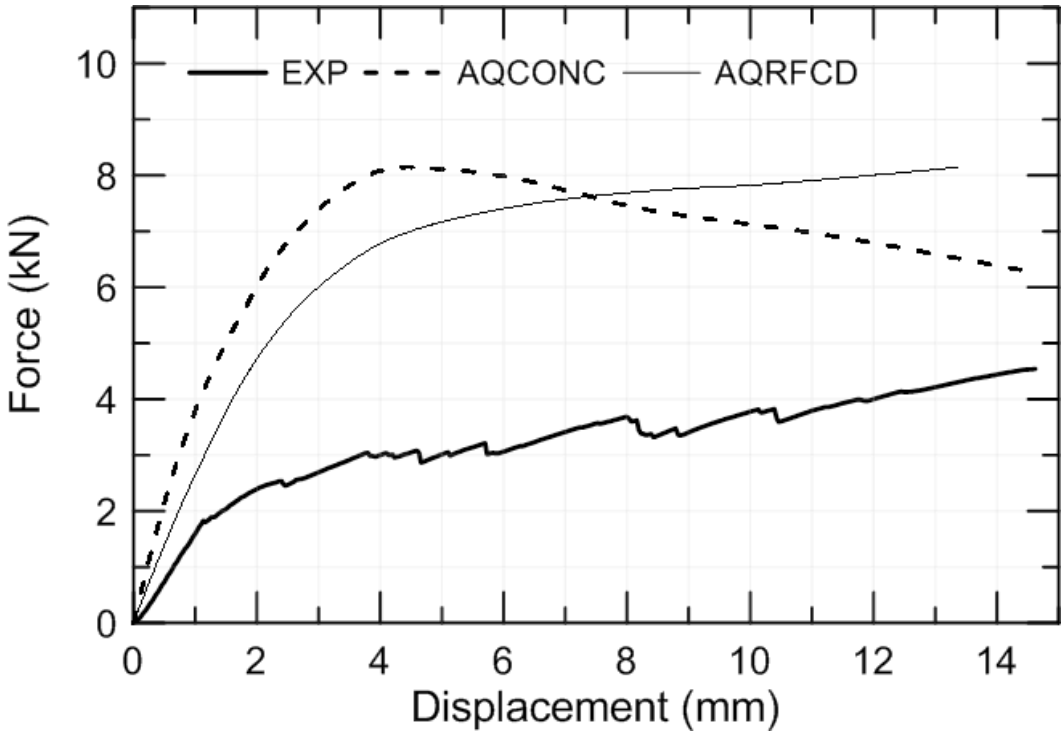

Figure 6.7a: Force-displacement curves for the experimental test (EXP), the Abaqus model with all elements set with concrete properties (AQCONC) and the Abaqus model simulating the basalt-reinforced TRC (AQRFCD).

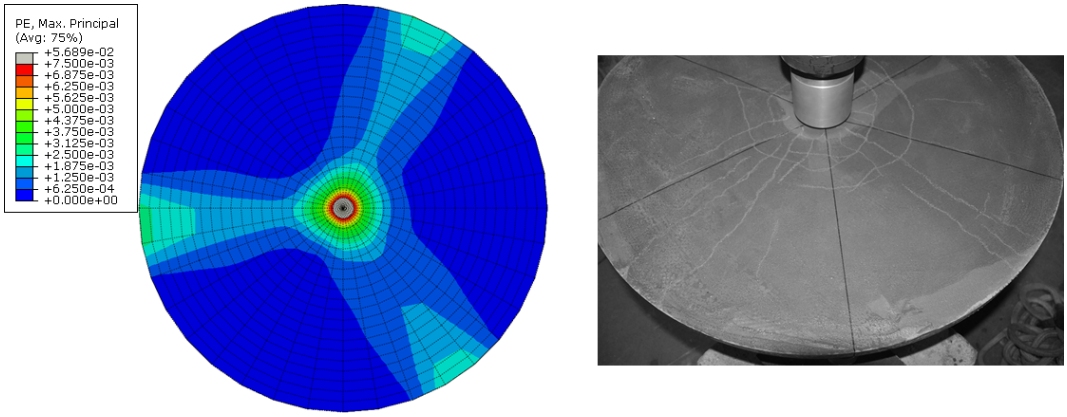

Figure 6.7b: Failure zones on the top layer of the matrix at the end of the simulation (left) and experimental test (right).

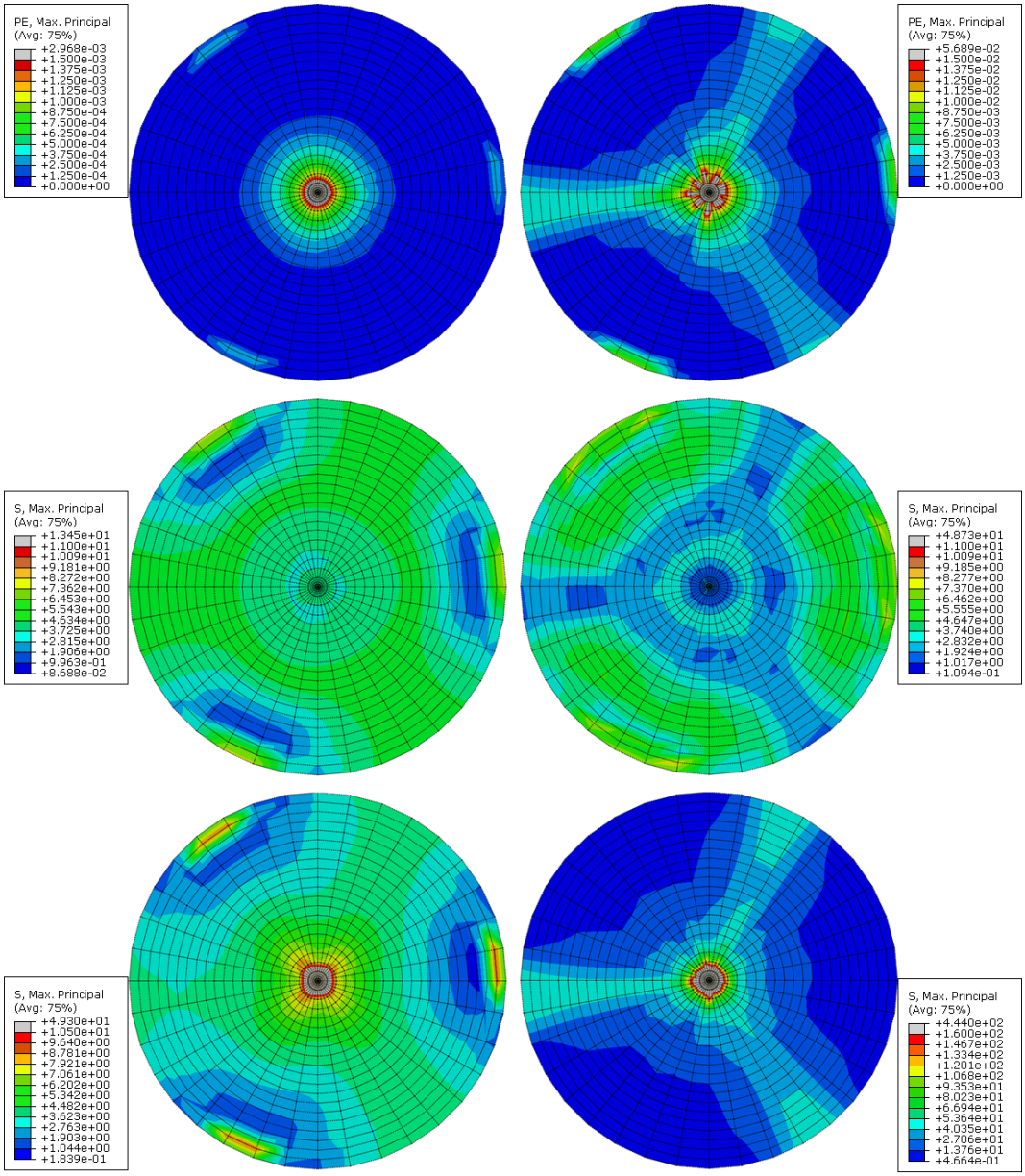

Figure 6.7c: Maximum plastic strain (top) and maximum principal stress (middle) on the bottom layer of the matrix and maximum principal stress on the bottom layer of the textile, at the prescribed displacement of 2.01 mm (left) and 11.15 mm (right).

7. Conclusions

An experimental program was conducted to determine mechanical behavior of a carbon-reinforced TRC and its individual components, i.e. cementitious matrix and carbon-textile. The parameters analyzed were: manufacture method, volume fraction of textile, size and interface adhesion.

Experimental results showed that the manufacturing method (i.e. hand-pressing the textile against the concrete matrix) and volume fraction affected bond strength. Test specimens with higher volume fraction and which had the reinforcement hand-pressed presented faster strain-hardening behavior and higher ultimate tensile strength.

Size of test specimens influenced the behavior of the composites as well. A more heterogeneous stress field was observed in smaller test specimens, which led to localized failure. Areas of stress concentration failed first, and, although load was transferred through the phases of the composite, higher, localized stresses caused crack growth rather than multiple cracking (i.e. Saint-Venant's principle).

Interface adhesion was altered by sand-coating the carbon textile. Comparison of results obtained from sand-coated and plain-coated test specimens showed no change in interface stiffness, as Young's moduli in the post-cracking branch of the stress-strain curves were not changed. However, interface shear strength was modified. The plain-coated test specimen presented an average crack-spacing of 70.0 mm and the sand-coated specimen presented an average crack-spacing of 27.3 mm and higher ultimate tensile strength.

An Abaqus finite elements (FE) model, based on results of the experimental program, was proposed to simulate mechanical behavior of TRCs. The model was created through a code in Lua, enabling alteration of model parameters (i.e. size, rigidity, damage criteria, etc.). Moreover, the code can be modified to insert random imperfections and details, better reproducing the physical TRC system. The numerical model consists of *Concrete Damaged Plasticity* constitutive response to reproduce the cementitious matrix, strain-dependent rigidity (added through a Fortran Routine) to model the textile structure and cohesive elements, following traction-separation law, to simulate the interface.

Validation of the FE model was made through comparison of numerical and

experimental results. Different sized carbon-reinforced TRCs with two distinct textile-coatings, as well as a basalt-reinforced TRC were used. Calibration of parameters was made with uniaxial tension tests of carbon-reinforced TRC and excellent agreement of results was obtained, as previously shown in this Section. The model was then altered to simulate the behavior of basalt-reinforced TRC containing five layers of textile reinforcement under uniaxial tension and flexure. In this case, no experimental data was acquired to describe the mechanical behavior of basalt yarns or the calcium-aluminate concrete matrix. Nonetheless, good agreement of results was found between experimental and numerical uniaxial tension tests.

From the FE results, textile behavior proved to have a profound influence on the cracking mechanism of composite. Specifically, multiple cracking under uniaxial tension was observed when the textile had a low Young's modulus until a certain strain was reached. The value of the strain varied, but generally it was slightly larger than the cracking strain of the matrix. Higher values of *dT0* and *L1* produced more cracks in the numerical uniaxial tension experiments. Calibration of multiple cracking behavior and hardening was implemented through parameters in the Fortran Routine, i.e. *d*, *dT0*, *L1*, *L2* and *CTE*.

Cracking behavior of the TRC in the FE model was affected by brittleness of the matrix. Variables under the **Concrete Tension Stiffening* tag described the softening behavior after matrix failure. Faster softening caused accentuated saw-shaped pattern in the stress-strain curve.

Interface numerical parameter *MAXS* was found to have good correlation to crack-spacing, as observed from comparison of test specimens TS14 and TS22. Experimental results showed average crack-spacing of 70.0 mm for TS14 and 27.3 mm for TS22. In the FE model, *MAXS* was altered from 0.16 MPa to 0.50 MPa to reproduce change in bond strength. Therefore, a decrease factor of 2.56 in crack-spacing caused an increase factor of 3.12 in *MAXS*.

Simulated uniaxial tension tests presented crack propagation direction from ends to center of the composite, creating a quasi-symmetric stress field. Contrastive behavior was observed in the sand-coated, carbon-reinforced TRC, which presented crack propagation from the fixed to the moving end of the model.

Overall, capability of the FE model exceeded expectations when simulating uniaxial tension tests. Every mechanical property of the system could be tailored and similarities to experimental uniaxial tension results were excellent. Simulation results of the round panel tests showed capability of the model to distribute loads in a multiaxial state of stress, although a gap between simulated and experimental results was observed. Hence, with some improvements, the proposed FE model should be able to reproduce mechanical behavior of larger test specimens under mixed load configurations, exhibiting great potential in dimensioning structural and semi-structural TRC components.

8. Suggestions for Future Works

A number of functionalities can be added to the Lua code to better represent the physical-mechanical phenomena of TRCs:

1. Heterogeneity of the matrix can be represented by random variation in ultimate tensile strength and Young's modulus of elements. This would cause non-linear cracks and different crack patterns for each generated model.

2. Boundary conditions should be improved to better represent the experimental tests, including a more refined mesh in stress concentration areas.

3. Geometry of the model should represent the interconnection between all matrix layers, creating a system where stress-transfer across different phases of the composite is made through interface and matrix elements. This geometry improvement would enhance performance of the FE model, especially in composites reinforced with three or more layers, where load-delay to inner elements was observed.

4. The mechanical behavior of the textile must be represented with a more realistic approach: an anisotropic response must be added.

Regarding the experimental program, a more detailed analysis of the interface should be carried. Specifically, a study to address load-activation speed of yarn filaments when embedded in a cementitious matrix. The results would facilitate calibration of different TRC models. Furthermore, experiments in larger scale would provide additional validation of the numerical model proposed and a study on crack formation (i.e. is there a section of the TRC which exhibits more cracks, is there an end on which cracking of the composite starts, stress concentrations, etc.) would provide data to improve the different phenomena simulated in the FE model. Finally, more data should be obtained for the textile structures, as biaxial and shear behavior.

Appendix I: Lua Code

The Lua code used to generate models in Abaqus is shown bellow. The parameters used describe the behavior shown in Figures 6.3a to 6.3d. Lua can be added to Mac OS through Homebrew (http://brew.sh/index.html) and typing in Terminal:

```
brew install lua
```

In Windows, Lua can be added following instructions suggested on the official website: https://www.lua.org/home.html. Lua documentation is also available at this web address. Once added, the Lua code is run through terminal (in Mac OS) or command prompt (in Windows). Navigate to the Lua code file directory and type the command:

```
lua file_name.lua
```

Press return to create the model_file.inp in the directory of the Lua code.

```
------------------------------------------------------------
--
-- model parameters.
--
------------------------------------------------------------
-- manual input data
local ntexlayers   = 2        -- number of textile layers
local textileH     = 0.3      -- textile layer height (mm)
local interfaceH   = 0.1      -- interface layer height (mm)
local matrixH      = 6.54/3   -- matrix layer height (mm)

local loadvalue    = {1, 0.5} -- axis (1=x, 2=y, 3=z), displacement value mm/min
local steps        = 20.      -- 1 step = 1 minute
-- type, max number of iterations, initial increment, time period, minimum
increment, maximum increment
local stepcontrol  = {"*Static", 1000000, 1e-8, 1., 1e-15, 0.025} -- step controls
-- command for stabilization:
-- *static , stabilize, factor=1e-6, allsdtol=0.05, continue=NO

local w  = 1000               -- width of the plate in mm (x axis)
local d  = 120                -- depth of the plate in mm (y axis)
local bc = 200                -- length of TRC inside one grip element (boundary
condition)

local matrixelemtype  = "C3D8"
local matrixdensity   = 1000  -- for dynamic simulations only
local matrixmodel     = {-- model type, youngs_modulus, poisson
                         {"*ELASTIC", 5880, 0.18}
                        }
local matrixdamage    = {-- tag, eccentricity, dilation angle, fb0/fc0, K,
viscosity parameter
                         {"*Concrete Damaged Plasticity", 36., 0.1, 1.16, 0.667,
1e-3},
                         -- tag, yield_stress_1, inelastic_strain_1, ...
yield_stress_n, inelastic_strain_n
                         {"*Concrete Compression Hardening",
                          78.0, 0.00},
                         -- tag, yield_stress_1, cracking_strain_1, ...
yield_stress_n, cracking_strain_n
                         {"*Concrete Tension Stiffening, type=displacement",
                          3.15, 0,
                          0.10, 0.06,
                         },
                         -- tag, damage_parameter_1, inelastic_strain_1, ...
damage_parameter_n, inelastic_strain_n
                         --{"*Concrete Compression Damage"},
```

```
                        -- tag, damage_parameter_1, cracking_strain_1, ...
damage_parameter_n, cracking_strain_n
                        {"*Concrete Tension Damage",
                         0.00, 0,
                        }
                       }
local interelemtype   = "COH3D8"
local interdensity    = 1000  -- for dynamic simulations only
local interfacemodel  = {-- tag, stress Sn @damage initiation, stress Tt @damage
initiation, stress Ts @damage initiation
                        {"*Damage Initiation, criterion=MAXS", 0.16, 0.16, 0.16},
                        -- tag, displacement at total failure, alpha
                        {"*Damage Evolution, type=DISPLACEMENT,
softening=EXPONENTIAL",
                         30, 0.1
                        },
                        {"*Damage Stabilization", 0.02},
                        -- tag, Kn = E/t, Ks = Kn/(2*(1+u)), Kt = Ks
                        {"*ELASTIC, type=TRACTION", 2500, 2500, 2500},
                       }
local textileelemtype = "C3D8"
local textiledensity  = 1000  -- for dynamic simulations only
local textilemodel    = {-- model type, youngs_modulus_1 MPa, poisson_1, temp1...
                         -- textile temperature control
                         --{"*ELASTIC",
                         -- 1250, 0.28, 0,
                         -- 1250, 0.28, 1,
                         -- 1500, 0.28, 2,
                         -- 1750, 0.28, 3,
                         -- 2000, 0.28, 4,
                         -- 32500, 0.28, 5,
                         --},
                         --{"*NO COMPRESSION"}
                         -- user defined material
                         {"*USER MATERIAL, CONSTANTS=1", 1}
                        }
local textilechange   = {-- loading step, temp value
                         -- controls textile Youngs modulus change
                         --{1, 1},
                         --{2, 2},
                         --{3, 3},
                         --{4, 5},
                         --{5, 5},
                        }
------------------------------------------------------------
-- automatic input data
matrixH            = matrixH/2    -- model considers 2 layers of matrix
local ninterlayers = 2*ntexlayers -- number of interface layers
local nmatlayers   = ntexlayers+1 -- number of matrix layers
local nx           = w/20+1        -- number of nodes in the x direction
local ny           = d/20+1        -- number of nodes in the y direction
local nz           = (ntexlayers+ninterlayers+2*nmatlayers)+1 -- number of nodes
in the z direction

local h = ntexlayers*textileH+ninterlayers*interfaceH+2*nmatlayers*matrixH --
height of the plate (mm)

local filename = os.date("%Y.%m.%d-%H.%M.%S").."-"..w.."x"..d.."x"..h.."-"
filename =
filename..math.floor(nx-1).."x"..math.floor(ny-1).."x"..math.floor(nz-1)..".inp"

local useQuadElement = false  -- if false, hex20 mesh. If true, hex8 mesh
------------------------------------------------------------
--
--  Writes Abaqus Inp File
--
------------------------------------------------------------
-- insert spaces into file for organization purposes
local function spaces (value)
  local s = string.len(tostring(value))
  local spaces = ","
  for n=1, 20-s do
    spaces = spaces .. " "
  end
  return spaces
end
-- write nodes to inp file
```

```
local function writeNodesToFile (nodes, filename)
  -- open file, write
  print(filename)
  local file = io.open(filename, "w")
  -- write nodes
  file:write("**********************************************************************
\n")
  file:write("*NODE \n")
  for i=1, #nodes do
    file:write(i)
    file:write(spaces(i))
    for j=1, 3 do
      file:write(nodes[i][j])
      file:write(spaces(nodes[i][j]))
      if (j==3) then file:write("\n") end
    end
  end
  file:close()
end
-- write elements to inp file
local function writeElementsToFile(cells, ntexlayers, nx, ny)
  -- open file, append
  local file = io.open(filename, "a")
  -- matrix elements
  file:write("**********************************************************************
\n")
  file:write("*ELEMENT, TYPE="..matrixelemtype.., ELSET=MATRIX \n")
  for i=1, ntexlayers+1 do
    for j=1+5*(i-1)*(nx-1)*(ny-1), 2*(nx-1)*(ny-1)+5*(i-1)*(nx-1)*(ny-1) do
      file:write(j)
      file:write(spaces(j))
      for k=1, 8 do
        file:write(cells[j][k])
        file:write(spaces(cells[j][k]))
        if (k==8) then file:write("\n") end
      end
    end
  end
  -- interface elements
  file:write("*ELEMENT, TYPE="..interelemtype.., ELSET=INTERFACE \n")
  for i=1, ntexlayers do
    -- preceeding textile
    for j=1+2*(nx-1)*(ny-1)+5*(i-1)*(nx-1)*(ny-1),
3*(nx-1)*(ny-1)+5*(i-1)*(nx-1)*(ny-1) do
      file:write(j)
      file:write(spaces(j))
      for k=1, 8 do
        file:write(cells[j][k])
        file:write(spaces(cells[j][k]))
        if (k==8) then file:write("\n") end
      end
    end
    -- succeeding textile
    for j=1+4*(nx-1)*(ny-1)+5*(i-1)*(nx-1)*(ny-1),
5*(nx-1)*(ny-1)+5*(i-1)*(nx-1)*(ny-1) do
      file:write(j)
      file:write(spaces(j))
      for k=1, 8 do
        file:write(cells[j][k])
        file:write(spaces(cells[j][k]))
        if (k==8) then file:write("\n") end
      end
    end
  end
  -- textile elements
  file:write("*ELEMENT, TYPE=".. textileelemtype..", ELSET=TEXTILE \n")
  for i=1, ntexlayers do
    for j=1+3*(nx-1)*(ny-1)+5*(i-1)*(nx-1)*(ny-1),
4*(nx-1)*(ny-1)+5*(i-1)*(nx-1)*(ny-1) do
      file:write(j)
      file:write(spaces(j))
      for k=1, 8 do
        file:write(cells[j][k])
        file:write(spaces(cells[j][k]))
        if (k==8) then file:write("\n") end
      end
    end
```

```
  end
  -- end part
  file:write("*********************************************************************
\n")
  file:write("*SOLID SECTION, ELSET=MATRIX, MATERIAL=matrix \n") -- could use
STACK DIRECTION
  file:write("*COHESIVE SECTION, ELSET=INTERFACE, MATERIAL=interface,
response=TRACTION SEPARATION \n1. \n")
  file:write("*SOLID SECTION, ELSET=TEXTILE, MATERIAL=textile \n")
  -- close file
  file:close()
end
-- write assembly to file
local function writeAssemblyToFile (bc, dx, nx, dy, ny, dz, nz)
  -- table of fixed nodes
  local bcnodesleft = {}
  local bcnodesright = {}
  local rest = bc%dx
  local bcx = (bc-rest)/dx + 1

  for k=1,2 do
    for j=1,ny do
      for i=1,bcx do
        -- bc nodes left
        bcnodesleft[#bcnodesleft+1] = i+(j-1)*(nx)+(k-1)*nx*ny*(nz-1)
        -- bc nodes right
        bcnodesright[#bcnodesright+1] = (nx-bcx)+i+(j-1)*(nx)+(k-1)*nx*ny*(nz-1)
      end
    end
  end
  local file = io.open(filename, "a")
  file:write("*********************************************************************
\n")
  file:write("*NSET, nset=ALLNODS \n") --, instance=PART-1-1, generate \n")
  file:write("1, "..math.floor(nx*ny*nz)..", 1 \n")
  file:write("*NSET, nset=FixedNodesLeft \n") --, internal, instance=TRCinstance
\n")
  for i=1,#bcnodesleft do
    file:write(bcnodesleft[i])
    file:write(spaces(bcnodesleft[i]))
    if (i%9==0 or i==#bcnodesleft) then file:write("\n") end
  end
  file:write("*********************************************************************
\n")
  file:write("*NSET, nset=MovingNodesRight \n") --, internal, instance=TRCinstance
\n")
  for i=1,#bcnodesright do
    file:write(bcnodesright[i])
    file:write(spaces(bcnodesright[i]))
    if (i%9==0 or i==#bcnodesright) then file:write("\n") end
  end
  file:write("*********************************************************************
\n")
  file:write("*NSET, nset=PlotNode \n") --, internal, instance=TRCinstance \n")
  file:write(bcnodesright[1])
  file:write(spaces(bcnodesright[1]))
  file:write("\n")
  file:close()
end
-- write material property tables to file
-- ncol defines the number of property columns
-- for new line placement
local function writeTableToFile (file, table, ncol)
  file:write(table[1].."\n") -- write header
  for i=2,#table do
    file:write(table[i]..", ") -- write content
    if (ncol==0) then
    -- write new line when needed
    elseif ((i-1)%ncol==0) then file:write("\n") end
  end
  if (ncol==0) then file:write("\n") end
end
-- write material tables to file
local function writeMaterialsToFile ()
  local file = io.open(filename, "a")
  file:write("*********************************************************************
\n")
```

```
  file:write("*MATERIAL, name=MATRIX \n")
  writeTableToFile(file, matrixmodel[1], 2)
  for i=1,4 do
    if i==1 then ncol=0 else ncol = 2 end
    writeTableToFile(file, matrixdamage[i], ncol)
  end
  file:write("*DENSITY \n"..matrixdensity.." \n")
  file:write("**********************************************************************
\n")
  file:write("*MATERIAL, name=INTERFACE \n")
for i=1,4 do
  if i==2 then ncol=2 elseif i==3 then ncol=1 else ncol=3 end
  writeTableToFile(file, interfacemodel[i], ncol)
end
  file:write("*DENSITY \n"..interdensity.." \n")
  file:write("**********************************************************************
\n")
  file:write("*MATERIAL, name=TEXTILE \n")
  writeTableToFile(file, textilemodel[1], 1)
  file:write("*DENSITY \n"..textiledensity.." \n")
  file:close()
end
-- write boundary conditions to file
local function writeBcToFile ()
  local file = io.open(filename, "a")
  file:write("**********************************************************************
\n")
  file:write("*BOUNDARY \n")
  for i=1, 3 do
    file:write("FixedNodesLeft, "..i.."..", "..i.."\n")
  end
  file:write("*Initial Conditions, type=TEMPERATURE \n")
  file:write("ALLNODS, 0 \n")
  file:close()
end
-- write step and load to file
local function writeLoadToFile (loadvalue, steps)
  local file = io.open(filename, "a")
  local axis = loadvalue[1]
  local displacement = loadvalue[2]
  local k = 1
  for i=1,steps do
    file:write("**********************************************************************
\n")
    file:write("*STEP, name=Loading"..i.."..", nlgeom=YES, inc="..stepcontrol[2].." ,
unsymm=YES \n")
    file:write(stepcontrol[1].." \n")
    for j=3,#stepcontrol do file:write(stepcontrol[j].."..", ") end
    file:write("\n")
    file:write("*controls, analysis=discontinuous \n")
    file:write("*BOUNDARY \n")
    file:write("MovingNodesRight, "..axis.."..", , "..displacement.." \n")
    --add temperature control
    if (#textilechange >= k) then
      if (i==textilechange[k][1]) then
        file:write("*TEMPERATURE \n")
        file:write("ALLNODS, "..textilechange[k][2].." \n")
        k=k+1
      end
    end
    file:write("*Restart, write, frequency=0 \n")
    file:write("*Output, field \n")
    file:write("*Node Output \n")
    file:write("CF, RF, U \n")
    file:write("*Element Output, directions=YES \n")
    file:write("DAMAGEMT, DAMAGET, LE, PE, PEMAG, S, SDEG, MAXSCRT \n") --STATUS,
DAMAGEC, DAMAGEMC, PEEQ, PEEQT,
    file:write("*Contact Output \n")
    file:write("CDISP, CSTRESS \n")
    file:write("*Output, history, variable=PRESELECT \n")
    file:write("*END STEP \n")
    displacement = displacement + loadvalue[2]
  end
  file:close()
end
------------------------------------------------------------
--
```

```
--  Mesh definition
--
------------------------------------------------------------
 local function modelDomain(dx, nx, dy, ny, dz, nz, ntexlayers, bc, quad,
filename)

  local qdx, qnx, qdy, qny, qdz, qnz = dx, nx, dy, ny, dz, nz
  if quad then
    qdx = dx / 2
    qdy = dy / 2
    qdz = dz / 2
    qnx = 2 * nx - 1
    qny = 2 * ny - 1
    qnz = 2 * nz - 1
  end
  -- Node list
  local nodes = {}
  -- Matrix
  for z=0,1 do
    for y=0,qny-1 do
      for x=0,qnx-1 do
        nodes[#nodes+1] = {x*qdx, y*qdy, z*matrixH}
      end
    end
  end
  for n=1, ntexlayers do
    -- Matrix
    for y=0,qny-1 do
      for x=0,qnx-1 do
        nodes[#nodes+1] = {x*qdx, y*qdy, matrixH + nodes[#nodes+1-nx*ny][3]}
      end
    end
    -- Interface
    for y=0,qny-1 do
      for x=0,qnx-1 do
        nodes[#nodes+1] = {x*qdx, y*qdy, interfaceH + nodes[#nodes+1-nx*ny][3]}
      end
    end
    -- Textile
    for y=0,qny-1 do
      for x=0,qnx-1 do
        nodes[#nodes+1] = {x*qdx, y*qdy, textileH + nodes[#nodes+1-nx*ny][3]}
      end
    end
    -- Interface
    for y=0,qny-1 do
      for x=0,qnx-1 do
        nodes[#nodes+1] = {x*qdx, y*qdy, interfaceH + nodes[#nodes+1-nx*ny][3]}
      end
    end
    -- Matrix
    for y=0,qny-1 do
      for x=0,qnx-1 do
        nodes[#nodes+1] = {x*qdx, y*qdy, matrixH + nodes[#nodes+1-nx*ny][3]}
      end
    end
  end
  -- Matrix
  for y=0,qny-1 do
    for x=0,qnx-1 do
      nodes[#nodes+1] = {x*qdx, y*qdy, matrixH + nodes[#nodes+1-nx*ny][3]}
    end
  end
  -- element list
  local cells = {}
  local N
  if quad then
    --N = function (r,c) return (r-1)*qnx*2 + (c-1)*2 + 1 end
  else
    N = function (i, j, k) return (k-1)*nx*ny + (j-1)*nx + i end
  end
  for z=1, nz-1 do
    for y=1, ny-1 do
      for x=1, nx-1 do
        if quad then

        else
```

```
          cells[#cells+1] = {N(x, y, z), N(x+1, y, z), N(x+1, y+1, z), N(x, y+1,
z),
                             N(x, y, z+1), N(x+1, y, z+1), N(x+1, y+1, z+1), N(x,
y+1, z+1)}
        end
      end
    end
  end
  -- write information to file
  writeNodesToFile(nodes, filename)
  writeElementsToFile(cells, ntexlayers, nx, ny)
  writeAssemblyToFile(bc, dx, nx, dy, ny, dz, nz)
  writeMaterialsToFile(matrixmodel, matrixprop, interfacemodel, interfaceprop,
textilemodel, textileprop)
  writeBcToFile()
  writeLoadToFile(loadvalue, steps)
  return
end
-- call function
modelDomain(w/(nx-1), nx, d/(ny-1), ny, h/(nz-1), nz, ntexlayers, bc,
useQuadElement, filename)
```

Appendix II: Fortran Routine

The Fortran routine defines the hardening curve of the textile.

```
C ----------------------------------------------------------------
C UMAT FOR ISOTROPIC ELASTICITY
C CANNOT BE USED FOR PLANE STRESS
C ----------------------------------------------------------------
C PROPS(1) - E
C PROPS(2) - NU
C ----------------------------------------------------------------
C
      SUBROUTINE UMAT(STRESS,STATEV,DDSDDE,SSE,SPD,SCD,
     1 RPL,DDSDDT,DRPLDE,DRPLDT,
     2 STRAN,DSTRAN,TIME,DTIME,TEMP,DTEMP,PREDEF,DPRED,CMNAME,
     3 NDI,NSHR,NTENS,NSTATV,PROPS,NPROPS,COORDS,DROT,PNEWDT,
     4 CELENT,DFGRD0,DFGRD1,NOEL,NPT,LAYER,KSPT,JSTEP,KINC)
C
C     DDSDDE - Constitutive Jacobian
C     NDI - Number of direct stress components at this point.
C     NSHR - Number of engineering shear stress components at this point.
C     NTENS - Size of the stress or strain component array (NDI + NSHR).
C     DSTRAN - Relative-displacements as “strains” (STRAN and DSTRAN)
C
      INCLUDE 'ABA_PARAM.INC'
C
      CHARACTER*80 CMNAME
      DIMENSION STRESS(NTENS),STATEV(NSTATV),
     1 DDSDDE(NTENS,NTENS),DDSDDT(NTENS),DRPLDE(NTENS),
     2 STRAN(NTENS),DSTRAN(NTENS),TIME(2),PREDEF(1),DPRED(1),
     3 PROPS(NPROPS),COORDS(3),DROT(3,3),DFGRD0(3,3),DFGRD1(3,3),
     4 JSTEP(4)
      REAL*8 E0, v,G0,K0,dT0,CTE,L1,L2,R,d

C
C ELASTIC PROPERTIES of the textile
C
C define dT0 and l
      L1=1795
      L2=2125
      R=L1/L2
      R=3.035*R*R*R-3.055*R*R+1.02*R
      dT0 = 0.0012
      CTE = 1
      d=0.0005
      IF (STRAN(1)<dT0) THEN
      E0 = 5.88E3
      v = 0.28
      ELSE IF (STRAN(1)<dT0+1*d*R) THEN
      E0 = 45E3
      v = 0.28
      ELSE IF (STRAN(1)<dT0+2*d*R) THEN
      E0 = 40E3
      v = 0.28
      ELSE IF (STRAN(1)<dT0+3*d*R) THEN
      E0 = 45E3
      v = 0.28
      ELSE IF (STRAN(1)<dT0+4*d*R) THEN
      E0 = 60E3
      v = 0.28
      ELSE IF (STRAN(1)<dT0+5*d*R) THEN
      E0 = 60E3
      v = 0.28
      ELSE IF (STRAN(1)<dT0+6*d*R) THEN
      E0 = 70E3
      v = 0.28
      ELSE IF (STRAN(1)<dT0+7*d*R) THEN
      E0 = 90E3
      v = 0.28
      ELSE IF (STRAN(1)<dT0+8*d*R) THEN
      E0 = 100E3
      v = 0.28
      ELSE IF (STRAN(1)<dT0+9*d*R) THEN
      E0 = 105E3
      v = 0.28
      ELSE IF (STRAN(1)<dT0+10*d*R) THEN
```

```
      E0 = 120E3*CTE
      v = 0.28
      ELSE IF (STRAN(1)<dT0+11*d*R) THEN
      E0 = 120E3*CTE
      v = 0.28
      ELSE IF (STRAN(1)<dT0+12*d*R) THEN
      E0 = 120E3*CTE
      v = 0.28
      ELSE IF (STRAN(1)<dT0+13*d*R) THEN
      E0 = 120E3*CTE
      v = 0.28
      ELSE IF (STRAN(1)<dT0+14*d*R) THEN
      E0 = 120E3*CTE
      v = 0.28
      ELSE IF (STRAN(1)<dT0+15*d*R) THEN
      E0 = 120E3*CTE
      v = 0.28
      ELSE IF (STRAN(1)<0.008) THEN
      E0 = 120E3*CTE
      v = 0.28
      ELSE IF (STRAN(1) > 0.008)THEN
      E0 = 120E3*CTE
      v = 0.28
      END IF
      E0=E0
C
      G0 = E0/(2*(1+v))
      K0 = E0/(3*(1-2*v))
C ELASTIC STIFFNESS
      DO K1 = 1, NDI
        DO K2 = 1, NDI
                DDSDDE(K2,K1) = K0 - (2/3)*G0
        END DO
            DDSDDE(K1,K1) = K0 + (4/3)*G0
      END DO
      DO K1 = NDI + 1, NTENS
         DDSDDE(K1, K1) = G0
      END DO
C CALCULATE STRESS
      DO K1 = 1, NTENS
         DO K2 = 1, NTENS
            STRESS(K2) = STRESS(K2) + DDSDDE(K2, K1)*DSTRAN(K1)
         END DO
      END DO
      RETURN
      END
```

9. References

[1] TAYLOR, H., **Cement Chemistry**, pp. 1–491, 1990.

[2] SPARAVIGNA, A., "Ancient concrete works," pp. 1–7, Oct. 2011.

[3] ASPDIN, J., "An Improvement in the Modes of Producing an Artificial Stone," pp. 1–2, Oct. 1824.

[4] AÏTCIN, P.-C., "Cements of yesterday and today," Cement and Concrete Research, vol. 30, no. 9, pp. 1349–1359, Sep. 2000.

[5] HASSAN, A. M. T.; JONES, S. W.; MAHMUD, G. H., "Experimental test methods to determine the uniaxial tensile and compressive behaviour of ultra high performance fibre reinforced concrete (UHPFRC)," Construction and Building Materials, vol. 37, pp. 874–882, Dec. 2012.

[6] BEHNOOD, A.; GHANDEHARI, M., "Comparison of compressive and splitting tensile strength of high-strength concrete with and without polypropylene fibers heated to high temperatures," Fire Safety Journal, vol. 44, no. 8, pp. 1015–1022, Nov. 2009.

[7] SHAFIGH, P.; JUMAAT, M. Z.; MAHMUD, H. B.; HAMID, N. A. A., "Lightweight concrete made from crushed oil palm shell: Tensile strength and effect of initial curing on compressive strength," Construction and Building Materials, vol. 27, no. 1, pp. 252–258, Feb. 2012.

[8] ROUMALDI, J. P.; BATSON, G. B., Mechanics of Crack Arrest in Concrete, vol. 89. Proceedings of the ASCEJ of Engineering Mechanics Division, 1963, pp. 147–168.

[9] ZOLLO, R. F., "Fiber-reinforced concrete: an overview after 30 years of development," Cement and Concrete Composites, vol. 19, no. 2, pp. 107–122, Jan. 1997.

[10] DE FELICE, G.; DE SANTIS, S.; GARMENDIA, L.; GHIASSI, B.; LARRINAGA, P.; LOURENÇO, P. B.; OLIVEIRA, D. V.; PAOLACCI, F.; PAPANICOLAOU, C. G., "Mortar-based systems for externally bonded strengthening of masonry," Mater Struct, vol. 47, no. 12, pp. 2021–2037, 2014.

[11] DONNINI, J.; CORINALDESI, V.; NANNI, A., "Mechanical properties of FRCM using carbon fabrics with different coating treatments," Composites Part B, vol. 88, no. C, pp. 220–228, Mar. 2016.

[12] TRIANTAFILLOU, T.; PAPANICOLAOU, C., "Innovative Applications of Textile-Based Composites in Strengthening and Seismic Retrofitting as Well as in the Prefabrication of New Structures," Advanced Materials Research, vol. 639, pp. 26–41, 2013.

[13] GOPINATH, S.; KUMAR, V. R.; SHETH, H.; MURTHY, A. R.; IYER, N. R., "Pre-fabricated sandwich panels using cold-formed steel and textile reinforced concrete," Construction and Building Materials, vol. 64, no. C, pp. 54–59, Aug. 2014.

[14] HEGGER, J.; HORSTMANN, M.; ZELL, M., "Textile Reinforced Concrete – Realization in applications," in Tailor Made Concrete Structures, CRC Press, 2008, pp. 357–362.

[15] KULAS, C., "Actual applications and potential of textile-reinforced concrete," GRCA International, pp. 1–11, Apr. 2015.

[16] GAO, T.; SHEN, L.; SHEN, M.; CHEN, F.; LIU, L.; GAO, L., "Analysis on differences of carbon dioxide emission from cement production and their major determinants," Journal of Cleaner Production, vol. 103, pp. 160–170, Sep. 2015.

[17] HEGGER, J.; BENTUR, A.; CURBACH, M.; MOBASHER, B.; PELED, A.; WASTIELS, J., "6.2 Mechanical Behaviour of Textile Reinforced Concrete," in Textile Reinforced Concrete - State-of-the-Art Report of RILEM, Report, 2006, pp. 133–186.

[18] GONG, R. H.; CHEN, X., "Technical yarns," in Handbook of Technical Textiles, Elsevier, 2000, pp. 42–61.

[19] SONDHELM, W. S., "Technical fabric structures – 1. Woven fabrics," in Handbook of Technical Textiles, Elsevier, 2000, pp. 62–94.

[20] JACQUEMIN, F., "The hygroscopic behavior of plant fibers: a review," pp. 1–12, Jan. 2014.

[21] DE ROOIJ, M.; QIAN, S.; VAN DE KUILEN, J.; GARD, W.; LIU, H., Using natural wood fibers to self heal concrete. CRC Press, 2008, pp. 123–124.

[22] BOISSE, P.; BORR, M.; BUET, K.; CHEROUAT, A., "Finite element simulations of textile composite forming including the biaxial fabric behaviour," Composites Part B: Engineering, vol. 28, no. 4, pp. 453–464, Jan. 1997.

[23] LORD, P. R.; RADHAKRISHNAIAH, P., "A Comparison of Various Woven Fabrics Containing Friction, Rotor, and Ring Spun Cotton Yarn Fillings," Textile Research Journal, vol. 58, no. 6, pp. 354–362, Jun. 1988.

[24] SEO, M. H.; REALFF, M. L.; PAN, N.; BOYCE, M.; SCHWARTZ, P.; BACKER, S., "Mechanical Properties of Fabric Woven from Yarns Produced by Different Spinning Technologies: Yarn Failure in Woven Fabric," Textile Research Journal, vol. 63, no. 3, pp. 123–134, Mar. 1993.

[25] GRIES, T.; ROYE, A.; OFFERMANN, P.; PELED, A., "3 Textile," in Textile Reinforced Concrete - State-of-the-Art Report of RILEM, Report, 2006, pp. 11–27.

[26] MIRAFTAB, M., "Technical fibres," in Handbook of Technical Textiles, Elsevier, 2000, pp. 24–41.

[27] PEIRCE, F. T., Tensile tests for cotton yarns–"the weakest link" theorems on the strength of long and of composite specimens. J. Textile Inst, 1926.

[28] WEIBULL, W., A statistical theory of the strength of materials. Vetensk. Akad. Handl, 1939.

[29] REALFF, M. L., "Mechanical properties of fabrics woven from yarns produced by different spinning technologies," Massachusetts Institute of Technology, 1992.

[30] MISAK, H. E.; ASMATULU, R.; MALL, S., "Tensile behavior of carbon nanotube multi-yarn coated with polyester," Journal of Composite Materials, vol. 49, no. 14, pp. 1–7, Jun. 2014.

[31] CAROZZI, F. G.; POGGI, C., "Mechanical properties and debonding strength of Fabric Reinforced Cementitious Matrix (FRCM) systems for masonry strengthening," Composites Part B: Engineering, vol. 70, pp.

215–230, Mar. 2015.

[32] PEIRCE, F. T., “5—THE GEOMETRY OF CLOTH STRUCTURE,” Journal of the Textile Institute Transactions, vol. 28, no. 3, pp. T45–T96, Mar. 1937.

[33] VASSILIADIS, S.; KALLIVRETAKI, A.; DOMVOGLOU, D.; PROVATIDIS, C., “Mechanical Analysis of Woven Fabrics:The State of the Art,” in Advances in Modern Woven Fabrics Technology, no. 3, InTech, 2011, pp. 1–25.

[34] RAMAKRISHNA, S., “Characterization and modeling of the tensile properties of plain weft-knit fabric-reinforced composites,” Composites Science and Technology, vol. 57, no. 1, pp. 1–22, Jan. 1997.

[35] OZGEN, B.; GONG, H., “Yarn Geometry in Woven Fabrics,” Textile Research Journal, vol. 81, no. 7, pp. 1–8, Nov. 2010.

[36] PELED, A.; SUEKI, S.; MOBASHER, B., “Bonding in fabric–cement systems: Effects of fabrication methods,” Cement and Concrete Research, vol. 36, no. 9, pp. 1661–1671, Sep. 2006.

[37] PELED, A.; COHEN, Z.; PASDER, Y.; ROYE, A.; GRIES, T., “Influences of textile characteristics on the tensile properties of warp knitted cement based composites,” Cement and Concrete Composites, vol. 30, no. 3, pp. 174–183, Mar. 2008.

[38] HARTIG, J.; HÄUSSLER-COMBE, U.; SCHICKTANZ, K., “Influence of bond properties on the tensile behaviour of Textile Reinforced Concrete,” Cement and Concrete Composites, vol. 30, no. 10, pp. 898–906, Nov. 2008.

[39] PORTAL, N. W.; PEREZ, I. F.; THRANE, L. N.; LUNDGREN, K., “Pull-out of textile reinforcement in concrete,” Construction and Building Materials, vol. 71, no. C, pp. 63–71, Nov. 2014.

[40] XU, S.; LI, H., “Bond properties and experimental methods of textile reinforced concrete,” J. Wuhan Univ. Technol., vol. 22, no. 3, pp. 529–532, Sep. 2007.

[41] SUEKI, S.; SORANAKOM, C.; MOBASHER, B.; PELED, A., “Pullout-Slip Response of Fabrics Embedded in a Cement Paste Matrix,” Journal of Materials in Civil Engineering, vol. 19, no. 9, pp. 718–727, Sep. 2007.

[42] AVESTON, J.; COOPER, G. A.; KELLY, A., The Properties of Fiber Composites, Conf. Proc. Nat. Phys. Lab.

[43] COX, H. L., “The elasticity and strength of paper and other fibrous materials,” Br. J. Appl. Phys., vol. 3, no. 3, pp. 72–79, 1952.

[44] MARSHALL, D. B.; COX, B. N.; EVANS, A. G., “The mechanics of matrix cracking in brittle-matrix fiber composites,” Acta Metallurgica, vol. 33, no. 11, pp. 2013–2021, Nov. 1985.

[45] WANG, Y.; LI, V. C.; BACKER, S., “Modelling of fibre pull-out from a cement matrix,” International Journal of Cement Composites and Lightweight Concrete, vol. 10, no. 3, pp. 143–149, 1988.

[46] NAAMAN, A. E.; SHAR, S. R., “PULL-OUT MECHANISM IN STEEL FIBRE-REINFORCED CONCRETE,” Journal of the Structural Division, vol. 102, Aug. 1976.

[47] MOBASHER, B., **Mechanics of Fiber and Textile Reinforced Cement Composites**. 2012, pp. 1–465.

[48] REINHARDT, H. W.; KRÜGER, M.; BENTUR, A.; BRAMESHUBER, W.; BANHOLZER, B.; CURBACH, M.; JESSE, F.; MOBASHER, B.; PELED, A.; SCHORN, H., "6.1 Bond," in Textile Reinforced Concrete - State-of-the-Art Report of RILEM, 2006, pp. 1–49.

[49] HÄUSSLER-COMBE, U.; HARTIG, J., "Bond and failure mechanisms of textile reinforced concrete (TRC) under uniaxial tensile loading," Cement and Concrete Composites, vol. 29, no. 4, pp. 279–289, Apr. 2007.

[50] MOBASHER, B.; DEY, V.; COHEN, Z.; PELED, A., "Correlation of constitutive response of hybrid textile reinforced concrete from tensile and flexural tests," Cement and Concrete Composites, vol. 53, no. C, pp. 148–161, Oct. 2014.

[51] NAAMAN, A. E.; NAMUR, G. G.; ALWAN, J. M.; NAJM, H. S., "Fiber Pullout and Bond Slip. I: Analytical Study," J. Struct. Eng., vol. 117, no. 9, pp. 2769–2790, Sep. 1991.

[52] PARK, J.-M.; KIM, J.-W.; YOON, D.-J., "Interfacial evaluation and microfailure mechanisms of single carbon fiber/bismaleimide (BMI) composites by tensile and compressive fragmentation tests and acoustic emission," Composites Science and Technology, vol. 62, no. 6, pp. 743–756, May 2002.

[53] LORENZ, E.; ORTLEPP, R., "Bond Behavior of Textile Reinforcements - Development of a Pull-Out Test and Modeling of the Respective Bond versus Slip Relation," in High Performance Fiber Reinforced Cement Composites 6, vol. 2, no. 58, Dordrecht: Springer Netherlands, 2012, pp. 479–486.

[54] VAN MIER, J., **Fracture processes of concrete**. 1997.

[55] MEHTA, P.; MONTEIRO, P., "Concrete: Microstructure, Properties and Materials," pp. 1–684, 2006.

[56] LANDIS, E. N.; BOLANDER, J. E., "Explicit representation of physical processes in concrete fracture," J. Phys. D: Appl. Phys., vol. 42, no. 21, p. 214002, Nov. 2009.

[57] GROSS, D.; SEELIG, T., "Classical fracture and failure hypotheses," in Fracture Mechanics, no. 2, Berlin, Heidelberg: Springer Berlin Heidelberg, 2011, pp. 39–50.

[58] HILLERBORG, A., "A model for fracture analysis," Report TVBM, 1978.

[59] AKIHAMA, S.; SUENAGA, T.; BANNO, T., "The behaviour of carbon fibre reinforced cement composites in direct tension," International Journal of Cement Composites and Lightweight Concrete, vol. 6, no. 3, pp. 159–168, Aug. 1984.

[60] PAPANICOLAOU, C. G.; PAPANTONIOU, I. C., "Mechanical Behavior of Textile Reinforced Concrete (TRC) / Concrete Composite Elements," Journal of Advanced Concrete Technology, vol. 8, no. 1, pp. 35–47, 2010.

[61] ARBOLEDA, D., "Fabric Reinforced Cementitious Matrix (FRCM) Composites for Infrastructure Strengthening and Rehabilitation: Characterization Methods," University of Miami, 2014.

[62] MATZENMILLER, A.; LUBLINER, J.; TAYLOR, R. L., “A constitutive model for anisotropic damage in fiber-composites,” Mechanics of Materials, vol. 20, no. 2, pp. 125–152, Apr. 1995.

[63] DE ANDRADE SILVA, F. V.; BUTLER, M.; HEMPEL, S.; FILHO, R. D. T.; MECHTCHERINE, V., “Effects of elevated temperatures on the interface properties of carbon textile-reinforced concrete,” Cement and Concrete Composites, vol. 48, no. C, pp. 26–34, Apr. 2014.

[64] BUTLER, M.; MECHTCHERINE, V.; HEMPEL, S., “Experimental investigations on the durability of fibre–matrix interfaces in textile-reinforced concrete,” Cement and Concrete Composites, vol. 31, no. 4, pp. 221–231, Apr. 2009.

[65] FRISCH, J., “Numerical Modelling - Introductory Approach.” pp. 1–22, Oct-2010.

[66] FELIPPA, C., “FEM Modeling: Introduction,” in Introduction to Finite Element Methods, 2004, pp. 1–15.

[67] JANKOWIAK, T.; LODYGOWSKI, T., “Identification of parameters of concrete damage plasticity constitutive model,” Foundations of Civil and Environmental Engineering, 2005.

[68] WAHALATHANTRI, B. L.; THAMBIRATNAM, D. P., “A material model for flexural crack simulation in reinforced concrete elements using ABAQUS | QUT ePrints,” presented at the Proceedings of the …, 2011.

[69] CHAUDHARI, S. V.; CHAKRABARTI, M. A., “Modeling of concrete for nonlinear analysis Using Finite Element Code ABAQUS,” International Journal of Computer Applications, vol. 44, no. 7, pp. 14–18, Apr. 2012.

[70] LOMOV, S. V.; HUYSMANS, G.; LUO, Y.; PARNAS, R. S.; PRODROMOU, A.; VERPOEST, I.; PHELAN, F. R., “Textile composites: modelling strategies,” Composites Part A: Applied Science and Manufacturing, vol. 32, no. 10, pp. 1379–1394, Oct. 2001.

[71] KING, M. J.; JEARANAISILAWONG, P.; SOCRATE, S., “A continuum constitutive model for the mechanical behavior of woven fabrics,” International Journal of Solids and Structures, vol. 42, no. 13, pp. 3867–3896, Jun. 2005.

[72] FILLEP, S.; MERGHEIM, J.; STEINMANN, P., “Computational modelling and homogenization of technical textiles,” Engineering Structures, vol. 50, pp. 68–73, May 2013.

[73] EISCHEN, J. W.; DENG, S.; CLAPP, T. G., “Finite-Element Modeling and Control of Flexible Fabric Parts,” IEEE Computer Graphics and Applications, vol. 16, no. 5, pp. 71–80, Sep. 1996.

[74] HIVET, G.; BOISSE, P., “Consistent 3D geometrical model of fabric elementary cell. Application to a meshing preprocessor for 3D finite element analysis,” Finite Elements in Analysis and Design, vol. 42, no. 1, pp. 25–49, Oct. 2005.

[75] CARVELLI, V.; CORAZZA, C.; POGGI, C., “Mechanical modelling of monofilament technical textiles,” Computational Materials Science, vol. 42, no. 4, pp. 679–691, Jun. 2008.

[76] DURVILLE, D., “Finite element simulation of textile materials at the fiber

scale," arXiv.org, vol. cond-mat.mtrl-sci. 07-Dec-2009.

[77] BOISSE, P.; GASSER, A.; HIVET, G., "Analyses of fabric tensile behaviour: determination of the biaxial tension–strain surfaces and their use in forming simulations," Composites Part A: Applied Science and Manufacturing, vol. 32, no. 10, pp. 1395–1414, Oct. 2001.

[78] NEKKANTY, S.; WALTER, M.; SHIVPURI, R., "A cohesive zone finite element approach to model tensile cracks in thin film coatings," Journal of Mechanics of Materials and Structures, vol. 2, no. 7, pp. 1231–1247, Sep. 2007.

[79] ELIASSON, S.; LUNDBERG, A., "Investigation and Comparison of Cohesive Zone Models for Simulation of Crack Propagation," 2015.

[80] SCHEIDER, I., "Cohesive model for crack propagation analyses of structures with elastic–plastic material behavior Foundations and implementation," GKSS research center, 2001.

[81] ZACHARIAH, A., "Finite Element Modelling of Adhesive Interface between Steel and CFRP," 2016.

[82] LAPCZYK, I.; HURTADO, J. A., "Progressive damage modeling in fiber-reinforced materials," Composites Part A: Applied Science and Manufacturing, vol. 38, no. 11, pp. 2333–2341, Nov. 2007.

[83] ŠEJNOHA, M.; ZEMAN, J., "Micromechanical modeling of imperfect textile composites," International Journal of Engineering Science, vol. 46, no. 6, pp. 513–526, Jun. 2008.

[84] AZZAM, A.; RICHTER, M., "Investigation of Stress Transfer Behavior in Textile Reinforced Concrete with Application to Reinforcement Overlapping and Development Lengths," Colloquium on Textile Reinforced Structures, pp. 103–116, Sep. 2011.

[85] WILLIAMS PORTAL, N.; LUNDGREN, K.; WALTER, A. M.; FREDERIKSEN, J. O.; NYHOLM THRANE, L., Numerical Modelling of Textile Reinforced Concrete. 2013, pp. 886–897.

[86] LARRINAGA, P.; CHASTRE, C.; BISCAIA, H. C.; SAN-JOSÉ, J. T., "Experimental and numerical modeling of basalt textile reinforced mortar behavior under uniaxial tensile stress," Materials & Design, vol. 55, pp. 66–74, Mar. 2014.

[87] SALVIATO, M.; KIRANE, K.; ASHARI, S. E.; BAŽANT, Z. P.; CUSATIS, G., "Experimental and numerical investigation of intra-laminar energy dissipation and size effect in two-dimensional textile composites," Composites Science and Technology, vol. 135, pp. 67–75, 2016.

[88] BAZANT, Z. P.; PLANAS, J., Fracture and size effect in concrete and other quasibrittle materials. 1997.

[89] SILVA, F. DE A.; BUTLER, M.; MECHTCHERINE, V.; ZHU, D.; MOBASHER, B., "Strain rate effect on the tensile behaviour of textile-reinforced concrete under static and dynamic loading," Materials Science and Engineering: A, vol. 528, no. 3, pp. 1727–1734, Jan. 2011.

[90] C09 COMMITTEE, "Standart Test Method for Slump Flow of Self-Consolidating Concrete - ASTM C1611," ASTM International, West Conshohocken, PA, Jun. 2014.

[91] STRAUSS RAMBO, D. A.; DE ANDRADE SILVA, F.; TOLEDO FILHO, R. D.; UKRAINCZYK, N.; KOENDERS, E., "Tensile strength of a calcium-aluminate cementitious composite reinforced with basalt textile in a high-temperature environment," Cement and Concrete Composites, vol. 70, pp. 183–193, Jul. 2016.

[92] SANJA, M.; MILICA, V.; JELENA, M.; BRANKO, M.; TATJANA, V.-H., "Thermal and mechanical properties of high alumina low cement castable," Metallurgical and Materials Engineering, vol. 18, no. 1, pp. 53–65, 2012.

[93] ABNT/CB COMITEE, "NBR 8522: Concrete - Determination of the elasticity modulus by compression," ABNT, pp. 1–16, Apr. 2008.

[94] OTSU, N., "A threshold selection method from gray-level histograms," Automatica, 1975.

[95] RILEM TECHNICAL COMMITTEE 232-TDT (WOLFGANG BRAMESHUBER), "Recommendation of RILEM TC 232-TDT: test methods and design of textile reinforced concrete," Mater Struct, vol. 49, no. 12, pp. 4923–4927, May 2016.

[96] C09 COMMITTEE, "Test Method for Flexural Toughness of Fiber Reinforced Concrete (Using Centrally Loaded Round Panel)," ASTM International, West Conshohocken, PA, 2012.

[97] CHUDOBA, R.; VOŘECHOVSKÝ, M.; KONRAD, M., "Stochastic modeling of multi-filament yarns. I. Random properties within the cross-section and size effect," International Journal of Solids and Structures, vol. 43, no. 3, pp. 413–434, Feb. 2006.

[98] ISHIKAWA, T.; MATSUSHIMA, M.; HAYASHI, Y., "Hardening non-linear behaviour in longitudinal tension of unidirectional carbon composites," J Mater Sci, vol. 20, no. 11, pp. 4075–4083, Nov. 1985.

[99] MORETON, R., "The effect of gauge length on the tensile strength of R.A.E. carbon fibres," Fibre Science and Technology, vol. 1, no. 4, pp. 273–284, 1969.

[100] ABAQUS/CAE User's Guide 6.14. 2014, pp. 1–1146.

[101] BRUGGI, M.; VENINI, P., "A numerical investigation on the size effect of fiber-reinforced concrete specimens in crack propagation," Computational Mechanics, vol. 50, no. 1, Jul. 2012.

[102] KONRAD, M.; CHUDOBA, R., "Textile Reinforced Concrete Part II: Multi-Level Modeling Concept," pp. 1–11, Apr. 2003.

[103] PARTON, G. M.; SHENDY-EL-BARBARY, M. E., "A finite element analysis for cement composite sandwich plates," International Journal of Cement Composites and Lightweight Concrete, vol. 5, no. 3, pp. 181–191, Aug. 1983.